UNIVERSIDADE FEDERAL DE SANTA CATARINA
CENTRO TECNOLÓGICO
DEPARTAMENTO DE ENGENHARIA QUÍMICA E ENGENHARIA DE ALIMENTOS
PROGRAMA DE PÓS-GRADUAÇÃO EM ENGENHARIA QUÍMICA

PAULO EMILIO FEUSER

SUPERPARAMAGNETIC POLY(METHYL METHACRYLATE) NANOPARTICLES FOR BIOMEDICAL APLLICATION

FLORIANÓPOLIS
2016

Paulo Emilio Feuser

SUPERPARAMAGNETIC POLY(METHYL METHACRYLATE) NANOPARTICLES FOR BIOMEDICAL APLLICATION

Tese de Doutorado submetida ao programa de Pós Graduação em Engenharia Química da Universidade Federal de Santa Catarina para a obtenção do Grau de doutor em Engenharia Química.

Orientador: Prof. D.Sc. Pedro Henrique Hermes de Araújo

Coorientadora: Prof[a]. D. Sc. Claudia Sayer
Coorientador: Prof. D.Sc. Eduardo Ricci Júnior

Florianópolis
2016

Ficha de identificação da obra elaborada pelo autor
através do Programa de Geração Automática da Biblioteca Universitária
da UFSC.

Feuser, Paulo Emilio
Superparamagnetic Poly(methyl Methacrylate) Nanoparticles for Biomedical Apllication / Paulo Emilio Feuser ; orientador, Pedro Henrique Hermes de Araújo ; coorientadora, Claudia Sayer ; coorientador, Eduardo Ricci Júnior – Florianópolis, SC, 2015
200 p.

Tese (Doutorado). Universidade Federal de Santa Catarina. Centro Tecnológico. Programa de Pós-Graduação em Engenharia Química.

Inclui referência

1. Engenharia Química. 2. ácido fólico. 3. poli(metacrilato de metila). 4. nanopartículas poliméricas. 5. polimerização em miniemulsão. I. De Araújo, Pedro Henrique Hermes. II. Sayer, Claudia. III. Júnior, Eduardo Ricci. IV. Universidade Federal de Santa Catarina. Programa de Pós-Graduação em Ciência dos Alimentos. V. Título.

SUPERPARAMAGNETIC POLY(METHYL METHACRYLATE) NANOPARTICLES FOR BIOMEDICAL APLLICATION

Tese de doutorado submetida ao Programa de Pós Graduação em Engenharia Química da Universidade Federal de Santa Catarina para a obtenção do Grau de doutor em Engenharia Química.

Florianópolis, 03 de março de 2016.

_____
Prof. Dr. Pedro Henrique Hermes de Araújo
Orientador

_____
Profª. Drª. Claudia Sayer
Coorientadora

_____
Eduardo Ricci-Júnior
Coorientador

_____
Profª. Drª. Cíntia Soares
Coordenadora

Banca Examinadora

_____
Profª. Drª. Debora de Oliveira
Membro interno

_____
Profª. Drª. Cristiane da Costa Bresolin
Membro interno

_____
Prof. Dr. Marcio Nele de Souza
Membro externo

_____
Prof. Dr. Marcelo Kaminski Lenzi
Membro externo

_____
Profª. Drª. Alexsandra Valério
Membro participante

AGRADECIMENTOS

Primeiramente queria agradecer meus pais e irmãs pelo carinho e apoio em todos os momentos, obrigado por tudo, hoje e sempre. Agradeço também minha esposa, Karla pelo apoio incondicional, carinho, atenção e mesmo estando longe em alguns momentos, obrigado por tudo.

Aos meus grandes "mestres": meu orientador, Prof. Pedro Henrique Hermes de Araújo, por todo apoio, compreensão e amizade. A minha coorientadora, Claudia Sayer, pelo carinho e atenção em todos os momentos. Ao meu coorientador Prof. Eduardo Ricci da Faculdade de Farmácia-UFRJ, pelo apoio, amizade e atenção. Ao Prof. Marcio Nele da Escola de Química-UFRJ, por ter me dado a minha primeira oportunidade e sempre me apoiando em todos os momentos. Tenho orgulho em ter vocês do meu lado. Não existem palavras para dizer o quanto vocês são importantes para mim.

A Prof(a) Maria Eliane e toda equipe do Laboratório de Oxidações da Universidade Federal do Paraná, pelo carinho e apoio em todos os momentos.

Ao Prof. Alexandre Cas Viegas pela atenção e pela possibilidade de realizar análises de magnetização e de Raio-X.

Ao Prof. Tedesco, bem como, a seus colaboradores do Centro de Nanotecnologia, Engenharia Tecidual e Fotoprocessos voltado a Saúde - Grupo de Fotobiologia e Fotomedicina da Universidade de São Paulo, pelo apoio e a possibilidade de realizar os ensaios *in vitro* de hipertermia.

A Profª. Maria Claudia e seus colaboradores do Departamento de Análises Clínicas desta Universidade.

Agradeço também à Universidade Federal de Santa Catarina, ao Programa de Pós-Graduação Engenharia Química, por todos os recursos que permitiram a elaboração deste trabalho. Em especial ao Laboratório de Controle de Processos (LCP) da UFSC, pela disponibilidade dos recursos físicos e pela oportunidade do desenvolvimento das atividades. Não posso esquecer de todo pessoal do LCP, que sempre me auxiliaram e me ajudaram de alguma forma a construir este trabalho.

Agradeço ainda ao LCME - Laboratório Central de Microscopia Eletrônica pela disponibilidade da estrutura física do laboratório e microscópios, que me propuseram a oportunidade do desenvolvimento das atividades necessárias para a realização deste trabalho.

Ao apoio financeiro do Conselho Nacional de Desenvolvimento Científico e Tecnológico (CNPq) e a Coordenação de Aperfeiçoamento de Pessoal de Nível de Superior (CAPES).

RESUMO

O câncer é o nome dado a um conjunto de mais de 100 doenças que tem em comum, o crescimento desordenado de células (maligno), que invadem os tecidos e órgãos podendo espalhar-se (metástase) para outras regiões do corpo e o câncer benigno, que significa simplesmente uma massa localizada de células que se multiplicam vagarosamente e se assemelham ao seu tecido original e raramente constitui risco de vida, dependendo do tempo de diagnóstico. Dados da Organização Mundial de Saúde (OMS) mostram que o câncer é a segunda principal causa de mortes em todo o mundo. Estima se que no ano de 2030, o câncer poderá matar 17 milhões de pessoas contra os 7,6 milhões de óbitos que provocou em 2007. Um grande esforço na busca de novos tratamentos para o câncer, como um tratamento mais seletivo das células cancerígenas vem ganhando destaque na literatura. A busca de novas formulações farmacêutica utilizando como ferramenta a nanotecnologia pode melhorar a eficácia terapêutica de fármacos já existente no mercado e consequentemente diminuir seus inúmeros efeitos adversos. Nanopartículas poliméricas (NPs) com propriedades superparamagneticas e superfície modificada com ácido fólico (FA) podem direcionar o fármaco encapsulado a uma célula tumoral alvo, no qual, melhora sua internalização celular (endocitose) e eficácia terapêutica, diminuindo assim seus efeitos tóxicos. Outra vantagem destes sistemas com propriedades superparamagnéticas, é que estas podem induzir a morte das células por hipertermia (HPT) (aumento da temperatura), sendo este tratamento muito mais eficaz quando associado a terapias convencionais, como a quimioterapia e a radioterapia. Tendo em conta as vantagens e desvantagens de diferentes estratégias terapêuticas, a ideia de combinar vários tratamentos, pode ser um atrativo para a próxima geração do tratamento do câncer. Com isso, o objetivo deste trabalho foi a síntese, caracterização e estudos *in vitro* das NPs de poli (metacrilato de metila) (PMMA) com propriedades superparamagnéticas, obtidas via polimerização em miniemulsão. A fim de verificar a eficácia das NPs como sistemas carreadores de fármacos, dois compostos antitumorais foram utilizados: a ftalocianina de zinco (ZnPc), um fotossensibilizante de segunda geração utilizado no tratamento do câncer via Terapia Fotodinâmica (PDT) e o lauril galato (G12), um derivado do ácido gálico. Com o intuito de melhorar a vetorização das NPs de PMMA, o AF foi usado como modificador de

superfície. Por fim, ensaios de citotoxicidade e internalização celular foram realizados em células que expressam receptores folatos, com o objetivo de avaliar o mecanismo de entrada dos sistemas preparados. As NPs de PMMA obtidas via polimerização em miniemulsão apresentaram um tamanho nanométrico, com potencial zeta negativo e biocompatibilidade em células tumorais e não tumorais. A partir destes excelentes resultados de biocompatibilidade, a ZnPc foi incorporada nas NPs de PMMA (PMMAZnPc). Ensaios de citotoxicidade em células leucêmicas (K562 e Jurkat) mostraram um maior efeito citotóxico da ZnPc encapsulada em NPs que ZnPc livre, sugerindo que a morte das células leucêumicas foi mediada por apoptose. Em outro estudo, NPs de PMMA com propriedades superparamagnéticas (MNPs-PMMA) foram obtidas via polimerização em miniemulsão. MNPs-PMMA NPs apresentaram biocompatibilidade em células tumorais e não tumorais, e induziram a morte das células U87MG (~50%) por HPT. O tratamento simultâneo (PDT e HPT) sobre as mesmas células (U87MG) com o encapsulamento simultâneo da ZnPc e NPMs em NPs de PMMA (MNPsZnPc-PMMA), apresentaram um efeito sinérgico. Os resultados *in vitro* mostraram que a aplicação da PDT e HPT simultaneamente podem ser mais eficazes quando aplicados simultaneamente. Por fim, visando uma melhor vetorização das NPs de PMMA quando o FA foi usado como agente ligante (FA-MNPsPMMA). A adsorção do FA nas NPs de PMMA com propriedades superparamagnéticas aumentou a internalização das NPs nas células que expressam receptores folatos (células K562). Em outro estudo o G12 foi incorporado nas NPs de PMMA. O encapsulamento simultâneo do G12 e NPMs em NPs de PMMA com superfície modificada, apresentou um maior efeito citotóxico sobre as células HeLa, quando comparado com as NPs sem FA. Ensaios de captação celular e citometria de fluxo demostraram uma maior internalização das NPs de PMMA com superfície modificada, sugerindo que estas são internalizadas via receptor folato mediado pelo mecanismo de endocitose. Além disso, o encapsulamento do G12 em NPs de PMMA diminui possíveis efeitos citotóxicos do G12, em células não tumorais e células do sangue.

Palavra chave: ácido fólico, poli(metacrilato de metila), nanopartículas poliméricas, polimerização em miniemulsão, superparamagnetismo.

ABSTRACT

Polymeric nanoparticles (NPs) with superparamagnetic properties and surface modified with folic acid (FA) can targeted drug delivery to tumors, which increase their cellular uptake (endocytosis) and therapeutic efficacy. Furthermore, NPs with superparamagnetic properties can induce cell death by hyperthermia (increasing cell temperature), and the combination of hyperthermia (HPT) with other methods like chemotherapy and radiotherapy turns these treatments much more effective. Having regard to the advantages and disadvantages of different therapeutic strategies, the idea of combining various treatments can be attractive for the next generation of cancer treatment. Thus the aim of this work was to synthesize by miniemulsion polymerization poly(methyl methacrylate) (PMMA) NPs with superparamagnetic properties for biomedical applications. In order to verify the effectiveness of NPs as drugs carrier systems, two antitumor compounds were used: zinc phthalocyanine (ZnPc), a second generation photosensitizer used in the treatment of cancer via photodynamic therapy (PDT) and lauryl gallate (G12), a derivative of gallic acid. With the aim to improve the drug delivery, the FA was used as a surface modifier of NPs. Finally, cytotoxicity and cellular uptake assay were performed in cells that express folate receptors (HeLa) to evaluate the entered mechanism of the prepared systems. The NPs obtained by minimeulsion polymerization presented a nanometric size, negative zeta potential and biocompatibility in tumor and non-tumor cells. From these excellent results of biocompatibility, ZnPc was encapsulated in PMMA NPs (PMMAZnPc). Cytotoxicity assays on leukemic cells (Jurkat and K562) showed a higher cytotoxic effect of PMMAZnPc than free ZnPc, suggesting that the death leukemic cells were by apoptosis. In another study, NPs with superparamagnetic properties (MNPs-PMMA) were obtained by miniemulsion polymerization. MNPs-PMMA NPs presented biocompatibility in tumor and non-tumor cells inducing the death of U87MG cells (~50%) by HPT. Simultaneous treatment by PDT and HPT in U87MG cells, with the simultaneous encapsulation of ZnPc and NPMs in PMMA NPs (PMMA-MNPsZnPc), showed a synergic effect when the treatments were combined. The *in vitro* results showed that the application of PDT and HPT together can be more effective than each of the two treatments applied separately. Finally, aiming to

improve the drug delivery efficacy, the surface of NPs were modified with folic acid (FA). The adsorption of the FA on PMMA NPs with superparamagnetic properties (FA-MNPsPMMA) increased internalization of NPs on cells that express folate receptors of type β (K562). In another study, the G12 was encapsulated in superparamagnetic PMMA NPs (MNPsG12PMMA-FA). The simultaneous encapsulation presented a higher cytotoxic effect of FA-MNPsG12PMMA than NPs without FA, when incubated in HeLa cells. Cellular uptake assays and flow cytometry demonstrated a higher cellular uptake of FA-MNPsG12PMMA than NPs without FA, suggesting that these are internalized by folate receptor-mediated endocytosis mechanism. Furthermore, the encapsulation of G12 in PMMA NPs decreases possible cytotoxic effects of G12, in non-tumor cells and blood cells.

Keywords: folic acid, poly(methyl methacrylate), polymeric nanoparticles, miniemulsion polymerization, superparamagnetic

FIGURES

CHAPTER 1

CHAPTER 2

CHAPTER 3

CHAPTER 4

CHAPTER 6

TABLES

CHAPTER 3

CHAPTER 4

CHAPTER 7

ABREVIATIONS

AIBN – azobisisobutyronitrile
AG – galic acid
AO-EB – Acridine orange – ethidium bromide
GC – Gas chromatography
DLS – dynamic light scattering
EE – encapsulation efficiency
FA –folic acid
FBS – 10% heat-inactivated fetal bovine serum
FR – folate receptor
FTIR – Fourier transform infrared spectroscopy
G12 – lauryl or dodecyl gallate
G8 – octyl gallate
Hc – coercive field
HeLa – uterine colon cancer
HPBL – human peripheral blood lymphocytes
HPT – Hyperthermia
J774 – murine macrophage
JURKAT – acute lymphoblastic leukemia cells
K562 – chronic myeloid leukemia in blast crisis cells
L929 – murine fibroblast cells
MMA – methyl methacrylate
MNPs – magnetic nanoparticles
FA-MNPsG12PMMA – folic acid-surface modified superparamagnetic poly(methyl methacrylate) nanoparticles loaded G12 by miniemulsion polymerization
MNPsOA – magnetic nanoparticles coated oleic acid
MNPs-PMMA – superparamagnetic poly(methyl methacrylate)
MNPsPMMA-FA – folic acid-surface modified superparamagnetic poly(methyl methacrylate) nanoparticles
MNPsZnPc-PMMA – superparamagnetic poly(methyl methacrylate) nanoparticles loaded zinc (II) phthalocyanine
Mr – remanent magnetization
MRI – magnetic resonance imaging
Ms – saturation magnetization
MTT – (3-[4,5-dimethylthiazol-2-yl]-2,5-diphenyltetrazolium bromide)
NIH-3T3 – normal human fibroblast cells
NMP – N-methylpyrrolidone

NPs – nanoparticles
OA – oleic acid
PBS - phosphate buffered saline
PDT – photodynamic therapy
PMMA - poly(methyl methacrylate)
PMMAZnPc – Zinc (II) phthalocyanine loaded poly(methyl methacrylate)
PSD – particle size distribution
ROS – oxygen reactive specie
RPMI – roswell park memorial institute medium
SDS – sodium dodecyl sulfate
TEM – transmission electron microscopy
TGA – thermogravimetric analyse
U87MG – human glioblastoma cells
UV-vis – ultraviolet-visivel spectrophotometer
VSM – vibrating sample magnetometer
XRD – X-ray diffraction
ZnPc – zinc (II) phthalocyanine

SUMMARY

CHAPTER 1

1. INTRODUCTION

Magnetic nanoparticles (MNPs) have been extensively studied for a variety of biological applications, such as, targeted drug delivery, in which can be guided by external magnetic field (ZHAO et al, 2011; ZHENG et al, 2005) and in cancer treatment by hyperthermia (FEUSER et al,. 2015a; KUMAR et al, 2011; SIMIONI et al, 2007). Cancer treatment by hyperthermia involves raising the temperature of tumor-loaded tissues to 40–43 °C (BASE et al, 2012; DANHIER et al, 2010; GUPTA and GUPTA 2005). Solid tumors have been shown to have increased susceptibility to small temperature rises compared to healthy tissue due to their increased rate of cell cycling, increased hypoxia, reducing fluid exchange, increased acidity (pH 2-4) (BASEL et al, 2012; ZEE, 2002). The combination of hyperthermia with radiotherapy, chemotherapy and photodynamic therapy (PDT) turns these much more effective. However, for application in biomedical field, MNPs must have combined properties of high magnetic saturation, biocompatibility and superparamagnetic properties, in order to improve the efficacy of thermal therapy as a cancer treatment (HAUSER et al, 2016; KUMAR et al,. 2011; ZHENG et al, 2005). The use of free MNPs for these applications are challenging due to the high surface to volume ratio and strong dipole–dipole interaction between the particles, which makes MNPs agglomeration possible (KUMAR et al, 2014; TANG et al, 2013). The agglomeration of MNPs can be attenuated with the encapsulation of MNPs in polymeric nanoparticles (NPs). The encapsulation of MNPs in polymeric NPs improves their chemical and physical stability, solubility, biological stability, target delivery and reduces the side effects of the encapsulated material (FAN et al, 2009; ZHANG et al, 2011; AKBARZADEH et al, 2012). The preparation of polymeric nanoparticles (NPs) with superparamagnetic properties can increase the site-specific drug concentration and reduce toxic effects on non-tumor cells or tissues, in which, it can be attracted by external magnetic field (targeted drug delivery) and also induce cell death by hyperthermia, as illustrated in Figure 1.1. (FEUSER et al, 2015a, 2015b GUPTA and GUPTA, 2005; XU and SU, 2013).

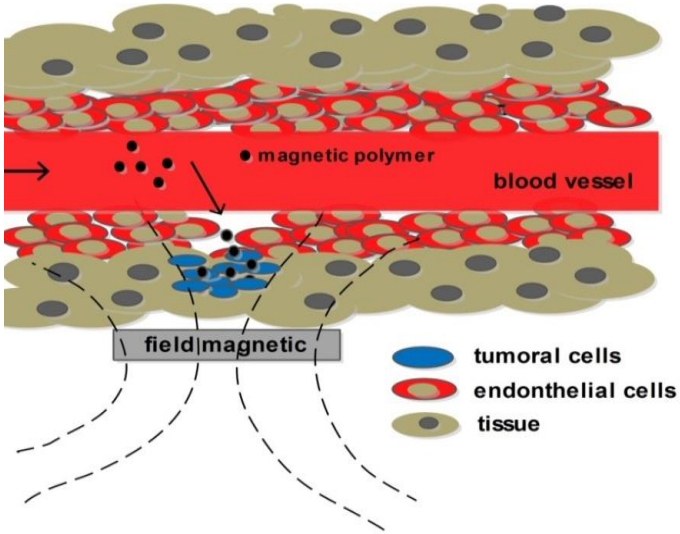

Figure 1.1 Illustration of targeted drug delivery and treatment by hyperthermia when polymeric NPs are systemically administered (adapted from Mody et al, 2013)

NPs are drugs carrier systems able of improve pharmacokinetic profile and decreased drugs toxic effects. Additionally, drugs carriers system can control the drugs release maintaining drug levels within the therapeutic window, decrease risk of toxicity and acting as controlled release system. Today, many studies have been developed in search of new carrier systems to the chronic diseases treatment, such as cancer, tuberculosis and Leishmania. The use of polymeric NPs to cancer treatment is a strategy excellent mainly due to physiological difference of non tumor and tumor cells, as can be seen in Figure 1.2.

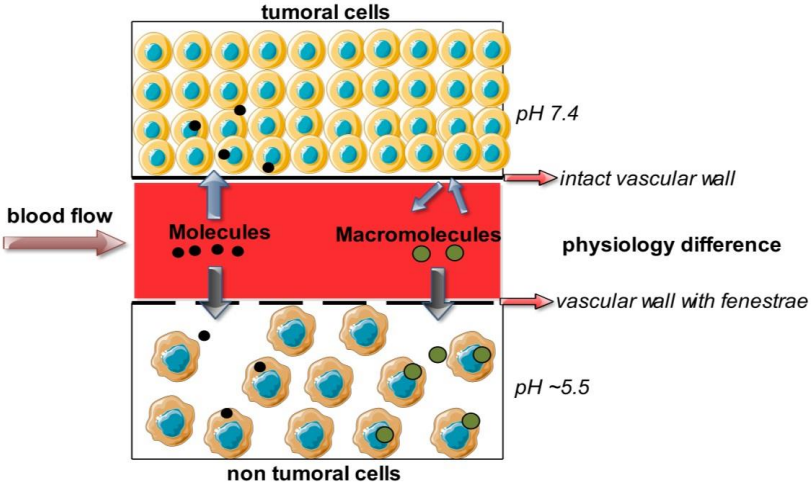

Figure 1.2 Anatomic and physiological difference of non-tumor and tumor cells (adapted from Chin et al, 1999)

The procedure to encapsulate drugs in polymeric NPs presents many advantages when compared with the use of free drugs, such as: protective effect against drug degradation controlled or sustained release, possibility of drug delivery within the target tissue, and reduction of side effects (DE JONG and BORN, 2008; FELICE et al, 2014; FEUSER et al, 2014; REN et al, 2013). NPs can be prepared by *in situ* polymerization (miniemulsion polymerization) and pre-formed polymer method (nanoprecipitation and miniemulsification solvent evaporation) and they can be classified, as nanocapsules (oil core) and nanospheres (polymeric matrix). The main advantage of the *in situ* polymerization when compared with the pre-formed polymer technique is the ability to produce complex nanostructures, including inorganic nanoparticle encapsulation in a single reaction step with fast polymerization rates and high drug encapsulation efficient (MAHDAVIAN et al, 2008; QUIU et al, 2007; ROMIO et al, 2009). In this work polymeric NPs were obtained from methyl methacrylate (MMA) monomer. Poly(methyl methacrylate) (PMMA), a polymer biocompatible and non-biodegradable, has been used in many

application in biomedical field, such as, adjuvant in vaccines and as carrier for many drugs including antioxidants, anti-inflammatories, antihistamines, antihypertensives, antidiabetics and antibiotics (BETTENCOURT and ALMEIDA, 2012; FEUSER et al, 2014; SCHADE and ROUKIS, 2010; SIVAKUMAR and RAO, 2000). Recent publications have shown an increasing interest in its applications as a drug carrier (GYERGYEKA et al, 2010; FU and KAO, 2010).

Another strategy used to improve the pharmacokinetic profile and drugs cellular uptake is the functionalization or surface modification of NPs with ligands, such as folic acid, that has been shown to result in uptake of NPs by endocytosis. Folic acid (FA) (Figure 1.3) is a water-soluble vitamin and it has been used in *targeted* therapy *drugs* in oncology (SAHOO et al, 2013; JIA-JYUN et al, 2009). The folate receptor (FR) is significantly overexpressed on the surface of different human tumor cells and limited expression on non-tumor cells (YANG et al, 2014; SAHOO et al, 2013; SALTAN et al, 2011; JIA-JYUN et al, 2009). FR-mediated drug delivery is facilitated by endocytosis, which may enable drug delivery (SUDIMACK and LEE, 2000; PENGCHENG et al,. 2009; CHEN et al,. 2013). The NPs can be internalized across a plasmatic membrane (passive diffusion) and through endocytosis (NPs are engulfed by endocytic vesicles) (WANG et al, 2012). Several *in vitro* studies have demonstrated that the modified surface of nanoparticles with FA increases the cellular uptake in tumor cells that overexpressed FR (ZHANG et al,. 2009; DUAN et al, 2012; SAHOO et al, 2013; YANG et al,. 2014). However, the functionalization or adsorption of the ligands cannot ensure targeted drug delivery when it is intravenously administered (*in vivo*). When the functionalized NPs enter the bloodstream they need to cross the blood vessel endothelial cells, which do not express FR, in order to reach the interstitial space of tumor sites (CHIN and FERREIRA, 1999; ANDHARIYA et al,. 2013). To overcome this, a drug delivery system with superparamagnetic properties was proposed that could be guided by external magnetic field and uptake *in vivo* by FR mediated by endocytosis (Zheng et al,. 2005; Xu et al,. 2014). Furthermore, MNPs can also induce cell death by hyperthermia (HPT), when external alternating magnetic fields are applied (XU et al,. 2014, MODY et al,. 2014; FEUSER et al,. 2015a and 2015b).

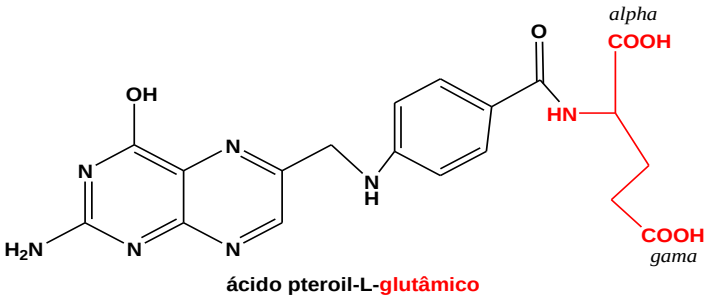

Figure 1.3 Chemical structure of folic acid

In this work two antitumor drugs models were used: Zinc (II) phthalocyanine (ZnPc) and dodecyl gallate (G12). ZnPc is a promising second-generation photosensitizer for PDT that belongs to the phthalocyanine class due to its high optical absorption coefficient (in the range of 600-800 nm). PDT has also been used in the treatment of solid tumors in the esophagus, lungs, larynx, and uterine cervix (DALMONS et al, 2003; DIES et al, 2013; WEN et al, 2012; ZHEN et al, 2013). Furthermore, there are several studies that show the use of PDT in the treatment of leukemia *in vitro* (FEUSER et al, 2015; FURRE et al, 2005) and a few studies that report the efficacy of *in vivo* PDT on leukemic cells (HUANG et al, 2009; WEN et al, 2012). NPs are promising delivery systems for use in PDT and HPT. PDT consists of therapeutic approaches involving the activation of photosensitized drugs by a visible light source, always associated with the generation of cytotoxic reactive oxygen species (ROS) and other free radicals, by type I or type II photochemistry pathway (FOOTE, 1991), to promote the selective destruction of target tissues (MARANHO et al, 2009; NAWALANY et al, 2012; RICCI-JÚNIOR and MARCHETTI, 2006; TRIESSCHEIJN et al, 2006). The combination of HTP and PDT has produced promising results indicating synergistic interaction and significant tumor regression (BOLFARINI et al, 2012; PRIMO and TEDESCO, 2013; XU and SU, 2013).The heat released by HPT induces changes in cell cycle, causing faster denaturation of malignant cells through aggregation of nuclear proteins, thereby enhancing the sensitivity of cells denatured previously with PDT (KUMAR and MOHAMAD, 2011).

Gallic acid (GA) is an important polyphenol compound presenting various biological activities. (ALVES et al, 2016; OW and STUPANS, 2003; WANG et al, 2007). The biological activity of GA and its derivatives has been described in the literature as antimalarial (KLEIN and WEBER, 2001), antioxidant (GRUNDHOFER and NIEMETZ, 2007; OW and STUPANS, 2003), antitumor (ZHAO and HU, 2013) and antibacterial (MANNA and KUO, 1999). G12 is an ester derivative of GA, with twelve carbon atoms in the side-chain, more efficient than GA in antiviral, antifungal, antioxidant and antitumoral activities (CORDOVA et al, 2011; LOCATELLI, 2013). These high biological activities have been correlated to the amphipathic character by increasing cell membranes affinity and permeability (SAEKI et al, 2000; LOCATELLI et al, 2013). Although some of these ester derivatives showed a high cytotoxic activity, the chemical derivatization decrease their water solubility, constituting a disadvantage for intravenous administration (STELLA et al, 2007). Other disadvantage involving in vivo administration of GA is poor pharmacokinetic profile (low bioavailability) (ALVES et al, 2016). Therefore the encapsulation of drugs in polymeric NPs with superparamagnetic properties and modified surface can increase site-specific drug concentration (increased bioavailability), reduce toxic effects on non-tumor cells or tissues, protecting and preventing possible aggregation of encapsulated drugs with suitable release profile. In addition, it can improve the intravenous administration, when it is dispersed in aqueous medium, providing an excellent strategy for cancer treatment and other disease (ORTEAG et al, 2011).

1.1 Objectives

1.1.1 General objective

The main goal of this work was the synthesis, characterization and *in vitro* cytotoxicity assay of MNPs and antitumor drugs simultaneous encapsulated in folic acid-poly(methyl methacrylate) nanoparticles obtained by miniemulsion polymerization.

1.1.2 Specific objectives:

- *in vitro* cytotoxicity studies of PMMA NPs obtained via miniemulsion polymerization;

- *in vitro* cytotoxicity studies by PDT of ZnPc loaded in PMMA NPs obtained via miniemulsion polymerization;
- *in vitro* cytotoxicity studies by HPT of PMMA NPs with superparamagnetic properties obtained via miniemulsion polymerization;
- *in vitro* cytotoxicity studies by PDT and/or HPT (simultaneous treatment) of ZnPc loaded in superparamagnetic PMMA NPs obtained via miniemulsion polymerization;
- synthesis and characterization superparamagnetic PMMA NPs with FA-surface modified obtained via miniemulsion polymerization and *in vitro* studies on cell that overexpress FR type β
- synthesis and characterization of G12 loaded in superparamagnetic PMMA NPs with FA-surface modified. *In vitro* cytotoxicity and cellular uptake assay on cell that overexpress FR type α.

The next chapters of this Thesis will be present as articles. Chapter 2 presents the article entitled: "*In vitro* cytotoxicity of poly(methyl methacrylate) nanoparticles and nanocapsules obtained by miniemulsion polymerization for drug delivery application", published in Journal of Nanoscience and Nanotechnology (**doi: 10.1166/jnn.2015.11610**). The Chapter 3 presents the article entitled: "Synthesis of Znpc loaded poly(methyl methacrylate) nanoparticles via miniemulsion polymerization for photodynamic therapy in leukemic cells", published in Materials and Engineering C (**doi: 10.1016/j.msec.2015.11.063)**. The Chapter 4 presents the article entitled: "Encapsulation of magnetic nanoparticles in poly(methyl methacrylate) by miniemulsion and evaluation of hyperthemia in U87MG cells", published in European Journal Polymer (**doi: 10.1016/j.eurpolymj.2015.04.029)**. The Chapter 5 presents the article entitled: "Simultaneous encapsulation of magnetic nanoparticles and zinc phthalocyanine in poly(methyl methacrylate) nanoparticles by miniemulsion polymerization and *in vitro* studies", published in Colloids an Surfaces B: Biointerfaces (**doi: 10.1016/j.colsurfb.2015.07.067)**. The articles presented in Chapter 6 entitled: "Superparamagnetic poly(methyl methacrylate) nanoparticles surface modified with folic acid presenting cell uptake mediated by

endocytosis" was published in the Journal of Nanoparticles Research. The article presented in Chapter 7 entitled "Synthesis of folic acid-superparamagnetic poly(methyl methacrylate) nanoparticles loaded with lauryl gallate by miniemulsion polymerization and *in vitro* studies" was submitted. Lastly, in Chapter 8 a general conclusion of the work performed in this Thesis is presented.

It is also important to mention that the method of simultaneous encapsulation of MNPs and drugs by miniemulsion polymerization was patented (BR 1020140133887) by Feuser et al. (2015).

CHAPTER 2

IN VITRO CYTOTOXICITY OF POLY(METHYL METHACRYLATE) NANOPARTICLES AND NANOCAPSULES OBTAINED BY MINIEMULSION POLYMERIZATION FOR DRUG DELIVERY APPLICATION

Abstract: With the objective to develop a new drug delivery systems without secondary effects, this study evaluated *in vitro* cytotoxicity in fibroblast cells, macrophage uptake and hemocompatibility of poly(methyl methacrylate) (PMMA) nanoparticles and nanocapsules obtained by miniemulsion polymerization. PMMA nanoparticles and nanocapsules presented spherical morphology, mean size 102 ± 4.2 nm and 211 ± 3.8 nm and negative zeta potential - 27 ± 3.2mV, - 41 ± 4.3 mV. *In vitro* cytotoxicity in fibroblast cells lines L929 and NIH-3T3 caused no significant reduction of cells viability, which, is critical regarding the biocompatibility of those carriers. Assay macrophages uptake showed that PMMA nanoparticles presented a significant increase (67%) in the phagocytic uptake, when compared with PMMA nanocapsules (44%), indicated that higher negative zeta potential and small mean size influenced in the macrophages uptake. Both polymeric systems, presented excellent blood biocompatibility. Finally, our results indicate, that these polymeric systems obtained by miniemulsion polymerization, have the potential to be used as drug delivery system in the treatment of diseases, in which, macrophages act as host cells.

Keywords: biomaterials, poly(methyl methacrylate); miniemulsion polymerization, i*n vitro* cytotoxicity.

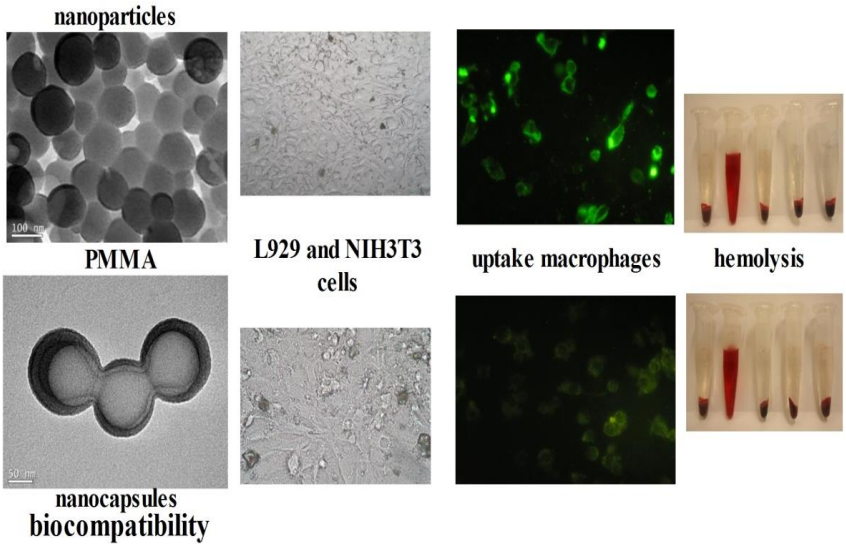

The manuscript was published in the Journal of Nanoscience and Nanotechnology

doi: 10.1166/jnn.2015.11610

2. INTRODUCTION

Polymeric nanoparticles and nanocapsules obtained by miniemulsion polymerization have been studied extensively as carriers for the drug delivery systems, whose main advantages are the protection of the drug, controlled release, the possibility of site-specific-site drug delivery in the target tissue and reduction of side effects (LANDFESTER et al, 2009; LANDFESTER and MAILANDER, 2013; MORA-HUERTAS et al, 2010). Nanoparticles are matrix-type systems composed of an entanglement of oligomer or polymer units, while nanocapsules are reservoir type systems, inside of which active components may be confined in a cavity which consists of a liquid nucleus (an oil which may dissolve lipophilic agents) and surrounded by polymer shell in the order of nanometers. Miniemulsion is defined as dispersions of relatively stable oil droplets with a size range 50–500 nm, prepared by shearing a system containing oil, water, surfactant and

costabilizer (AL-GHAMDI et al, 2006; ANTONIETTI and LANDFESTER, 2002; ROMIO et al, 2013; TEIXEIRA et al, 2005;

The development of biocompatible polymers, as poly(methyl methacrylate) (PMMA) obtained by miniemulsion polymerization has drawn much attention in the last decades due to their excellent physicochemical properties, and the potential value has been discussed for a variety of pharmaceutical, medical, and cosmetic applications, such as, medium for drug release and carries system (BETTENCOURT et al, 2010; FEUSER et al, 2013; LEKSHMI et al, 2010). An important factor in the preparation of polymeric systems for biomedical application is synthesis conditions and their physical-chemical characteristics, that will determine the type of application and the therapeutic level to be achieved (CHELLAT et al, 2005)

However, the most important in the preparation of polymeric systems for biomedical application, is their biocompatibility, preventing toxic effects on the physiological system (DESHAYES and KASKO, 2013). To verify the *in vitro* biocompatibility of these polymeric systems, fibroblast cells lines are useful models for research since they provide large amounts of consistent cells for prolonged use and because most cellular characteristics are maintained reliable experimental data can be compared among research reports, in which, the same cell lines are used. Mouse fibroblast (L929) is a popular cell line in many experiment aspects such as material biocompatibility testing (BRETAGNOL et al, 2008; Zange et al, 1997) drug cytotoxicity testing (Faria et al, 2009; NORDIN et al, 1991) and cell biology studies (CARTWRIGHT et al, 1996; Taniguchi et al, 2006). Macrophage uptake assays, is another important study, to evaluate the accumulation of polymeric systems into macrophages.

The interaction between polymeric system and macrophages, cells that specialize in the internalization of foreign particles is of interest. Macrophages enact rapid clearance of particles from the circulation, decrease circulating half-life of a drug. One the other hand, nanoparticles targeted to macrophages can be attractive, especially for treatment of diseases, in which, macrophages act as host cells, as for example, in the treatment of leishmaniasis and inflammatory diseases (CHELLAT et al, 2005; JAIN et al, 2015; LUNOV et al, 2011; SHARMA et al, 2010)

In order to develop new drug delivery systems without secondary effects, the final purpose of this study was to evaluate the *in vitro* cytotoxicity in murine fibroblast (L929) and normal human fibroblast (NIH-3T3), hemocompatibility and *in vitro* macrophage uptake (J774) of PMMA nanoparticles and nanocapsules, obtained by miniemulsion polymerization with the final goal of evaluate the biological activities of these nanostructured systems

2.1 MATERIALS AND METHODS

2.1.1 MATERIALS

For PMMA nanoparticles and nanocapsules preparation the following reagents were used: monomer methyl methacrylate (MMA) from Arinos chemistry, azobisisobutylonitrile (AIBN), sodium phosphate monobasic (NaH_2PO_4) and sodium phosphate dibasic (Na_2HPO_4) were purchased from Vetec chemistry, lecithin of Alpha Aesar, as co-stabilizer Crodamol (Croda) and distilled water was used throughout the experiments.

2.2.2 METHODS

2.2.1.1 Synthesis of PMMA nanoparticles

The preparation of PMMA nanoparticles via miniemulsion polymerization was the same described by FEUSER and collaborates (2013). In a beaker containing 20mL distilled water (aqueous phase) added the organic phase containing: 79 wt% MMA, 3.6 wt% Lecithin, 4 wt% Miglyol and 14 wt% AIBN (in relation organic phase). The organic phase was added dropwise under higher shear with amplitude of 70% (Fisher Scientific, Sonic Dismembrator, 500 W). The higher shear was kept for 5 min (10 s on, and 1 s off) in a beaker immersed in an ice bath to avoid the temperature increase during sonication. The miniemulsion was transferred to glass tubes (10 mL) at 70 °C where the polymerization took place for 3 hours under light protection. Afterwards, the material was cooled, centrifuged and washed several times with phosphate buffered saline (PBS) at pH 7.4. Subsequently nanoparticles were transferred to glass vials, frozen in liquid nitrogen and lyophilized (Lyophilizer, FreeZone 4.5-L Benchtop Freeze Dry

System; Labconco, Kansas City, MO). The lyophilized powder was stored at room temperature (25 °C) before analysis.

2.2.1.2 Synthesis of PMMA nanocapsules

In a beaker containing 20mL distilled water (aqueous phase) added the organic phase containing: 44.4 wt% MMA, 2wt% Lecithin, 44 wt% Miglyol and 8 wt% AIBN (in relation organic phase). The organic phase was added dropwise under higher shear with amplitude of 70% (Fisher Scientific, Sonic Dismembrator, 500W). The higher shear was kept for 5 min (10 s on and 1 s off) in a beaker immersed in an ice bath to avoid the temperature increase during sonication. The miniemulsion was transferred to glass tubes (10 mL) at 70 °C where the polymerization took place for 4 hours. Afterwards, the material was cooled, centrifuged and washed several times with phosphate buffered saline (PBS) at pH 7.4 and lyophiolized.

2.2.1.3 Preparation of PMMA nanoparticles and nanocapsules labeled with 6-coumarin

6-coumarin, a highly fluorescent molecule, was dissolved in Miglyol to form a uniform solution (0.5mg.mL^{-1}). This solution (6-coumarin/Miglyol) was used in the preparation of the miniemulsion. In a beaker containing 20mL distilled water (aqueous phase) added the organic phase containing: 79 wt% MMA, 3.6 wt% Lecithin, 4 wt% Miglyol and 14 wt% AIBN or 44.4 wt% MMA, 2 wt% Lecithin, 44wt% 6-coumarin/Miglyol and 8 wt% AIBN (in relation organic phase) to preparation of nanoparticles and nanocapsules, respectively. The organic phase was added dropwise under higher shear with amplitude of 70% (Fisher Scientific, Sonic Dismembrator, 500W). The higher shear was kept for 5 min (10 s on and 1 s off) in a beaker immersed in an ice bath to avoid the temperature increase during sonication. The miniemulsion was transferred to glass tubes (10 mL) at 70 °C where the polymerization took place for 4 hours under light protection. Afterwards, the material was cooled, centrifuged and washed several times with phosphate buffered saline (PBS) at pH 7.4 and lyophiolized.

2.3 Characterization of PMMA nanoparticles and nanocapsules

Average diameters (intensity averages) PMMA nanoparticles and nanocapsules were measured by dynamic light scattering (DLS-Malvern Instruments, Zeta Sizer Nano S). Surface charge of the nanoparticles was investigated through zeta potential measurements (Zetasizer, Malvern Instruments, U.K.). All samples were analyzed five times, from which were calculated the average and standard deviation. The analysis was performed at 28 ^{o}C. PMMA nanoparticles and nanocapsules morphology were observed using Transmission Electronic Microscopy (TEM), model JEM 2100 F 100 kV.

2.4 In vitro studies

2.4.1 Cell culture

Mouse fibroblasts cells L929 (kindly provided by Dr. Jamil Assreuy, Federal University of Santa Catarina, Florianopolis, SC, Brazil) and NIH-3T3 (kindly provided by Dr. Antônio Cláudio Tedesco, University of Sao Paulo, São Paulo, SP, Brazil) were cultivated in Dulbecco's Modified Eagle Medium (DMEM) (GIBCO, São Paulo, SP, Brazil) and supplemented with 10% fetal bovine serum (FBS) (GIBCO, São Paulo, SP, Brazil), 100 U/mL penicillin-streptomycin (GIBCO, São Paulo, SP, Brazil) and 10 mM HEPES (GIBCO, São Paulo, SP, Brazil) incubated at 37 ^{o}C in a humidified atmosphere with 5% CO_2, in plastic culture flasks.

2.4.2 In vitro cytotoxicity assay

In order to determine PMMA nanoparticles and nanocapsules cytotoxicity, *in vitro* cytotoxicity MTT (3-[4,5-dimethylthiazol-2-yl]-2,5-diphenyltetrazolium bromide) assay (purchased from Amresco LLC, Solon) was performed using L929 mouse fibroblasts (ATCC, Manassas, VA). Cells were arranged in flat bottom 96-well tissue culture plates (starting concentration: $5.0x10^4$ cells/mL, 200 mL/well). PMMA nanoparticles and nanocapsules were dispersed in phosphate buffered saline (PBS) (Laborclin, Pinhais, PR, Brazil) at final concentration of micrograms per millimeter. For treatment were made different dilution in culture media starting with concentration of 2 mg/mL. After

incubation, cells were exposed to different dilutions test samples for 24 h at 37 ^{o}C in a humidified atmosphere with 5% of CO_2.

Cells viability was measured by MTT assay. MTT solution was added to cell cultures in a final concentration of 0.5 mg/mL and cells were incubated for 3 h. Thereafter, 100 mL of lysis solution (20% sodium dodecyl sulphate in 50% n,n-dimethylformamide, 0.4% acetic acid, and 0.04 N HCl) was added and the conversion of MTT to formazan by metabolically viable cells was measured by a Organon Teknika microplate reader (Organon Teknika, Brussels, Belgium) at 540 nm. Each dilution was tested in three replicates. 50% of inhibition concentration (IC_{50}) was determined by GraphPad Prism version 5.01 (GraphPad Software Inc, La Jolla, CA, USA).

2.4.3 Cell analysis by fluorescence microscopy

The intracellular fate of carrier systems marked with 6-coumarin (nanoparticles and nanocapsules labeled) were evaluated with fluorescence microscopy. L929 and NIH-3T3 cells (starting concentration: $1.0x10^6$ cells/mL, 200 mL/well) were incubated with carrier systems, at concentration of 250 µg/mL. After 24 h of incubation, cells were washed with PBS and the coverslips covering the bottom of the plate were removed and placed on a glass slide. Cells were analyzed under a fluorescence microscope (Olympus BX41). The cell morphology was evaluated by optical microscopy and the fluorescence of 6-coumarin was monitored by fluorescence microscopy. Cells images were acquired using emission mode with 20 x objectives after exciting the sample from 450 to 490 nm using barrier filter. Fluorescence imaging in wavelength of 505 nm was collected. In order to quantify the 6-coumarin fluorescence, image analysis was performed using ImageJ software.

2.4.4 Macrophage Uptake Studies

Phagocytic uptake and intracellular fate of fluorescent free 6-coumarin, PMMA nanoparticles and nanocapsules labeled with 6-coumarin at concentration 300 $\mu g.mL^{-1}$ were monitored by fluorescence microscopy upon incubation with murine macrophage-like J774 cells. Cell uptake was determined in cells grown near to confluence on coverslips in 24-well plates. After 60 minutes of incubation with free 6-

coumarin, PMMA nanoparticles and nanocapsules labeled with 6-coumarin at 37 ºC, the treatment solutions were removed, and cells were washed with phosphate buffered saline (PBS). For uptake analysis by fluorescence microscopy, the coverslips were mounted on a fluorescence microscope (Olympus BX-FLA) and the fluorescence of 6-coumarin was monitored. Cells images were acquired using emission mode with 40x objectives after exciting the sample from 450 to 490 nm using barrier filter. Fluorescence imaging in wavelength of 505 nm was collected. In order to quantify the macrophage uptake, image analysis was performed using ImageJ software.

2.4.5 Hemolysis assay

Citrate-stabilized human blood was freshly collected according to an approved University of Utah Institutional Review Board protocol used within 3 hours of being drawn. 4 mL of whole blood was added to 8 mL of a sterile solution of sodium chloride in water (saline) and the RBCs were isolated from serum by centrifugation at 10,000 × *g* for 5 minutes, this method was previous described in the literature (WANG et al, 2009; YU et al, 2011). The RBCs were further washed five times with saline solution. Following the last wash, the RBCs were diluted to 2 mL of saline. 120 µL of the diluted RBC suspension was added to 880 µL of water or saline. Samples were treated with PMMA nanoparticles and nanocapsules at 10 µl (70 $\mu g.mL^{-1}$), 25µl (150 $\mu g.mL^{-1}$ and 50 µl (300 $\mu g.mL^{-1}$) volume. All samples were prepared in triplicate and the suspension was briefly vortexed before leaving under gentle stirring at 37 °C for 60 minutes. After that, the mixture was briefly vortexed again and centrifuged at 10.000 × *g* for 5 minutes. 100 µL of supernatant was transferred to a 96-well plate. The absorbance value of hemoglobin at 570 nm was measured with the reference wavelength at 540 nm. 120 µL of the diluted RBC suspension incubated with 880 µL of water and saline were used as the positive and negative control, respectively. Hemolysis percent was calculated as:

Hemolysis (%) = [(Sample absorbance – negative control)/(positive control – negative control)] × 100

2.5 Statistical Analysis

The results are presented as means ± SEM. The statistical significance between groups was determined by analysis of variance (ANOVA) followed by Bonferroni's multiple comparison test. *P*-values less than 0.05 were considered indicative of significance. IC_{50} values were determined by graphical interpolation from individual experiments.

2.6 RESULTS AND DISCUSSIONS

The evaluation of the morphology and particle size is of fundamental importance, when it is desired obtain polymeric systems for biomedical application, which, may have important biological implications on cellular uptake and biological processes (HE et al, 2010; ZHANG et al, 2008; DANHIER et al, 2010). Figure 2.1 shows mean size determinate by DLS and TEM analysis. The results obtained by DLS showed that PMMA nanoparticles and nanocapsules exhibited low polydispersity index (PdI) and mean diameter of approximately 102 ±4.2 nm and 211 ±3.8 nm respectively, for PMMA nanoparticles and nanocapsules. TEM analysis corroborate with results obtained by DLS. PMMA nanoparticles and nanocapsules presented spherical morphology and regular size distribution of nanoparticles and nanocapsules.

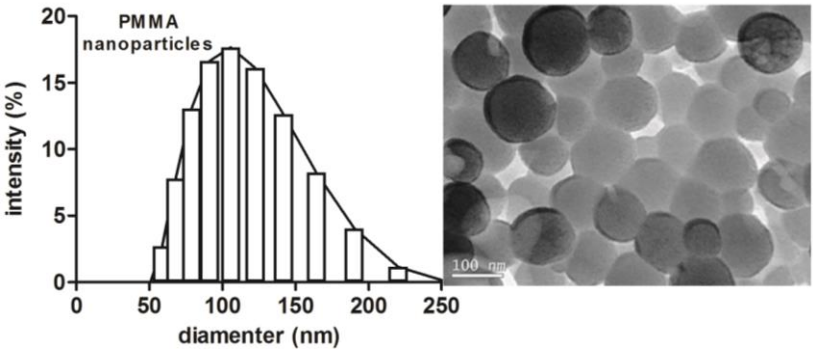

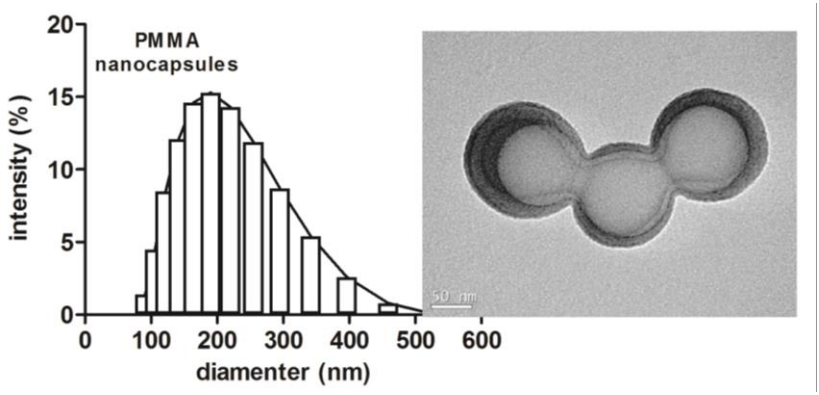

Figure 2.1 Dynamic light scattering (left) and transmission electron microscopy images (right) of PMMA nanoparticles and PMMA nanocapsules.

Other important factor in the polymeric systems preparation is the surface charge, which gives information about the colloidal stability, blood time circulation and possible interactions between nanoparticles and biological medium (HE et al, 2010; ZHANG et al, 2008; DANHIER et al, 2010). PMMA nanoparticles and nanocapsules presented negative surface charge, -40 ± 4.3 mV and -27 ± 3.2mV, respectively. The negative charge is associated with the presence of surfactants (lecithin) adsorbed in the PMMA nanoparticles and nanocapsules surface. Lecithins have compounds, such as, free acids or negatively charged phospholipids, which confer a negative charge (ROMIO et al, 2013). The difference of zeta potential, between PMMA nanoparticles and nanocapsules, can be related with the lecithin, located on the core oil of polymer, wherein, the polymeric wall formed around the oil droplets very thick and consequently decreasing the surface charge (LOSA et al, 1993; CALVO et al, 1996).

Cytotoxic effect of PMMA nanoparticles and nanocapsules were analyzed in L929 and NIH-3T3 mouse fibroblast cells by MTT assay for 24 hours (Figure 2.2). When the L929 and NIH-3T3 cells were exposed with PMMA nanoparticles and nanocapsules both cells presented a slightly reduced of cell viability, approximately 81% and 84% in the L929 cells and 84% and 81% in the NIH-3T3 cells respectively at concentration 750 $\mu g.ml^{-1}$ (Figure2.2).

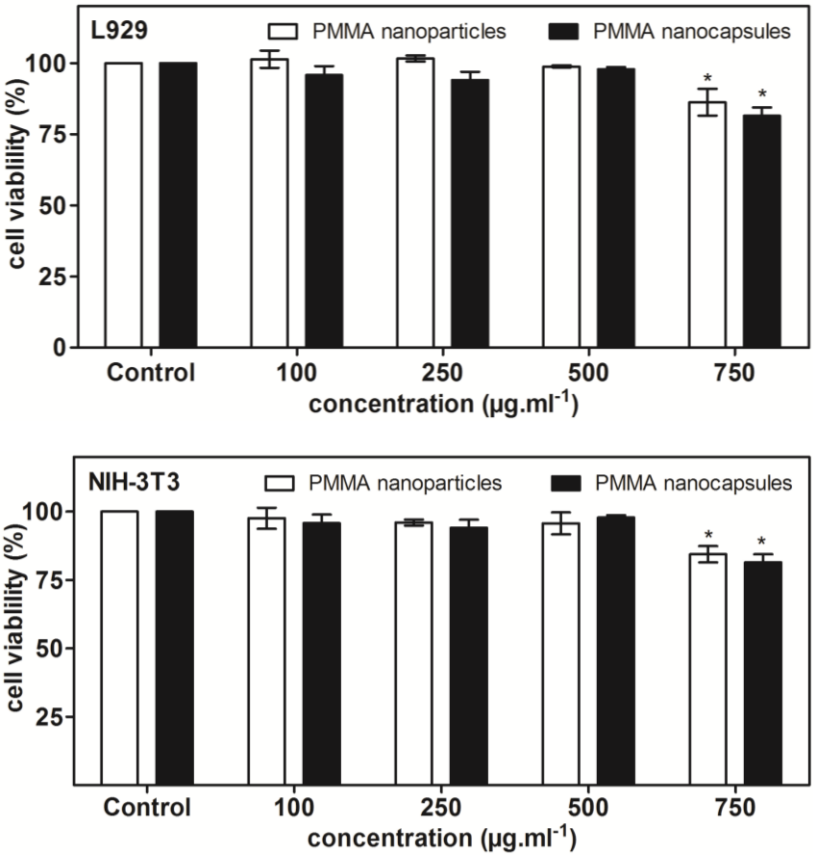

Figure 2.2 *In vitro* cytotoxicity of PMMA nanoparticles and nanocapsules in L929 and NIH3T3 cells exposed 24 h. (*p>0.05 Bonferroni's multiple comparison test)

The effect of polymeric systems on fibroblasts morphology was evaluated by optical microscopy, and fluorescence microscopy using 6-coumarin as fluorescent dye. It can be seen in Figure 2.3 that there were no significant changes in cell morphology even after the incorporation of 6-coumarin. The use of L929 cells are recommended by ISO 10993-5 to *in vitro* cytotoxicity assay of news materials for biomedical application. According to ISO 10993-5, cell viability <70% compared to

untreated cells are considered cytotoxic. Therefore it can be said that the nanoparticles and nanocapsules obtained in this work via miniemulsion polymerization exhibit biocompatibility.

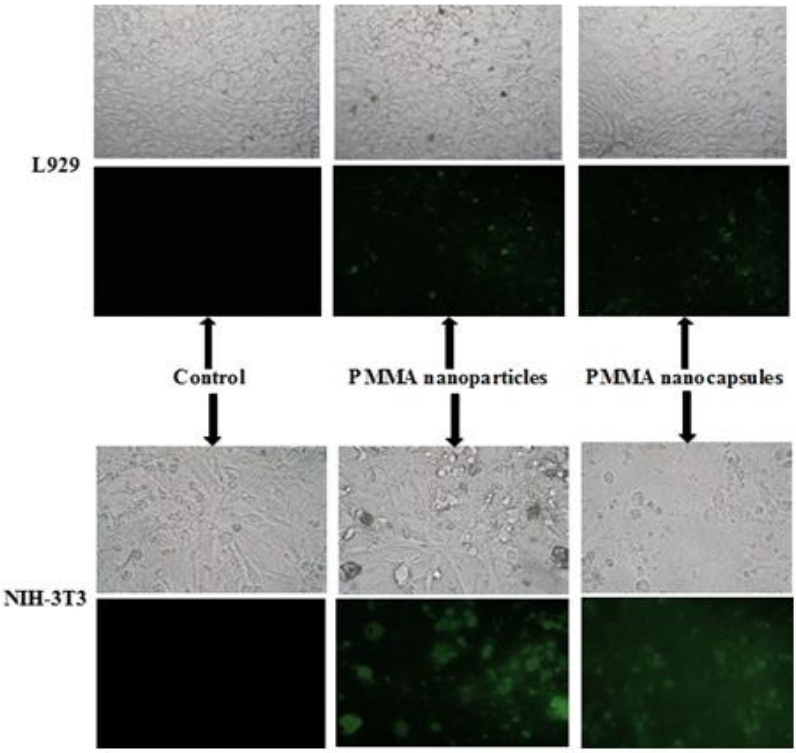

Figure 2.3 Optical and fluorescence microscopy images of L929 and NIH-3T3 cells after 24 hours of incubation with PMMA nanoparticles and nanocapsules labeled with 6-coumarin. (*p <0.001) using one-way ANOVA followed by post-test Bonferroni's.

Uptake of 6-coumarin-loaded nanoparticles by macrophages was monitored by morphologic observation of the cells after 60 min of incubation (Figure 2.5). Green fluorescence indicates the intracellular accumulation of 6-coumarin. PMMA nanoparticles and nanocapsules labeled with 6-coumarin seemed scarcely captured by cells, as can be observed by the weak fluorescence in the cytoplasm of the

macrophages. On the other hand, free 6-coumarin was actively phagocytized and accumulated into the cells, as evidenced by their bright fluorescence. The quantification of intracellular fluorescence (Figure 2.4) to the PMMA nanoparticles (67%) showed a higher phagocytic uptake when compared with PMMA nanocapsules (44%). This increase in the phagocytic uptake of PMMA nanoparticles, can be related, with the mean size, morphology, surface charge and surface chemistry of polymeric systems (HE et al, 2010; KIM et al, 2011; SHANG et al, 2014). In this study, PMMA nanoparticles were phagocytized more efficiently by J774 cells. This difference in the macrophages uptake is attributed with surface charge and surface chemistry of polymeric systems, as previously discussed. Our results indicated PMMA nanoparticles and nanocapsules can be used as a platform for drug transport, especially for treatment of diseases, in which, macrophages act as host cells (CHELLAT et al, 2005). Macrophages play a central role in inflammation and act as reservoirs for bacterium and parasites, which are involved with infectious diseases, as tuberculosis and leishmanisis (JAIN et al, 2015; LUNOV et al, 2011; SHARMA et al, 2010).

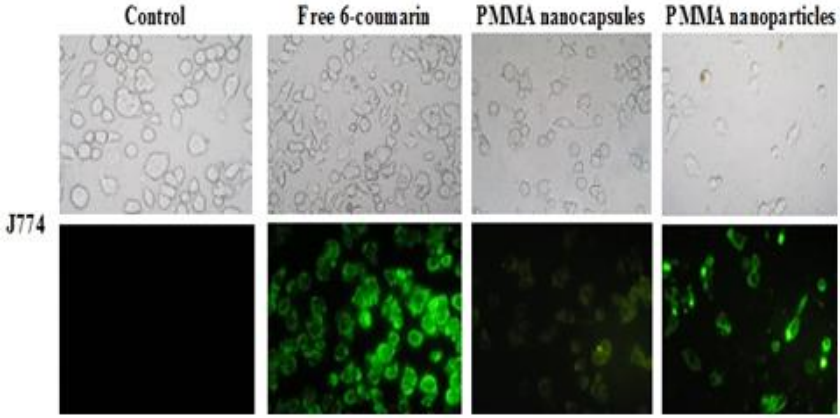

Figure 2.4 Macrophages Uptake Assay. Optical and fluorescence microscopy images of J774 cells after 60 minutes incubation in the dark with free 6-coumarin, PMMA nanoparticles and nanocapsules labeled with 6-coumarin. (*p <0.001) using one-way ANOVA followed by post-test Bonferroni's.

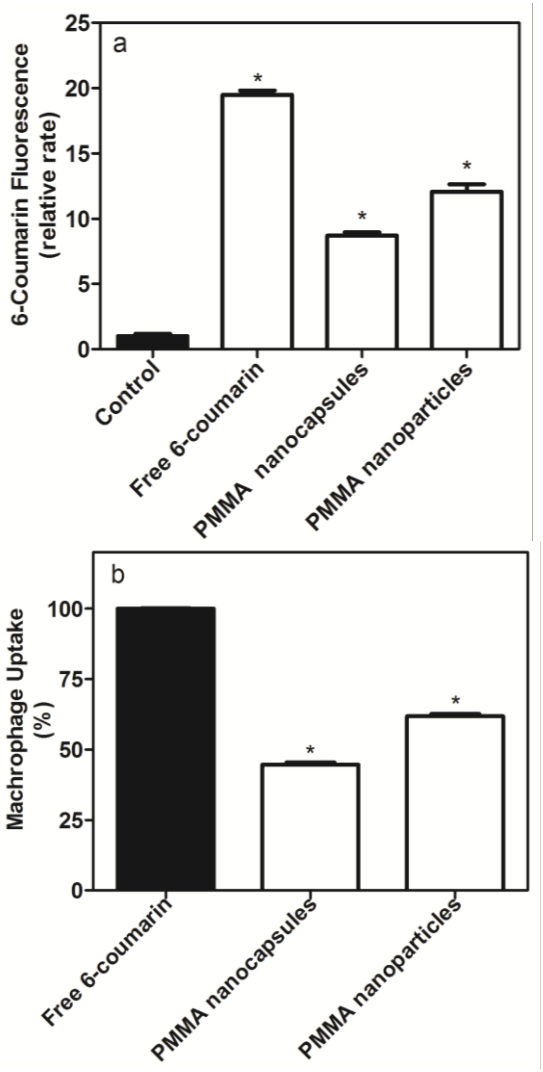

Figure 2.5 Effects of nanoparticles systems on 6-coumarin macrophages uptake. Optical and fluorescence microscopy images of J774 cells upon 60 minutes incubation in the dark with free 6-coumarin, PMMA nanoparticles and nanocapsules labeled with 6-coumarin (* $p < 0.001$) using one-way ANOVA followed by posttest Bonferroni's.

The impact of nanoparticle and nanocapsules on human red blood cells (RBCs) was evaluated by hemolysis assay. The quantitation of hemoglobin in the supernatant of nanoparticle-RBC mixture was done recording the absorbance of hemoglobin at 540 nm. Treatment with 10 µl, 25 µl and 50 µl of PMMA nanoparticles and nanocapsules was not able to cause hemolysis of RBCs suggesting that these systems do not have hemolytic capacity, even when administered at high concentrations (Figure 2.6). In others words are similar to the original plasma, which indicates that the materials have no obvious activation to coagulation factors and thrombin generation (ZHOU et al, 2011). The hemolysis assay is considered to be a supplementary assay for assessment of cytotoxicity and plays an important role in evaluation of biosafety. The results showed that PMMA nanoparticles and nanocapsules obtained by miniemulsion polymerization have high blood biocompatibility, which can be an alternative for drugs carrier systems administered systemically. The results showed that the hemolytic ratio of the nanoparticles and nanocapsules are within the range of less than 5%, the critical safe hemolytic ratio for biomaterials according to ISO/TR 7406, which indicated that the damage of the sample on the erythrocytes was little.

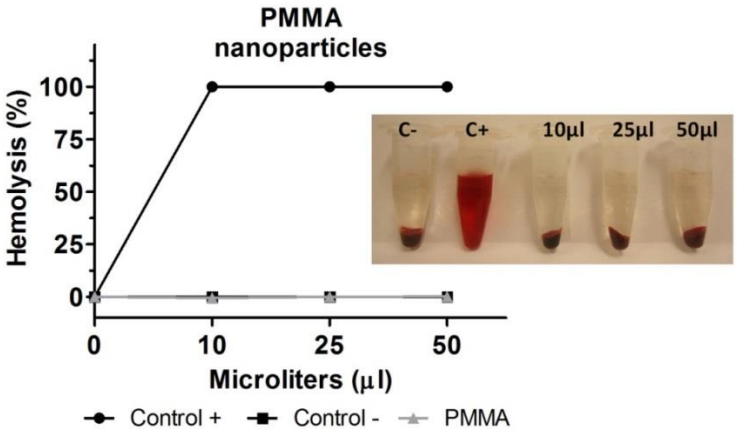

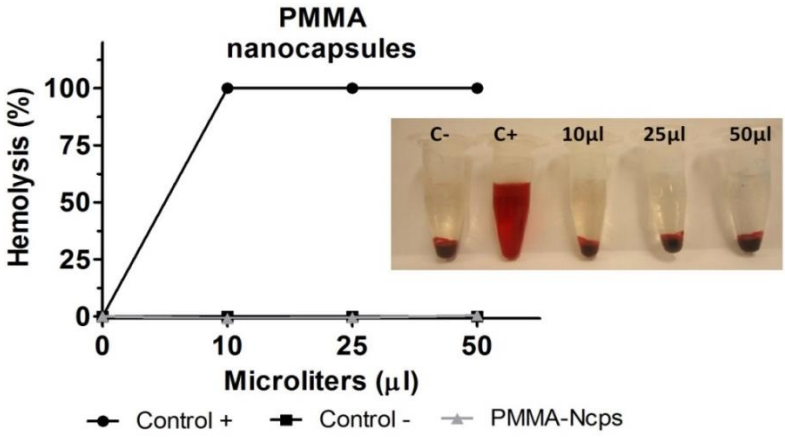

Figure 2.6 Hemolysis assay. Relative rate of hemolysis in human RBCs upon incubation with PMMA nanoparticles and nanocapsules respectively at 10 µl, 25 µl and 50 µl volume. Data were mean ± SD (n=3). (*p <0.001) using one-way ANOVA followed by posttest Bonferroni's.

2.7 CONCLUSIONS

The synthesis of PMMA nanoparticles and nanocapsules obtained by miniemulsion polymerization resulted in a stable polymeric system in aqueous dispersion, with low polydispersity index and good biocompatibility using high concentrations of nanoparticles. Hemolysis assay showed that polymeric systems can be systemically administered without causing any damage to the blood system. Altogether, this study showed that PMMA nanoparticles can be used as drug delivery, in the diseases treatments, in which, macrophages act as host cells. PMMA nanocapsules proved to be less efficient in macrophages uptake, may increasing blood circulating half-life. Finally, conclude that polymeric systems obtained by miniemulsion polymerization, can be used as drug delivery system in macrophages. Future studies, such as, encapsulation of drugs for leishmaniasis treatment and internalization assay in leishmaniasis parasites will be underway.

CHAPTER 3

SYNTHESIS OF ZNPC LOADED POLY(METHYL METHACRYLATE) NANOPARTICLES VIA MINIEMULSION POLYMERIZATION FOR PHOTODYNAMIC THERAPY IN LEUKEMIC CELLS

Abstract: The goal of this work was to synthesize and characterize ZnPc loaded poly(methyl methacrylate) (PMMA) nanoparticles (NPs) by miniemulsion polymerization. Biocompatibility assays were performed in murine fibroblast (L929) cells and human peripheral blood lymphocytes (HPBL). Finally, photobiological assays were performed in two leukemic cells: chronic myeloid leukemia in blast crisis (K562) and acute lymphoblastic leukemia (Jurkat). ZnPc loaded PMMA NPs presented an average diameter of 97 ± 2.5 nm with a low polydispersity index and negative surface charge. The encapsulation efficiency (EE %) of ZnPc PMMA NPs was 87 % ± 2.12. The release of ZnPc from PMMA NPs was slow and sustained without the presence of burst effect, indicating homogeneous drug distribution in the polymeric matrix. NP biocompatibility was observed on the treatment of peripheral blood lymphocytes and L929 fibroblast cells. Phototoxicity assays showed that the ZnPc loaded in PMMA NPs was more phototoxic than free ZnPc after activation with visible light at 675 nm, using a low light dose of 2 J/cm^2 in both leukemic cells (Jurkat and K562). The results from fluorescence microscopy (EB/OA) and DNA fragmentation suggest that the ZnPc loaded PMMA NPs induced cell death by apoptosis. Based on presented results, our study suggests that PDT combined with use of polymeric NPs, may be an excellent alternative for leukemia treatment.

Keywords: leukemia, miniemulsion, polymeric nanoparticles, photodynamic therapy.

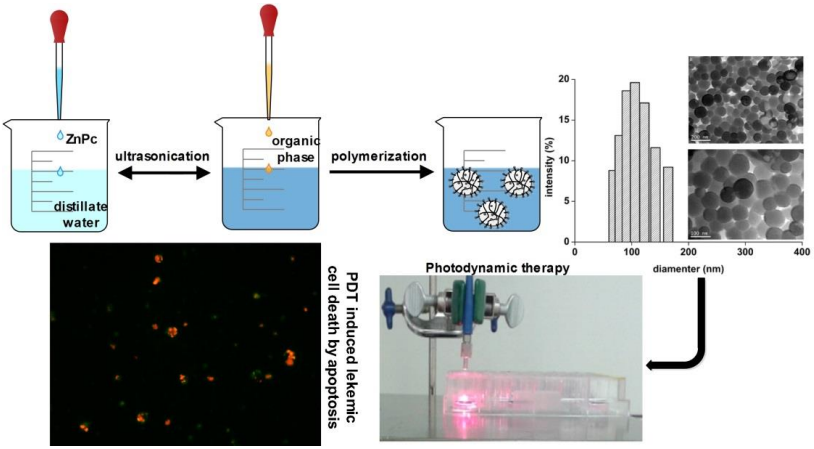

The manuscript was published in the Journal of Materials and Engineering Science C
doi: 10.1016/j.msec.2015.11.063

3. Introduction

The development of polymeric nanoparticles (NPs) as drug carriers has been drawing significant interest in recent years, due to their promising applications in cancer therapy. The procedure to encapsulate drugs in NPs presents many advantages when compared with the use of free drugs, such as: protective effect against drug degradation controlled or sustained release, possibility of drug delivery within the target tissue, and reduction of side effects (DE JONG and BORN, 2008; FELICE et al, 2014; FEUSER et al, 2014; REN et al, 2013). Poly(methyl methacrylate) (PMMA), a biocompatible and non-biodegradable polymer, has been used as an adjuvant in vaccines and is a carrier for many drugs (BETTENCOURT and ALMEIDA, 2012; FEUSER et al, 2014), including antioxidants, anti-inflammatories, antihistamines, antihypertensives, antidiabetics and antibiotics (BETTENCOURT and ALMEIDA, 2012; SCHADE and ROUKIS, 2010; SIVAKUMAR and RAO, 2000). Polymeric NPs can be prepared by miniemulsion polymerization or preformed polymers (GUTERRES et al, 2007; SCHAFFAZICK et al, 2003; HUANG et al, 2007; MORA-HUERTAS,

2010). Miniemulsion polymerization allows the synthesis of polymeric NPs with unique characteristics, great commercial interest, and possibility of incorporation of drugs with low solubility in the continuous phase. In general, miniemulsions consist of small droplets (50-500nm) dispersed in an aqueous phase. In order to stabilize such a direct miniemulsion, droplet coalescence is suppressed by the surfactant that stabilizes the particles electrostatically or sterically. Since the miniemulsion features a distribution in droplet size, the bigger droplets can grow due to a mass flux from the smaller ones as Laplace pressure increases with decreasing droplet size, this phenomenon is known as molecular diffusion degradation or Ostwald ripening. The ultrahydrophobe prevents diffusion degradation by introducing a counterforce to the Laplace pressure, since the smaller particles would contain a higher concentration of the ultrahydrphobe, which increases the osmotic pressure (ASUA, 2014; HIGUCHI and MISRA, 1962). The main advantage of the miniemulsion polymerization process is the ability to produce complex nanostructures, including inorganic nanoparticle encapsulation in a single reaction step with fast polymerization rates (MAHDAVIAN et al, 2008; QIU et al, 2007).

PDT is a current therapy that involves the administration of a non-toxic dye and the activation of photosensitizers with visible light (SIQUEIRA-MOURA et al, 2007). The activated photosensitizers are able to react with tissue oxygen producing reactive oxygen species (ROS) and other free radicals. ROS and free radicals are cytotoxic and formed by photochemical reactions type 1 or 2, respectively (FOOTE, 1991). Tumor cells are selectively eliminated after visible light application in the lesion site (DALMONS et al, 2003); MARANHO et al, 2009; OLEINEICK et al, 2002; RICCI-JÚNIOR and MARCHETTI, 2007; SAVOLAINEN et al, 2008; TRIESSCHEIJN et al, 2007; ZHEN et al, 2013). Efficient photosensitizers should have high absorbance at a wavelength suitable for the desired application (RAI et al, 2010), generally, near the maximum absorbance wavelength of the PS, avoiding interference from natural endogenous molecules. PDT has been widely used for treating superficial tumors such as skin, head, and neck tumors (PRIMO and TEDESCO, 2013; RAI et al, 2010; ROCHA et al, 2012). PDT has also been used in the treatment of solid tumors in the esophagus, lungs, larynx, and uterine cervix (DALMONS et al, 2003; DIES et al, 2013; ie et al, 2012; ZHEN et al, 2013). Furthermore,

there are several studies that show the use of PDT in the treatment of leukemia *in vitro* (FEUSER et al, 2015; FURRE et al, 2005). However, there are a few studies that report the efficacy of *in vivo* PDT on leukemic cells (HUANG et al, 2009; WEN et al, 2012). In an *in vivo* study, Wen and collaborators (2014), evaluated the efficacy of PDT on (A20) murine B-lymphoma leukemia cells, where microphotofibers (200 μm diameter) were inserted into tail veins and irradiated with a laser. The results showed an excellent efficacy of PDT on leukemic cells, resulting in cell death by apoptosis. This study showed that PDT could be an excellent alternative for leukemia treatment. According to Barth and collaborators (2011) leukemia only presents a challenge to photosensitizer or nanoparticle uptake when compared with solid tumors. Moreover, manifestation of leukemia throughout the body creates added challenges to the successful light delivery necessary for PDT. Currently, the development of optical fibers and laser devices with high light diffusion, associated with endoscopic minimum invasive treatment, allows us to use T-cell lymphoma and B-cell lymphoma, not only as model to understand the interaction and cellular behavior of the photosensitizers with this kind of cell, but also to imagine the use of PDT in the future treatment of these diseases, which is supported by previous reported studies (BICALHO et al, 2013; LONGO et al, 2013; TANAKA et al, 2001).

Zinc (II) phthalocyanine (ZnPc) is a second-generation photosensitizer for PDT. It belongs to a class of lipophilic phthalocyanines and has high optical absorbance coefficient within the 600-800 nm range. These photosensitizers are insoluble in water and prone to self-aggregation in aqueous solutions, which drastically reduces the photosensitizing efficiency restricting its direct use in biological fluids (RICCI-JÚNIOR and MARCHETTI, 2007). Many drug delivery systems containing photosensitizers have been described in the literature, and the results demonstrate a higher therapeutic efficacy by PDT than free photosensitizers, in which these drug delivery systems tend to prevent aggregation and photosensitizers toxicity (RICCI-JÚNIOR and MARCHETTI, 2007; ROCHA et al, 2012; SIQUEIRA-MOURA et al, 2007). Finally, the goal of this study was to synthesize and characterize ZnPc loaded poly(methyl methacrylate) (PMMA) obtained by miniemulsion polymerization (PMMAZnPc). Biocompatibility assays were performed in murine fibroblast (L929)

cells and human peripheral blood lymphocytes (HPBL). Finally, phototoxicity activity was evaluated in two leukemic cells: chronic myeloid leukemia in blast crisis (K562) and acute lymphoblastic leukemia (Jurkat).

3.1 MATERIALS AND METHODS

3.2 Materials

For the synthesis of ZnPc loaded PMMA NPs the following reagents were employed: the monomer methyl methacrylate (MMA), purchased from Arinos; azobisisobutylonitrile (AIBN), sodium dodecyl sulfate (SDS), NaH_2PO_4 (sodium phosphate monobasic) and Na_2HPO_4 (sodium phosphate dibasic), purchased from Vetec; lecithin (Alpha Aesar); miglyol 812 (Sazol) and zinc (II) phthalocyanine (ZnPc) and N-methylpyrrolidone (NMP), both purchased from Sigma Aldrich. Distilled water was used throughout the experiments.

3.3 Methods

3.3.1 Synthesis of ZnPc loaded in PMMA NPs via miniemulsion polymerization (PMMAZnPc)

ZnPc loaded in PMMA NPs was obtained by miniemulsion polymerization. Briefly, 1 mL of NMP containing 6 mg of ZnPc was added dropwise in a beaker containing 20 mL of distilled water (aqueous phase) under sonication with a 70% amplitude (Fisher Scientific, Sonic Dismembrator, 500 W). Next, the organic phase (containing 2 g of MMA, 0.1 g of lecithin, 0.1 g of miglyol and 0.04 g of AIBN) was added dropwise under high shear to the previous aqueous ZnPc dispersion. The sonication was continued for five minutes (10 s on and 1 s off) in a beaker immersed in an ice bath to avoid temperature increases during sonication. The miniemulsion was transferred to glass tubes (10 mL) at 70°C, where the polymerization took place for three hours under the protection from light. Afterwards, the material was cooled, centrifuged and washed several times with PBS at pH 7.4. Subsequently, NPs were transferred to glass vials, frozen in liquid nitrogen and lyophilized (FreeZone 4.5-L Benchtop Freeze Dry System;

Labconco, Kansas City, MO). The lyophilized powder was stored at room temperature (25°C) before analysis.

3.3.2 Characterization

Monomer consumption was followed by gravimetric analysis as described by Bernardy nd collaborates (2010). Latex samples taken at different time intervals were put into aluminum capsules that contained 0.3 g of 1 wt % hydroquinone aqueous solution. The NPs were dried at 60 °C until weight was constant. Conversion was determined as the ratio between experimental and theoretical polymer content, disregarding the fraction of non-volatile components, such as emulsifiers, co-stabilizers, photosensitizers and hydroquinone that was added to stop the polymerization reaction. The final residual monomer content was determined by GC (GC2010AF Shimadzu). Intensity mean diameters of the monomer droplets and polymeric NPs were measured by dynamic light scattering (DLS-Malvern Instruments, Zeta Sizer Nano S, UK). The surface charge of the NPs was investigated through zeta potential measurements (Zetasizer, Malvern Instruments, U.K.). All samples were analyzed five times at room temperature (28^{o}C) and the results were presented as mean and standard deviation. The NPs morphology was analyzed using transmission electron microscopy (TEM) (model JEM 2100F, 100 Kv). For this analysis, several drops of the diluted samples were placed on a 200-mesh Formvar/carbon copper grid (Electron Microscopy Science). After drying, samples were sputter-coated with a thin carbon film to avoid PMMA degradation under the electron beam and observed at 100 kV.

UV-vis analysis was performed in order to evaluate the photochemical properties of ZnPc loaded PMMA NPs. A known amount of ZnPc loaded PMMA NPs were extracted with NMP ($3\mu g.mL^{-1}$) and the wavelength was analyzed in the visible range (500 – 800 nm). The ZnPc release and the encapsulation efficiency (EE%) were determined by UV-vis spectrophotometry. NPs (10 mg) were dissolved in NMP, which is an excellent solvent for both drug and polymer. The ZnPc concentration was measured at 675 nm (region visible spectrum) using a calibration curve with different concentrations of ZnPc dispersed in NMP. The coefficient of determination (r^2) exceeded 0.999, with excellent linearity (20-200 ng). The EE% was calculated from Eq 1:

$$EE\ (\%) = {}^{M_1}/_{M_t} \times 100 \quad (1)$$

where EE (%) is the ZnPc encapsulation efficiency, M_1 is the mass of ZnPc loaded NPs, and M_t is the ZnPc mass used in formulation. The experiments were conducted in triplicate (n = 3).

The crystalline phase of the ZnPc and NPs were identified by measurements of X-ray diffraction (XRD) using Cu-Kα (1.54056 Å) at 45 kV/40 mA in an XRD model Xpert-Pro. NP chemical characterization was performed by Fourier transform infrared spectroscopy (FTIR) using KBr pellets.

3.4 *In vitro* studies

3.4.1 *In vitro* release of ZnPc from PMMA NPs

The *in vitro* release followed studies described by Ricci-Junior and Marchetti (2006). NPs (5 mg) were weighed and added to 30 mL of the receptor medium, composed of PBS (pH 7.4) and 2 wt.% SDS. The NPs suspension was continuously stirred (100 rpm) and the temperature was maintained at 37 ^{o}C in a thermostatically controlled water bath. At given time intervals, six samples (n = 6) of 3 ml were withdrawn and centrifuged at 10,000 × g for 30 min (Beckman J-25 centrifuge, USA). The precipitates were re-suspended in 3 ml of fresh medium and placed in the respective dissolution vessels. The drug released in the receptor medium was quantified by spectrophotometry using the visible region of the spectrum (670 nm). The release profile was obtained by associating the percentage of drug released with time. The release data were fitted utilizing the zero order, first order and Higuchi mathematical models described by Costa and Lobo (2001).

3.4.2 Photobiological activity

Two human leukemia cell lines were used in this study: chronic myeloid leukemia in blast crisis (K562) and acute lymphoblastic leukemia (Jurkat). Cells were cultured in Roswell Park Memorial Institute Medium (RPMI) (GIBCO, São Paulo, SP, Brazil) supplemented with 10% heat-inactivated fetal bovine serum (FBS),

100 U/ml penicillin, 100µg.mL^{-1} streptomycin and 10 mM HEPES under 5% CO_2 humidified atmosphere in 75 cm^2 flasks at 37°C. Cell lines were purchased from American Type Culture Collection (ATCC, Rockville, MD, USA). Cell viability counts were obtained using the Trypan blue exclusion assay. In order to assess the cytotoxic effect, K562 and Jurkat cells were cultured at a density of 5 x 10^4 and 1 x 10^5, respectively, in 96-well plates. Cells were incubated (1 h) with PMMA NPs at concentrations of 10, 20, 40 and 100 µg.mL^{-1} of PMMA, and free and loaded ZnPc in PMMA NPs at concentrations of 24.50, 30.62, 49.00 and 61.25 ng of ZnPc. The incubation time was determined according to the experimental protocol described in PDT cell culture literature (LONGO et al, 2013). Following the incubation time, cells were centrifuged, resuspended with 200µL of RPMI, exposed to a visible light (675 nm) dose of 2 J/cm^2 (Photon Lase I, DMC, Brazil), and incubated for 24 h. Cell viability was assessed using the classic MTT assay (Sigma, MO, USA). Cells without treatment were irradiated with a visible light (675 nm) dose of 2 J/cm^2, and used as a negative control, in order to evaluate light cytotoxicity. The viability of the control group was considered as 100%. The half maximal inhibitory concentration (IC_{50}) was determined for ZnPc loaded in PMMA NPs. In order to verify the cytotoxic effect of ZnPc loaded PMMA NPs without light exposure, cells were incubated for 1h and submitted to the same protocol described above.

Murine fibroblast cells (L929) were cultivated in Dulbecco's Modified Eagle Medium (DMEM) (GIBCO, São Paulo, SP, Brazil) and incubated (5% CO_2, 37°C) for 24 h. DMEM was supplemented with 10% fetal bovine serum (FBS) (GIBCO, São Paulo, SP, Brazil), 100 U/mL penicillin-streptomycin (GIBCO, São Paulo, SP, Brazil) and 10 mM HEPES (GIBCO, São Paulo, SP, Brazil). After 24 h, cells L929 were treated with ZnPc loaded PMMA NPs at concentrations near IC_{50} and free PMMA NPs at a final concentration of 50µg.mL^{-1} and incubated (5% CO_2, 37°C) for 1 h. After incubation, the medium containing the NPs was discarded and the cells were washed with PBS. Afterwards, the cells were incubated with fresh medium for an additional 24 h, until the cell viability assay (MTT) was performed.

3.4.3 MTT assay

The cell MTT proliferation method was used to assess cell viability after both the cytotoxic assays. Briefly, aliquots of 100 µl MTT solution (5 mg.mL^{-1}) and 100 µl medium were added to each well. The cells were then incubated for 4 h (37°C and 5% CO_2) to allow the formazan formation reaction. Following incubation, the medium containing the MTT solution was removed and the formazan crystals were dissolved in dimethyl sulfoxide (DMSO). The optical density was measured at 550 nm using a Safire^2 microplate reader (Tecan Group Ltd.). Results are presented as survival percentage, considering the control (untreated cells) as 100%.

3.4.4 Human peripheral blood lymphocytes (HPBL)

This study was approved by the Medical Ethics Committee 238/03. Five non-smoking healthy volunteers, who had never been treated with any cancer drugs, participated in this study between August 2011 and September 2011 at the *Polydoro Ernani de São Thiago* University Hospital (Florianópolis, Brazil). Blood samples were collected and human peripheral blood lymphocytes were isolated using the Ficoll-Hypaque method. After diluting blood with PBS, lymphocytes were isolated by centrifugation over a Ficoll-Hypaque density gradient (density = 1.070 g/ml) for 30 min at 2000 rpm. Cells were washed twice with PBS and subsequently suspended in RPMI with 10% fetal bovine serum. The isolated lymphocyte viability was measured using the Trypan blue exclusion assay and found to be around 95%. The HPBL cells (1 x 10^6 cells/200 µL) were incubated for 1 h with ZnPc loaded PMMA NPs at final concentrations of 35.07 and 46.88 ng.mL^{-1} (concentrations near IC_{50}) at 37^{o}C in a humidified atmosphere with 5% CO_2. After incubation for 1 h, cells were centrifuged, resuspended with 200 µL of RPMI, exposed to a visible light (675 nm) dose of 2 J/cm^2 and incubated again for 24 h. Two controls were used: a non-treated group and a group treated with 25 µg.mL^{-1} of taxol, a compound already used in leukemia treatment clinical protocols. The protocol used for cytotoxic activity evaluation is the same as previously described.

3.4.5 Acridine orange – ethidium bromide (AO-EB) staining and DNA fragmentation

Apoptotic cells were stained with acridine orange - ethidium bromide (AO-EB) and examined with a fluorescence microscope. For morphological observations, K562 and Jurkat, with concentrations of 5×10^5 and 1×10^6 cells/well respectively, were treated with ZnPc loaded NPs at concentration near IC_{50}. After 1 h incubation, cells were centrifuged, resuspended with 200 µL of RPMI, exposed to a visible light (675 nm) dose of 2 J/cm^2 and incubated again for 24 h. The supernatant was removed and the cells were stained with a 1% AO-EB (1:1) solution and observed under a fluorescence microscope (Olympus BX41). Fields were photographed with a digital camera.

DNA fragmentation assay is another technique used to evaluate apoptotic cells. K562 and Jurkat cells were treated with ZnPc loaded PMMA at concentrations of IC_{50} (6×10^6 cells/well, IC_{50}) with an incubation time of 1 h. Subsequently, the cells were washed with PBS and separated by centrifugation. Cells were exposed to a visible light (675 nm) dose of 2 J/cm^2 and incubated for 24 h. After incubation, the cells were separated by centrifugation and lysed cells were suspended in PBS solution. The genomic DNA was obtained using the mini preparation kit with a spin column. The genomic DNA was separated on a 2% agarose gel stained with 1 µg.mL^{-1} ethidium bromide for 40 min at 80 V.

3.5 Statistical analysis

Data are presented as the mean±standard deviation of three determinations. One-way ANOVA followed by the Bonferroni post-hoc test were used to compare the cytotoxicity of the samples at different concentrations. Statistical analyses were performed using the Statistical Package for Social Sciences for Windows (SPSS Inc. version 13.0, USA). The statistical significance level was set at $p < 0.05$ for all analyses.

3.6 RESULTS AND DISCUSSION

Measurements of the conversion reaction (Figure 3.1) indicated that after 170 minutes of reaction the conversion reached almost 100%. The reactions kinetics showed that ZnPc presence did not affect the polymerization rate. The final conversion was slightly below 100%, probably due to the loss of monomer (MMA) by evaporation during the stages of emulsification and polymerization. Monomer evaporation may occur due to high vapor pressure of the MMA (FEUSER et al, 2014). Residual monomer (MMA) was not detected by GC analysis after lyophilization of ZnPc loaded PMMA NPs. The non-presence of MMA is an important factor when the focus for these NPs is their biomedical application. MMA presence can cause serious toxicity problems. The zeta potential is another important characteristic of the NPs and it provides information about the colloidal stability and the possible interactions between the NPs and the biological medium. ZnPc loaded PMMA NPs exhibited a high negative charge surface (-45 ±0.09 mV at pH 7.4 ±0.1), contributing to a higher colloidal stability of NPs (ANTONIETTI and LANDFESTER, 2002; SIQUEIRA-MOURA et al, 2013). The negative charge is associated with the presence of surfactants adsorbed on the nanoparticle surface.

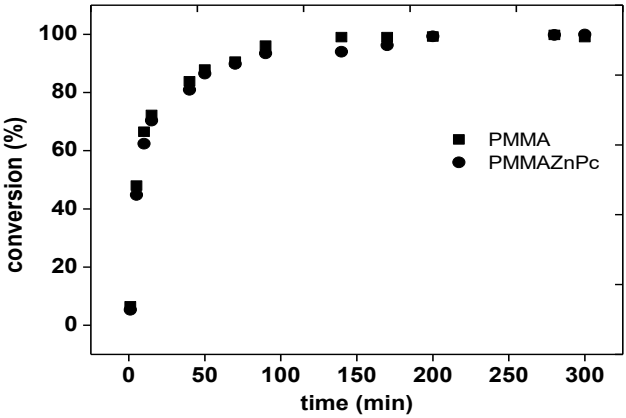

Figure 3.1 Conversion gravimetric of the PMMA, ZnPc loaded PMMA NPs.

Figure 3.2 shows the TEM images and the particle size distribution (PSD) obtained by DLS. ZnPc loaded PMMA NPs presented nanometric size with a narrow size distribution and spherical morphology, as can be seen clearly in Figure 3.2b and c. Table 3.1 shows the mean diameter and polydispersity index (PdI) obtained by DLS. The DLS results corroborate with the TEM analysis. The low polydispersity index (PDI), around 0.1, indicates that both samples have a narrow size distribution. In addition, the osmotic pressure would be sufficient to prevent Ostwald ripening, which increases the stability of the miniemulsion (ANTONIETTI and LANDFESTER, 2002; SHORK, 2005). It is likely that the dominant nucleation mechanism was the polymerization of the monomer (ANTONIETTI and LANDFESTER, 2002; BERNARDY et al, 2010; FEUSER et al, 2014). Both morphology and particle size have important biological implications on cellular uptake and biological processes (DANHIER et al, 2010; HE et al, 2010).

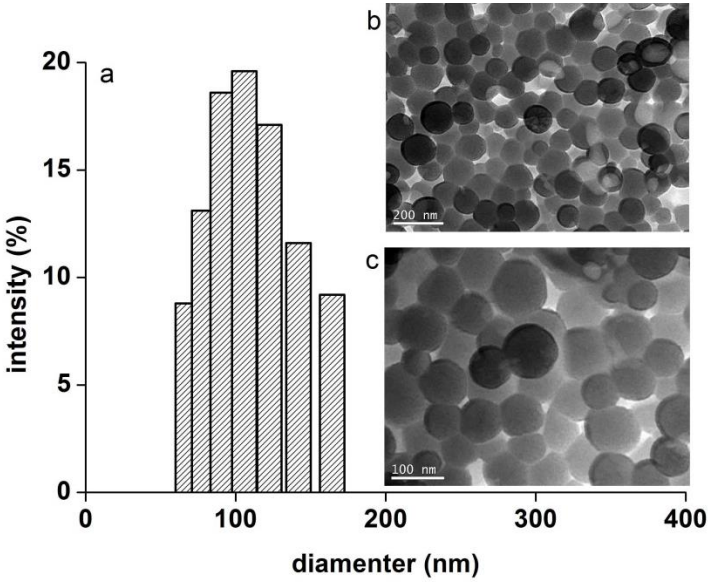

Figure 3.2 Particle size distribution obtained by dynamic light scattering (a) and transmission electron microscopy image (b and c) of ZnPc loaded PMMA NPs.

Table 3.1 Intensity mean diameter: droplets (DP_g) and Nps (DP_{NP}); Polydispersity index: droplets (PdI_g) and NPs (PdI_{NP}) obtained by DLS.

Samples	DP_g (nm)	DP_{Nps} (nm)	PdI_g	PdI_{NP}
PMMA NPs	85 ±2.3	89 ±1.9	0.09 ±0.04	0.09 ±0.05
ZnPc loaded PMMA	92 ±2.2	97 ±2.5	0.10 ±0.05	0.11 ±0.02

For encapsulation of the photosensitizer, ZnPc, into PMMA NPs using miniemulsion polymerization, a solution of ZnPc in NMP was added to the aqueous phase under high shear using a sonic dismembrator. Subsequently, the organic phase was added to the aqueous phase with continuous homogenization during five minutes using a sonic dismembrator. The addition of the organic phase, which contains the monomer and ZnPc, coalesced with the monomer droplets. The dispersion was stabilized by the lecithin present in the organic phase. This technique showed a high EE% (87 ±2.1 %). Tests performed with a high HLB (Hydrophilic-Lipophilic Balance) surfactant dispersed in the aqueous phase, such as SDS (sodium dodecyl sulphate), presented low encapsulation efficiency (> 20%) (data not shown). The presence of the surfactant with high HLB stabilized the photosensitizer dispersion in the aqueous phase, and reduced the coalescence between the photosensitizer and monomer droplets resulting in low encapsulation efficiency. UV-vis analysis showed that the ZnPc loaded PMMA NPs did not suffer changes in its spectroscopic properties after encapsulation (Figure 3.3). The soret and Q bands remained in the same position. Free ZnPc and ZnPc loaded PMMA NPs have similar spectroscopic behavior with wavelength of maximum absorbance at 675 nm for one of the Q bands (FEUSER et al, 2015).

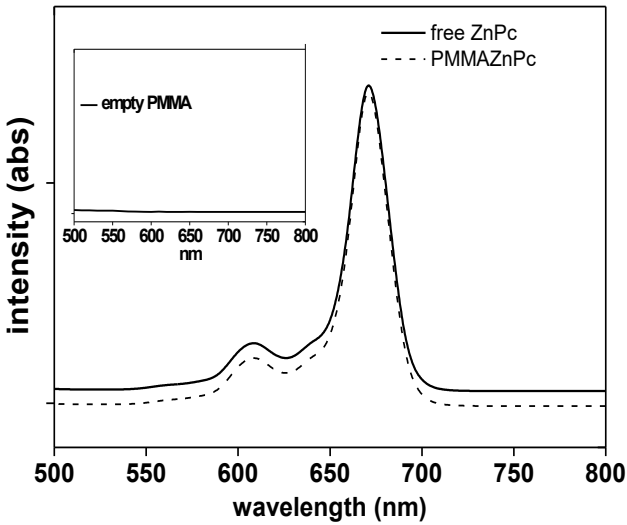

Figure 3.3 Absorption spectra in the UV-vis: free ZnPc, PMMA and ZnPc loaded in PMMA Nps.

X-ray diffraction (XRD) of free ZnPc, PMMA NPs, ZnPc loaded PMMA NPs is exhibits in Figure 3.4a. XRD profile of Free ZnPc exhibited a diffraction profile of crystalline material (β-phase of monoclinic structure) with several intense peaks (Figure 3.4). Free ZnPc has three different polymorphic forms (α, β and γ phases), where the β-form is thermodynamically stable (SHOCK et al, 1988). Our results are similar to the results reported by Iwatsu and collaborates (1980) and Choi and collaborates (2014) for the polymorphic β-form of ZnPc. However, these peaks were not observed in the diffractograms from NPs. Therefore, the diffractograms of the NPs (Figure 3.3a) indicated that the drug (ZnPc) can be molecularly dispersed in the polymeric matrix. Similar results have been reported in literature (HONG et al, 2008; LEKSHMI et al, 2010; WANG et al, 2014). FT-IR spectrum (Figure 3.4b) of ZnPc loaded PMMA NPs (Figure 4b) showed signals in 1736 cm^{-1} corresponding to the PMMA C=O groups. In addition, the bands in the 3000 – 2800 cm^{-1} region are attributed to the stretching of

C–H bonds of the PMMA saturated alkane. The free ZnPc presented peak characteristics (718, 747 and 783 cm^{-1}) of β-ZnPc (HUSSEIN, 2011), corroborating with XRD analysis. The FTIR spectrum of free ZnPc, PMMA, ZnPc loaded PMMA NPs confirmed that there was no significant interaction between drug and polymer. These results corroborate with XRD analysis, indicating that the drug, ZnPc, can be molecularly dispersed in the polymeric matrix (LEKSHMI et al, 2010).

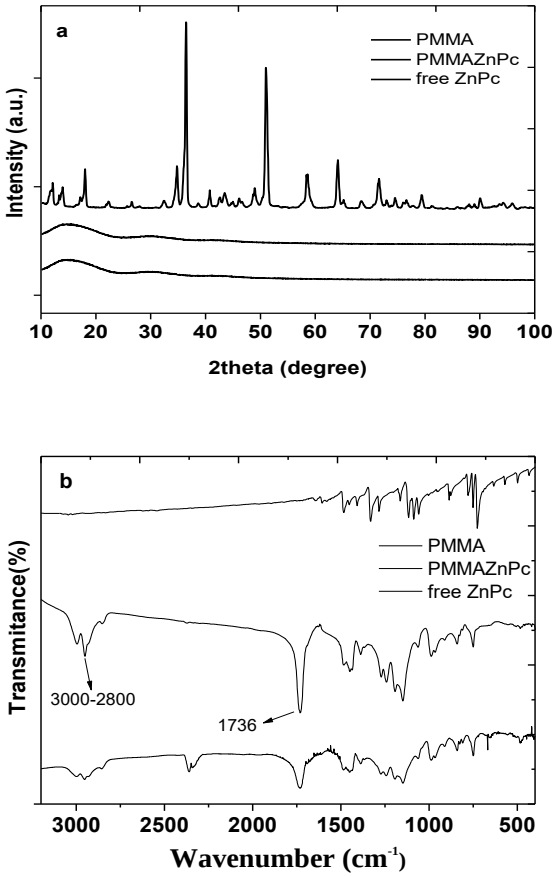

Figure 3.4 X-ray powder diffraction patterns (a) and FTIR analyses (b) of: free ZnPc, PMMA, ZnPc loaded PMMA NPs.

3.7 In vitro studies

3.7.1 In vitro ZnPc release study

Release study was performed in order to evaluate the release profile of ZnPc encapsulated in PMMA NPs. ZnPc loaded PMMA NPs presented a slow and sustained release profile. As can be seen in Fig. 3.5, the amount of ZnPc released from PMMA NPs reached 20% in 120 h. After 120 h of contact with the aqueous medium, the polymer matrix becomes less resistant to diffusion of the drug (LEKSHMI et al, 2010). Consequently, a linear increase can be observed in the drug release after 120 h. Eighty-five percent of the drug was released in the acceptor solution in 300 h. In addition, no burst effect was detected, indicating that ZnPc was entrapped within the PMMA NPs and possibly homogeneously dispersed in the polymeric matrix of the NPs and not at the surface (KUMARI et al, 2010; MADERUELO et al, 2011), corroborating with the results from the XRD and FTIR analyses.

The extended release may be attributed to the slow diffusion of ZnPc through the polymeric matrix of the PMMA NPs that present slow rate of disintegration aqueous medium (FU and KAO, 2010; LEKSHMI et al, 2010; VAN DER ENDE et al, 2010). Furthermore, the low solubility of ZnPc could contribute with the reduction the drug diffusion through the polymeric matrix, and consequently slowing the drug release (GAO et al, 2011). Sustained release systems are able to maintain the constant drug concentration in the blood plasma for a prolonged period, improving patient compliance (decreases the number of daily administrations) and therapeutic efficacy (GAO et al, 2011; HUANG et al, 2001).

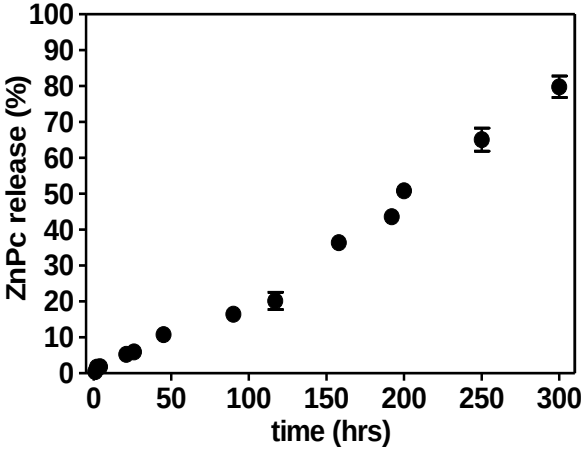

Figure 3.5 Release profiles of ZnPc loaded PMMA NPs. Data refer mean ± standard deviation (n =3) different experiments (pH 7.4).

The zero order, first order, and Higuchi mathematical models were used in this study to evaluate the release kinetics (Table 3.2). Mathematical models were applied to the release data. The choice of the model was based on the highest coefficient of determination (r^2). As shown in Figure 5, release kinetics was best explained by the zero order model, with the highest value of r^2 (0.9699), followed by the Higuchi model (0.8833) and the first order (0.7895). According to Costa and Lobo (2001) the zero order model is adequate for drug dissolution from delivery systems that do not disintegrate. The release profile showed that ZnPc flux is constant and it was released almost immediately from PMMA NPs with a small Lag Time as can be seen in the Table 3.2. Lag time is the time required for initial drug release (LEOPOLD et al, 2001; ROTHEN-WEINHOLD et al, 2000). The release of drugs from non-degradable polymeric delivery systems is more likely to be diffusion driven, which is associated with concentration gradient, diffusion distance and the swelling degree (FU and KAO, 2010). Finally, our results suggest that release of ZnPc from PMMA NPs was by diffusion, typical of non-biodegradable polymer (GAO et al, 2011; RAO AND GECKELER, 2011).

Table 3.2 Mathematical models and kinetic parameters

mathematical models	*Equation*	r^2	*Flux (ZnPc Release % / h)*	*lag time (h)*
Zero order	$Qt = Q_0 + K_0 t$	0.9699	0.0040	0.0161
First order	$\ln Qt = \ln Q_0 + K_1 t$	0.7895	4.3051	9.9294
Higuchi	$Qt = K_H t^{1/2}$	0.8833	0.0119	2.7045

3.7.2 Biocompatibility assays

The cytotoxic effects of PMMA NPs on K562 and Jurkat cells were found by MTT assay. Figure 3.6 shows the cytotoxicity profile of K562 and Jurkat cells incubated for 1 h with various NPs concentrations, in the absence of visible and red light exposure there was no cytotoxic effect when compared with the control group. The HPBL and L929 cells incubated with ZnPc loaded PMMA NPs and exposed to red light, also didn't present any cytotoxic effect. Other studies showed that PMMA NPs obtained by miniemulsion polymerization presented biocompatibility in human leukemic (THP1) and human lung adenocarcinoma cell lines (A549) (FEUSER et al, 2014). The non-cytotoxicity of the L929 cells is an important factor; ISO 10993-5 recommends the *in vitro* cytotoxicity assay of new material (MADERUELO et al, 2011). The non-cytotoxicity in HPBL cells is another key factor to leukemia and solid tumor treatment, where ZnPc loaded PMMA NPs can be systemically administered without causing a toxicity effect on human blood cells (DEDA et al, 2009).

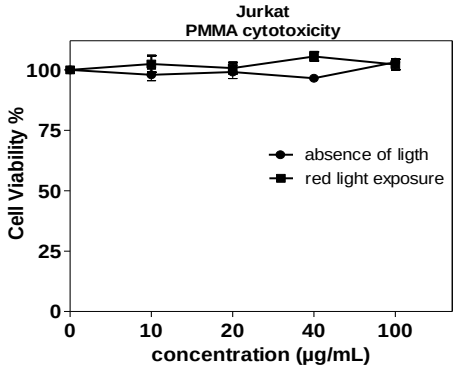

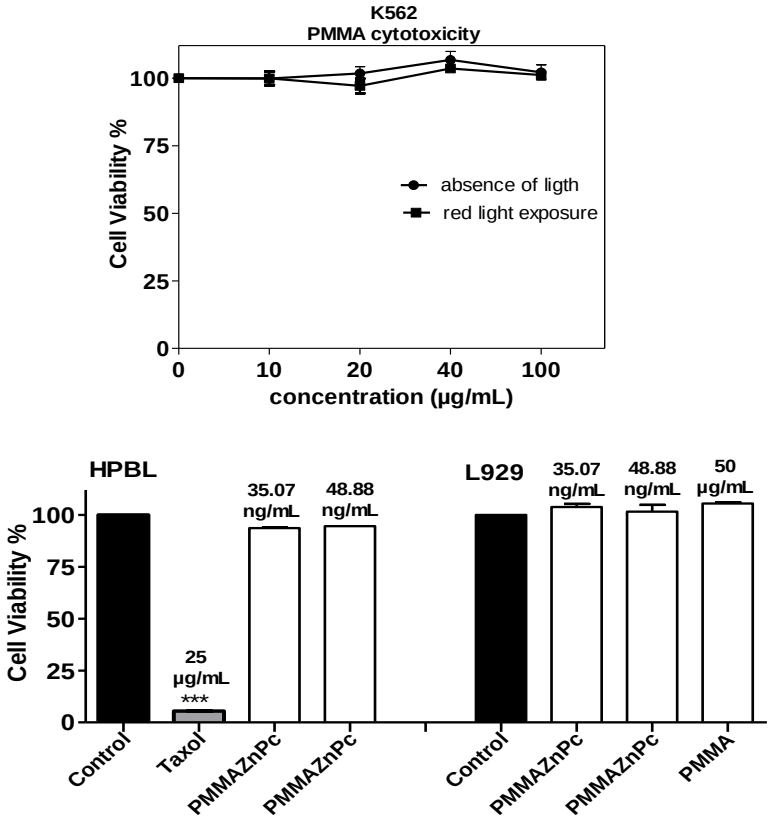

Figure 3.6 Cytoxicity effect of different concentrations of free PMMA NPs (10 - 100 µg.mL^{-1}) on leukemia cell lines (K562 and Jurkat) without and with red light. *p <0.05 compared to control groups, using ANOVA followed by the Bonferroni post-hoc test. Cytotoxic effects of ZnPc loaded PMMA in Nps on normal peripheral blood mononuclear human (HPBL) cells and normal mouse fibroblast (L929) cells, after red light exposure. ***$p < 0.001$ compared with control group, using ANOVA followed by the Bonferroni post-hoc test.

3.7.3 Photobiological activity

The phototoxicity assay (Figure 3.7) of free ZnPc and ZnPc loaded PMMA NPs on Jurkat and K562 cells was performed. The

results presented in Figure 7, showed that in the absence of red light, free ZnPc and ZnPc loaded PMMA NPs did not present cytotoxic effects on the leukemic cells (Figure 3.7). However, after irradiation with red light free ZnPc and ZnPc loaded PMMA NPs induced cell death in a concentration-dependent manner when compared with the control group (only cells) (Figure 3.7). The IC_{50} values of free ZnPc and ZnPc loaded PMMA Nps for Jurkat and K562 cells were 39.05 ±0.96 (Figure 3.7a), 47.43 ±1.20 (Figure 3.7b), 28.24 ±0.97 (Figure 3.7c) and 28.52 ±1.06ng/mL (Figure 3.7d), respectively. The phototoxicity assay showed that the ZnPc loaded PMMA NPs that incubated for 1 h were more phototoxic than the free ZnPc. The low incubation times (1 h) used in this study reflect the amount of photosensitizer delivered to the cells. The increase in phototoxic activity of ZnPc loaded PMMA NPs may be related to a higher delivery of ZnPc into cells. The non-aggregation of ZnPc in biological mediums also contributes to a higher phototoxicity. The photobiological activity is highly dependent on the photosensitizer's cellular uptake mechanism. In an aqueous medium, a free ZnPc is generally absorbed by diffusion across the plasmatic membrane (lipophilic) leading to a low intracellular concentration. Moreover, lipophilic ZnPc tends to aggregate in aqueous mediums, which reduce the photodynamic activity (CHARTTEJEE et al, 2008; DEDA et al, 2009; DOLMANS et al, 2003; RICCI-JÚNIOR and MARCHETTI, 2006). The results showed that the encapsulated ZnPc in polymeric NPs (PMMA) is an excellent strategy for leukemia treatment by PDT.

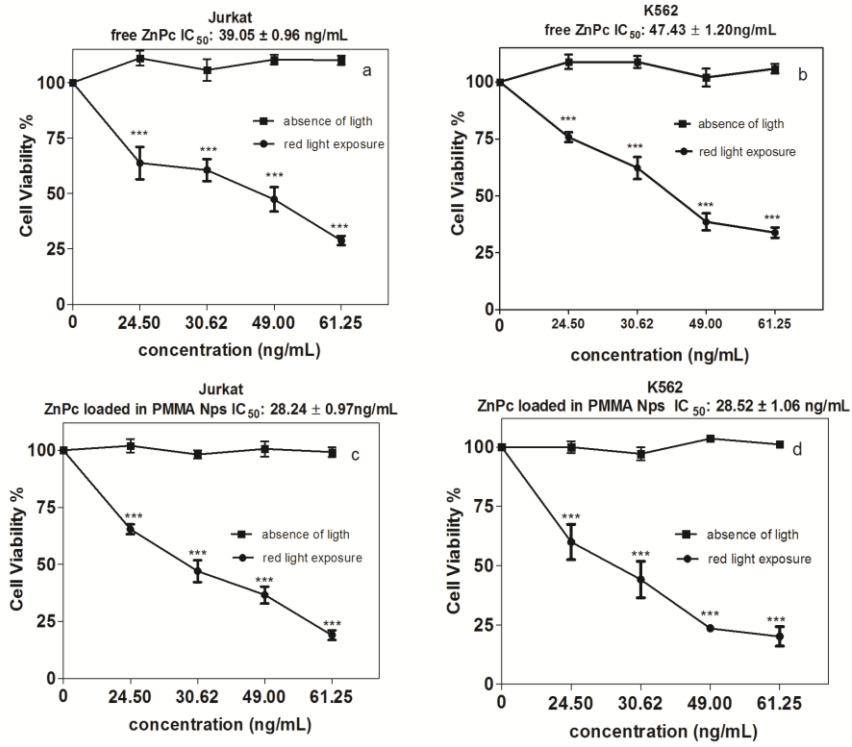

Figure 3.7 Phototoxicity assay of free ZnPc using Jurkat (a) and K562 (b) cells, and ZnPc loaded in PMMA Nps using Jurkat (c) and K562 (d) cells. *** $p<0.05$ compared to control groups, using ANOVA followed by the Bonferroni post-hoc test.

3.7.4 Evaluation of cell death by AO-EB staining and DNA fragmentation

PDT can induce cell death by apoptosis and/or necrosis after visible light exposure. To evaluate the cell death pathway, cell morphology was examined using fluorescence microscopy by AO-EB staining (Figure 3.8). K562 and Jurkat cells were treated with ZnPc loaded PMMA NPs, irradiated with red light (675 nm, light dose 2 J/cm^2) and incubated for 1 h. Viable cells exhibit green fluorescence

due to dye uptake. On the other hand, apoptotic cells exhibit orange-red fluorescence in the nucleus due to intercalation of ethidium bromide into damaged DNA (SHAO et al, 2012). As can be clearly seen in Figure 3.8, Jurkat and K562 cells presented orange fluorescence due to loss of membrane integrity, condensed or fragmented chromatin and presence of apoptotic bodies (white arrow) (ELMORES, 2007; GOSWAMI et al, 2014). Initial apoptosis can be observed in K562 cells, which present intact membranes and green fluorescence (yellow arrow), with condensed chromatin and nuclear fragmentation. This study's results were similar to the work of Goswasmi and collaborators where PDT was used to induce cell death by apoptosis in Hela and MCF-7 cells. The cell death by apoptosis was observed in a variety of tumor cell lines after PDT application with different photosensitizer derivatives (MARANHO et al, 2009; SHAO et al, 2012; SIQUEIRA-MOURA et al, 2009). Apoptosis is an intrinsic physiological event, which can also be triggered by external stimuli like oxidative stress attributable to PDT. Light absorption by the dye in the presence of oxygen, triggers photophysical and biological processes that result in the formation of ROS capable of damaging cellular components and causes cell death by apoptosis or necrosis (DOLMANS, 2003; FABRIS et al, 2001; OLEINEICK et al, 2002. The low light dose and low drug concentration used in the PDT is an important factor to induce cell death by apoptosis (DOLMANS, 2003; FABRIS et al, 2001; OLEINEICK et al, 2002; SHAO et al, 2012). Our results suggest that low ZnPc concentration and low light dose induced cell death by apoptosis. These results were corroborated with DNA fragmentation assays, as can be seen in Figure 3.9. DNA fragmentation assay induced the "staircase" fragmentation pattern characteristic of cell death by apoptosis.

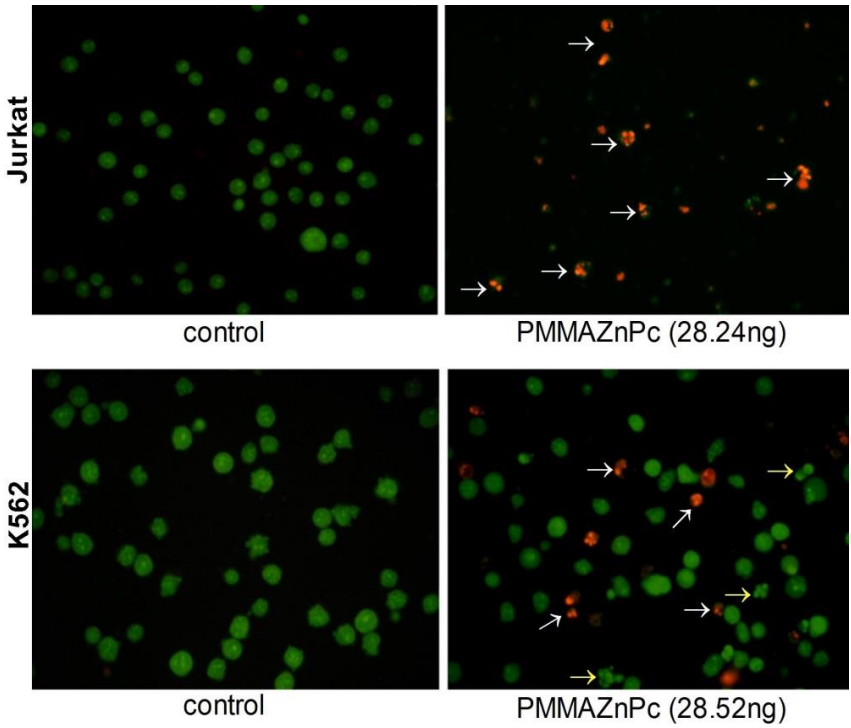

Figure 3.8 Acridine orange–ethidium bromide (AO-EB) staining of Jurkat and K562 cells at concentration of IC_{50} of ZnPc loaded PMMA NPs. The group without treatment was taken as the control group.

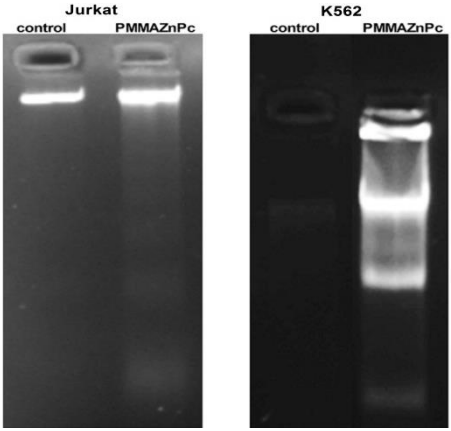

Fig. 3.9 DNA fragmentation analysis of ZnPc loaded PMMA NPs on K562 and Jurkat cells. The level of DNA fragmentation was determined using the genomic DNA mini preparation kit to obtain the genomic DNA. This was then separated in 2 % agarose gel with 1 $mg.mL^{-1}$ ethidium bromide for 40 min at 80 V.

3.8 CONCLUSIONS

The encapsulation method of ZnPc loaded PMMA NPs by miniemulsion polymerization showed high encapsulation efficiency of ZnPc (87 % ±2.1), and resulted in stable aqueous dispersion with an average size diameter around 100 nm. The release profile test and mathematical models used in this study showed that the ZnPc loaded in PMMA NPs had a sustained release, maintaining drug release for extended periods of time. Cytotoxicity and phototoxicity studies in leukemic cells (K562 and Jurkat) associated with non-cytotoxic activity in human peripheral blood lymphocyte cells and on normal fibroblast cells (L929) showed that the ZnPc loaded PMMA NPs can be considered an effective strategy for treatment of leukemic cells by PDT, based on low IC_{50} values and light dose. All the photobiological studies performed allow us conclude that ZnPc loaded PMMA NPs are promising drug carrier systems, improving the photobiologycal activity of the ZnPc on leukemic cells.

CHAPTER 4

ENCAPSULATION OF MAGNETIC NANOPARTICLES IN POLY(METHYL METHACRYLATE) BY MINIEMULSION AND EVALUATION OF HYPERTHEMIA IN U87MG CELLS

Abstract: Magnetic nanoparticles (MNPs) are promising materials for hyperthermia treatment and magnetic targeting systems. The objective of this work was to synthesize and characterize magnetic nanoparticles coated with oleic acid (MNPsOA) loaded with poly(methyl methacrylate) prepared by miniemulsion polymerization (MNPs-PMMA) and evaluate their cytotoxicity in murine fibroblast (L929) cells, blood biocompatibility (hemolysis assay) and hyperthermia (HPT) in human glioblastoma (U87MG) cells. The MNPs-PMMA nanoparticles presented average mean diameter of 99 ±1.9 nm with a polydispersity index (PdI) of 0.13 ±0.015 and saturation magnetization (Ms) value of 34emu/g of iron oxide, as well as superparamagnetic properties. The MNPs-PMMA nanoparticles did not present cytotoxicity in murine fibroblast (L929) and U87MG cells. HPT assays were applied, demonstrating that AC magnetic field application (1 MHz and 40 Oe) for 3 min or 6 min reduced the viability cells by 75% and 52% respectively. Morphological analyses showed that U87MG cells treated with 0.1 $\mu g.mL^{-1}$ of MNPs-PMMA nanoparticles shrank after AC magnetic field application for 6 mim, resulting in a region of hypoxia. Hemolysis assay showed that MNPs-PMMA nanoparticles presented high blood biocompatibility. Our results indicate that MNPs-PMMA nanoparticles obtained by miniemulsion polymerization have the potential to be used as carrier systems for HPT.

Keywords: biomaterials, hyperthermia, polymers, superparamagnetic nanoparticles.

The manuscript was published in the European Polymer Journal
doi: 10.1016/j.eurpolymj.2015.04.029

4. INTRODUCTION

Magnetic nanoparticles (MNPs) have been widely used in various biomedical applications (FERREIRA et al, 2012; GUPTA and GUPTA 2005; LAURENT et al, 2010; TEJA and KOH, 2009), such as targeted drug delivery (DORNIANI et al, 2012; KUMAR and MOHAMAD, 2011; SHI et al, 2013; ZHA et al, 2013; ZHAO et al, 2005; ZHENG et al, 2005), hyperthermia (FERREIRA et al, 2012; LATTUADA and HATTON, 2007; SAHOO et al, 2013; SIMIONI et al, 2007; TEJA and KOH, 2009) and magnetic resonance imaging (MRI) (ABULATEEFEH et al, 2011; FERREIRA et al, 2012; GUPTA and GUPTA 2005; LAURENT et al, 2010; TEJA and KOH, 2009). For these applications, MNPs must have combined properties of high magnetic saturation, superparamagnetic properties and biocompatibility (KUMAR and MOHAMAD, 2011; ZHENG et al, 2005). MNPs are promising materials for hyperthermia treatment and have been used in cancer therapy for decades, usually applied as an adjuvant to radiotherapy and chemotherapy. Additionally, induced hyperthermia for cancer treatment involves raising the temperature of tumor-loaded tissues to 40–43 °C (BASE et al, 2012; DANHIER et al, 2010; GUPTA and GUPTA 2005). Solid tumors have been shown to have increased susceptibility to small changes in temperature compared to healthy tissue due to their increased rate of cell cycling, increased hypoxia, reduced fluid exchange and increased cellular acidity (pH 2-4) (DANHIER et al, 2010; TANG et al, 2013).

In cancer therapy, the major difficulty is to destroy tumor cells without harming the surrounding normal tissue. The use the polymeric nanoparticles (Nps) for drug delivery results in increased local drug concentrations, reducing toxic effects on healthy cells or tissues, providing a new strategy for cancer treatment. Nps are solid spherical structures ranging around 100 nm in size and can be prepared from natural or synthetic polymers (LANDFESTER and MAILANDER, 2013). Nps have the function of protecting and preventing aggregation of MNPs (TANG et al, 2013). On the other hand, MNPs can ensure the mobility of the Nps when a magnetic field is applied, enabling their use for drug transport. A large number of strategies have been proposed in the literature to encapsulate MNPs in polymeric colloidal particles including emulsion polymerization (BOURGEOUT-LAMI E,

LANSALOT, 2010), inverse miniemulsion polymerization (ROMIO et al, 2012) and direct miniemulsion polymerization (HE et al, 2008; STAUDT et al, 2013).

Poly(methyl methacrylate) (PMMA) is widely used in biomedical materials due to its biocompatibility. Recent publications have shown an increasing interest in its applications as a drug carrier (GYERGYEKA et a, 2010; FU and KAO, 2010). PMMA, since it is not biodegradable, can increase the circulation time in the blood and therapeutic index of encapsulated drugs (FU and KAO, 2010). PMMA based particulate carriers can be prepared either by polymerization in dispersed phase or from preformed polymer-based techniques (BETTENCOURT and ALMEIDA, 2012; ZHENG et al, 2005). Miniemulsion polymerization allows the production of polymeric nanocapsules or nanospheres with unique characteristics of great commercial interest. Miniemulsion polymerization produces stable aqueous dispersions of droplets (50-500 nm) containing monomer, surfactant, ultrahydrophobe, initiator and water insoluble compounds (e.g., hydrophobic MNPs) by applying high shear stress (ASUA, 2014; CRESPY and LANDFESTER, 2010; HIGUCHI and MISRA, 1962; LANDFESTER, 2009; QIU et al, 2007). In order to stabilize such a direct miniemulsion, droplet coalescence is suppressed by the surfactant that stabilizes the particles electrostatically or sterically. As the miniemulsion features a distribution in droplet size, the bigger droplets can growth due to a mass flux from the smaller ones as Laplace pressure increases with decreasing droplet size, this phenomena is known as molecular diffusion degradation or Ostwald ripening. The ultrahydrophobe prevents diffusion degradation by introducing a counterforce to the Laplace pressure as the smaller particles would contain a higher concentration of ultrahydrphobe increasing the Osmotic pressure (HIGUCHI and MISRA, 1962). As the colloidal stability is attained, monomer droplets act as the primary polymerization *loci* and behave as "nano-reactors" and thus lead to a similar concentration of hydrophobic MNPs inside the polymeric particles if a high adhesion interaction between the polymer and the shells of metal nanoparticles is attained (ASUA, 2014). The main advantage of the miniemulsion polymerization process is the ability to produce complex nanostructures, including the encapsulation of inorganic nanoparticles, in a single

reaction step with fast polymerization rates (MAHDAVIAN et al, 2008; LANDFESTER K, MAILANDER, 2013; QIU et al, 2007).

The goals of this work were to synthesize and characterize MNPs loaded in poly(methyl methacrylate) (PMMA) by miniemulsion polymerization and to evaluate *in vitro* the cytotoxicity in murine fibroblast (L929) cells, hemolysis and the efficacy of HPT treatment using human glioblastoma (U87MG) cells.

4.1 MATERIALS AND METHODS

4.1.1 Materials

For synthesis of magnetic nanoparticles coated with oleic acid (MNPsOA), the following reagents were employed (high purity grade): ferrous sulfate ($FeSO_4 \cdot 4H_2O$), iron (III) chloride hexahydrate ($FeCl_3 \cdot 6H_2O$), ammonium hydroxide (99%), and oleic acid (OA), all purchased from Vetec Química Fina. For the encapsulation of MNPsOA, the following reagents were employed: methyl methacrylate (MMA), obtained from Arinos Química Ltda., azobisisobutyronitrile (AIBN), purchased from Vetec, lecithin, obtained from Alpha Aesar, and Miglyol 812 (as co-stabilizer), purchased frolm Sasol. Distilled water was used throughout the experiments.

4.2.2 Methods

4.2.2.1 Synthesis of magnetic nanoparticles coated with oleic acid (MNPsOA)

MNPsOA nanoparticles were prepared by co-precipitation (MEIORIN et al, 2014). Briefly, $FeCl_3.6H_2O$ and $FeSO_4.7H_2O$ (mole ratio of 1:1.2) were dissolved in a beaker containing distilled water under mechanical stirring in the range of 800 rpm. Then an ammonium hydroxide solution (11 mL) was rapidly added to the solution. After 1 h, 30 mL was added to the OA and the stirring process was continued (800 rpm) for 30 min. The MNPsOA produced was centrifuged and washed three times with ethanol to remove the unreacted OA.

4.2.2.2 Encapsulation MNPs in PMMA nanoparticles by miniemulsion polymerization (MNPs-PMMA)

For encapsulation of MNPs by miniemulsion polymerization, an organic phase containing 2 g of MMA with 1 g of MNPsOA, 0.1 g of lecithin, 0.1 g of Miglyol and 0.4 g of AIBN was added to a beaker containing 20 mL of distilled water (aqueous phase). The organic phase was added dropwise under higher shear with amplitude of 70% (Fisher Scientific, Sonic Dismembrator, 500 W). The high shear was maintained for 5 min (10 s on and 1 s off) in a beaker immersed in an ice bath to avoid increased temperature during sonication. The miniemulsion product was transferred to glass tubes (10 mL) at 70 °C for polymerization during 3 h. Afterwards, the material was cooled, centrifuged and washed three times with phosphate buffered saline (PBS) at pH 7.4. Subsequently, Nps were transferred to glass vials, frozen in liquid nitrogen and lyophilized (FreeZone 4.5-L Benchtop Freeze Dry System; Labconco, Kansas City, MO). The lyophilized powder was stored at room temperature (25 °C) before analysis. The magnetic fluid concentration used to produce the MNPs-PMMA was about $1.2x10^{17}$ particles/mL.

4.2.3 MNPsAO and MNPs-PMMA nanoparticles characterization

Average diameters (intensity averages) of monomer droplets (Dg) and of polymer particles were measured by dynamic light scattering (DLS-Malvern Instruments, Zetasizer Nano S). The Nps morphology was observed using transmission electron microscopy (TEM), with a JEM 2100F microscope operating at 100 kV. The XRD experiments were performed to identify the crystallographic structure of Nps. The crystalline phase of Nps was identified by measurements of X-ray diffraction using Cu-Kα (1.54056 Å) 45 kV/40 mA in an Xpert-Pro diffractometer. The average crystal size is calculated according to the Debye-Scherrer equation, $D = R\lambda/ß\cos\theta$ (where D is the particle diameter, R is the Scherrer constant (0.89), λ is the incident light wavenumber, β is the peak width of half-maximum, and θ is the diffraction angle. The average crystallite size is obtained from the most intense peak (311). Fourier-transform infrared spectroscopy (FT-IR) was used to confirm the chemical structure of the MNPs and PMMA using a KBr pellet. The MNPsOA and MNPs-PMMA nanoparticles

were measured through TGA runs under a nitrogen atmosphere at a heating rate of 10 °C/min. A MicroSense model EV9 vibration sample magnetometer (VSM) was used to measure the hysteresis loops of MNPsOA and MNPs-PMMA nanoparticles.

4.3 *In vitro* studies

4.3.1 *In vitro* cytotoxicity assay of MNPs-PMMA nanoparticles on L929 cells

The murine fibroblast (L929) cell lines were selected to evaluate cytotoxicity as a direct contact test, as recommended by ISO 10993 for *in vitro* toxicity. The cells were cultured in Dulbecco's Modified Eagle's medium (DMEM) supplemented with 10% fetal bovine serum, penicillin (100 units/ml), streptomycin (100 mg/mL), and 4 mM/L of glutamine at 37 °C in tissue culture flasks with 5% CO_2. For experimental purposes, trypsinized cells were adjusted to a concentration of $1x10^4$ cells/well and plated in a 96 well flat bottom culture plate. For cytotoxicity study, the cells were incubated with three concentrations of MNPs-PMMA nanoparticles (10, 20, 50µg.mL^{-1}) for 24 h at 37 °C in a humidified 5% CO_2 incubator and cell viability was measured by the MTT (3-(4, 5-dimethiazolzyl)-2-5-diphenyltetrazolium bromide) assay.

4.3.2 Cytotoxicity assay of MNPs-PMMA nanoparticles without hyperthermic application on U87MG cells

U87MG cells were seeded at $1x10^4$ cells/well in a 96-well plate to assess the intrinsic cytotoxic effect of the MNPs-PMMA nanoparticles. After 24 h, the cells were kept in the dark and incubated with a mixture of fresh medium and MNPs-PMMA. Nps at a final concentration of 0.05 and 0.1µg of MNPs were maintained for 3 h at 37 °C and 5% CO_2. After incubation, the medium containing the MNPs-PMMA nanoparticles was discarded and the cells were washed with sodium phosphate buffered saline (PBS). In the next step, the cells were incubated with fresh medium for an additional 24 h, after which the cell viability assay (MTT) was performed. Control cells were incubated with culture medium alone (untreated cells) or medium containing unloaded

MNPs-PMMA nanoparticles, both in the dark. Toxicity experiments in darkness were carried out in triplicate, with 36 wells for each condition.

4.3.3 MNPs-PMMA nanoparticles hyperthermia effect on U87MG cells

In order to evaluate the MNPs-PMMA nanoparticles hyperthermia effect on U87MG cells *in vitro*, the cells were seeded at $1x10^5$ cells/well in 24-well plate. After 24 h, the cells were treated with a medium containing MNPs-PMMA nanoparticles at two concentrations: 0.05 µg and 0.1 µg (5% CO_2, 37 °C). Following incubation (3 h), the medium loaded with Nps was removed, the cells were rinsed with PBS (1X) and incubated with conditioned medium. After 24 h, the cells were treated during 6 minutes with alternating magnetic fields operating at 1 MHz and 40O e amplitude, in fresh medium without bovine serum. After the hyperthermic application, the cells were incubated (5% CO_2, 37 °C) in fresh conditioned medium for a further 24 h, after which the MTT cell viability assay was performed. Control cells were incubated with culture medium alone without MNPsOA encapsulation and magnetic field, or encapsulated MNPsOA mixed with medium (encapsulation control). The cytotoxicity assay was carried out in triplicate, with 36 wells for each condition.

4.3.4 MTT viability assay

The MTT cell proliferation assay was employed to assess cell viability after both the cytotoxic assays. Briefly, 80-µl aliquots of MTT solution (5 $mg.ml^{-1}$) and 420 µl of medium without phenol red were added to each well. The cells were then incubated for 4 h, at 37 °C and 5% CO_2 to allow the formazan-formation reaction. Following incubation, the medium containing the MTT solution was removed, and the formazan crystals were dissolved in 2-propanol. The optical density was measured at 570 and 690 nm using a *Safire2* microplate reader (Tecan Group Ltd.). The results are presented as survival percentage, taking the control (untreated cells) as 100%.

4.3.4 Morphological analyses

Morphological analyses, consistent with observation of changes in cells morphology, were carried out by inverted microscopy. Cells were treated with MNPs-PMMA nanoparticles at MNPs concentration of 0.1µg.mL^{-1}. As negative controls, cells were incubated with culture medium alone without magnetic field (control cells), MNPs-PMMA nanoparticles mixed with medium without magnetic field (control group), or medium alone with magnetic field (hyperthermia control). The morphological changes of the cells were observed 1 h and 24 h after treatment.

4.3.5 Hemolysis assay

This study was approved by the medical ethics committee of Polydoro Ernani de São Thiago University Hospital (Florianopolis, Brazil). Citrate-stabilized human blood was freshly collected and used within 3 h of being drawn. 4 mL of whole blood was added to 8 mL of a sterile solution of sodium chloride in water (saline) and the human red blood cells (RBCs) were isolated from serum by centrifugation at 10,000 × *g* for 5 minutes. The RBCs were further washed five times with saline solution. Following the last wash, the RBCs were diluted in 2 mL of saline solution and then 120 µL of the diluted RBC suspension was added to 880 µL of water or saline. The MNPs-PMMA nanoparticles coated with 0.1µg.mL^{-1} were treated at 10 µl, 25 µl and 50 µl volume. All samples were prepared in triplicate and the suspension was briefly vortexed before gentle stirring at 37 °C for 60 minutes. After that, the mixture was briefly vortexed again and centrifuged at 10,000 × *g* for 5 minutes. 100 µL of supernatant from the sample tube was transferred to a 96-well plate. The absorbance value of hemoglobin at 570 nm was measured with the reference wavelength at 540 nm. 120 µL of the diluted RBC suspension incubated with 880 µL of water and saline were used as the positive and negative control, respectively. The hemolysis percent (%) was calculated from Equation 1:

$$\text{Hemolysis (\%)} = \frac{(\text{sample absorbance-negative control})}{(\text{positive control-negative control})} \times 100\% \quad (1)$$

4.4 RESULTS AND DISCUSSION

4.4.1 MNPs-PMMA nanoparticles characterization

The MNPsOA and MNPs-PMMA nanoparticles were examined by transmission electron microscopy (TEM) to determine their shape, size, and uniformity under optimum conditions. This analysis is very important to verify the presence of secondary nucleation and degradation mechanisms, especially when the final material will have biomedical use (FEUSER et al, 2014). Figure 4.1(a)-(b) show that these MNPsOA particles had a very small size, of around 5-13 nm in diameter, with narrow size distribution.

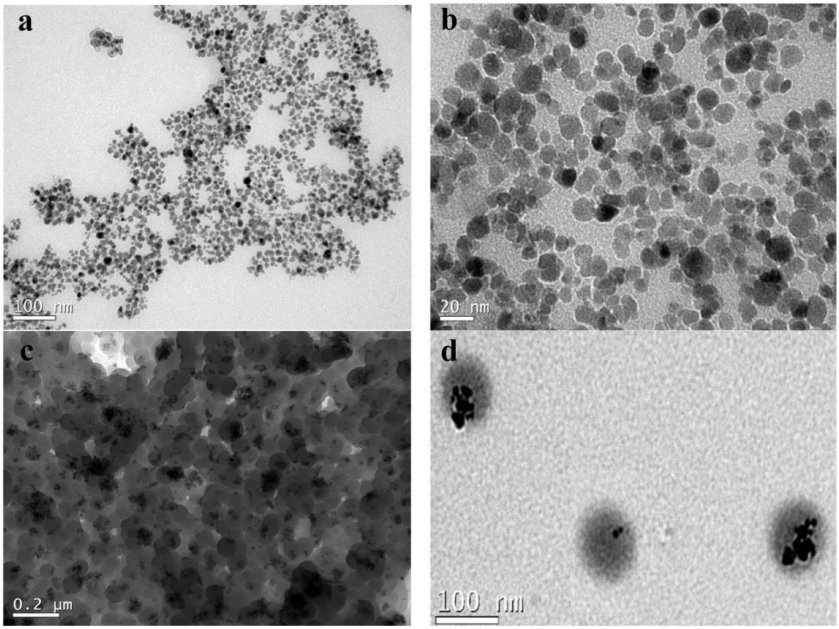

Figure 4.1 Transmission electron micrographs (TEM) of (a and b) MNPsOA and (c and d) MNPs-PMMA nanoparticles.

Figure 4.1c and d, shows some darker regions, which is attributed to the core formed by MNPs in PMMA with an approximate value of 100 nm, with spherical morphology and relatively narrow size distribution. Table 4.1 shows average droplets (Dp_I) and particles (Dp_F)

and polydispersity index (PdI) given by DLS. These results corroborate those of the TEM analysis (Figure 4.1). The low PdI indicates that both samples have narrow average size distribution and that the osmotic pressure would be sufficient to prevent Ostwald ripening (ASUA, 2014; LANDFESTER and MAILANDER, 2009; SHORK et al, 2015). The TEM and DLS showed that the size distribution of the MNPs-PMMA nanoparticles is uniform and it is likely that the dominant nucleation mechanism was polymerization of monomer droplets in preference to other possible mechanisms, such as micellar or homogeneous nucleation, as would be expected when employing a hydrophobic initiator (LANDFESTER and MAILANDER, 2009).

Table 4.1 Analysis of average droplet (Dg) and particle (Dp) diameter and initial and final polydispersity index (PdI_g and PdI_p) of NP miniemulsion polymerization by DLS

Samples	*Dg(nm)*	*Dp(nm)*	PdI_g	PdI_p
MNPs-PMMA	92±2.3	99±1.9	0.11±0.011	0.13±0.015

The powder X-ray diffraction (XRD) patterns for the naked MNPsOA and MNPs-PMMA nanoparticles are shown in Figure 4.2. For both samples (MNPsOA and MNPs-PMMA), six characteristic peaks can be observed at 2θ: (220), (311), (400), (422), (511) and (440) (DALLAS et al, 2006; DORNIANI et al, 2012; HONG et al, 2008; SAHOO et al, 2013). The XRD patterns of MNPsOA and MNPs-PMMA nanoparticles (Figure 4.2a and c respectively) indicate that the diffraction peaks' intensity weakened but did not disappear. The weakness of diffraction intensity of MNPs-PMMA nanoparticles may be due to the lower content of MNPs. During the synthesis process, the structure of MNP nanoparticles was unchanged. Therefore, the results demonstrated that the MNPs-loaded PMMA nanoparticles have the expected crystalline structure of Fe_3O_4 (HONG et al, 2008; ZHENG et al, 2005). Using the XRD results and Debye-Scherrer equation, the average crystallite sizes of MNPs and MNPs-PMMA nanoparticles were estimated to be 8 nm and 10 nm, respectively, similar to the result from TEM (Figure 4.1). According to Mody and collaborates (2014), when MNPs have a critical diameter of about 5-10 nm, they can become superparamagnetic nanoparticles.

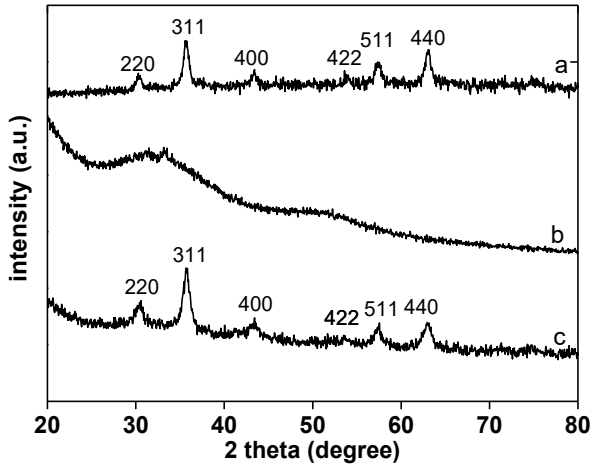

Figure 4.2 Powder x-ray diffraction (XRD) patterns for (a) MNPsOA, (b) PMMA and (c) MNPs-PMMA nanoparticles.

FT-IR analysis (Figure 4.3) can verify the presence of the absorption bands of the functional groups present in samples. In Figure3a, the peak at about 577cm^{-1} is related to the vibration of the Fe-O bond, which matches well with the characteristic peak of MNPs (SAHOO et al, 2013). The spectrum of MNPs-PMMA nanoparticles is shown in Figure 4.3c. The adsorption peak at 577cm^{-1} was the characteristic absorption of Fe-O bond, confirming the presence of MNPs in PMMA nanoparticles (HONG et al, 2008). A new adsorption at 1736 cm^{-1} corresponds to C=O groups of PMMA. In addition, the bands in the 3000–2800 cm^{-1} region are attributed to the stretching of C-H bonds of the saturated alkane in PMMA, indicating the existence of PMMA (Figure 4.2b) (FEUSER et al, 2014). On the basis of the above analysis, the MNPs and MNPs-PMMA nanoparticles were confirmed to be present in the composite particles (HONG et al, 2008).

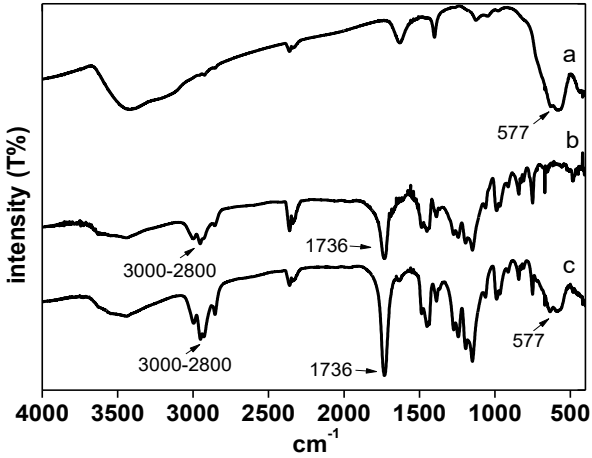

Figure 4.3 FTIR spectra of MNPsOA (a), PMMA (b) and MNPs-PMMA nanoparticles (c).

The thermal decompositions of pure MNPsOA and MNPs-PMMA nanoparticles were studied using thermogravimetry. Figure 4a and b show there was no mass loss in the temperature range 0 to 100 °C, which can indicate the material is free of impurities (LANDFESTER an RAMIREs, 2003). Figure4a shows two mass loss events, the first, of 30%, observed between temperatures of 200 and 280 °C, and the second, of 13%, observed between 300 and 410 °C. According to Landfester and Ramires (2003), the presence of two peaks indicates that different species of OA are present in the sample. In the case of MNPs in PMMA nanoparticles (Figure 4.4b), mass loss is gradual and it can be clearly seen that the PMMA nanoparticles are completely degraded when reaching about 410 °C. The residual concentration of 20% corresponds to the MNPs. The other 80% corresponds to the PMMA and AO present in MNPs. This analysis is very important to determine the total concentration of MNPs in the formulation.

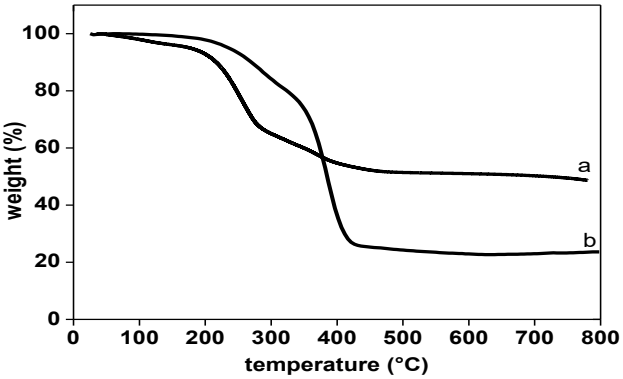

Figure 4.4 TGA analysis of MNPsOA (a) and MNPs-PMMA nanoparticles (b).

The magnetic properties of MNPsOA and MNPs-PMMA nanoparticles were characterized by vibrating sample magnetometry (VSM). Figure 4.5 shows the hysteresis loops as a function of the magnetic field at room temperature. The magnetic parameters, including saturation magnetization and remnant magnetization, are shown in Table 4.2. Saturation magnetization values in emu/g were obtained considering the iron oxide mass obtained from TGA analysis.

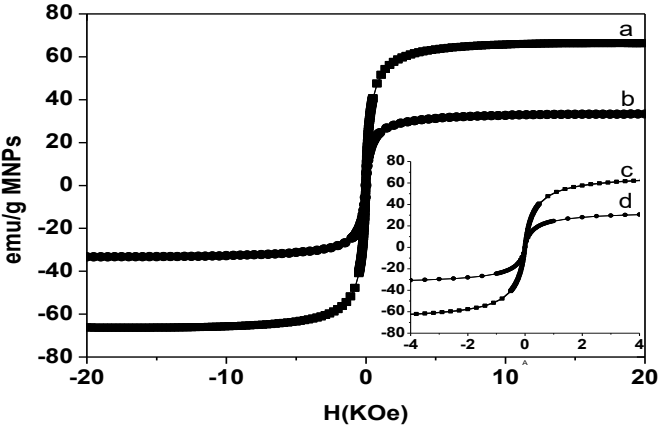

Figure 4.5 Magnetic properties of MNPs(AO) and MNPs-PMMA, magnetic field of 20 KOe (a)-(b) and magnetic field of 4 KOe (c)-(d), respectively.

Table 4.2 Magnetic properties of MNPs(OA) and MNPs-PMMA nanoparticles

Samples	*Ms (emu/g)*	*Mr (emu/g)*	*Hc (Oe)*	*Mr/Ms*
MNPs(OA)	66	0.0058	2.0	$8.7\ x10^{-5}$
MNPs-PMMA	34	0.0138	0.2	$3.8\ x10^{-5}$

The saturation magnetization of the MNPs-PMMA nanoparticles was about 34 emu/g of MNPs (Figure 4.5a and c), while that of the MNPs(AO) was about 66 emu/g of MNPs (Figure 4.5b and d). The decrease in saturation magnetization relative to the bulk value Ms=100 emu/g may be due to oxidation processes during sonication, which leads to the formation of some iron oxides without magnetization or with low saturation magnetization (Ms), such as maghemite (γ-Fe_2O_3), which has a lower Ms of 60–80 emu/g compared to 92-100 emu/g for Fe_3O_4 (LANDFESTER and RAMIREs, 2003). It also can be attributed to the dense coating of the non-magnetic polymer, or because during the polymerization, some of the Fe_3O_4 converts to another iron oxide, like γ-Fe_2O_3, due to the presence of the oxidizing initiator fragments (DALLAS et al, 2006; HONG et al, 2008; MODY et al, 2014; RAMIRES and LANDFESTER, 2003). However, the nanoparticles presented a significantly lower Ms compared with the bulk values, due to finite-size effects (BATLLE and LABARTA, 2002). All of the ferrofluids showed typical superparamagnetic behavior at room temperature, with absence of hysteresis loop, low Mr/Ms ratio and small Hc values (Table 4.2) (CHANDRASEKHARANA et al, 2011; MODY et al, 2014). The superparamagnetic properties of Nps are very important for biomedical applications. Therefore, without an external magnetic field, their overall magnetization value is randomized to zero, preventing active behavior of the particles when there is no applied field (DALLAS et al, 2006; GUPTAab, 2005; ZHENG et al, 2005).

Figure 4.6 shows that the amount of MNPs in PMMA nanoparticles does not influence the Ms (Figure 4.6a and b) and the general shape of the magnetization curve (Figure 4.6c and d), indicating non-observable interacting effects among MNPs. This clearly indicates that the MNPs with a diameter of 10 nm are still well separated in the polymer matrix (XU et al, 2014). This Ms value is enough for encapsulated MNPs to move quickly and be easily separated from the aqueous phase by the action of an external magnetic field gradient, as can be seen in Figure 4.7. MNPs-PMMA nanoparticles can be directed

towards a specific target in the human body, with application of an external magnetic field, such as, after intravenous administration.

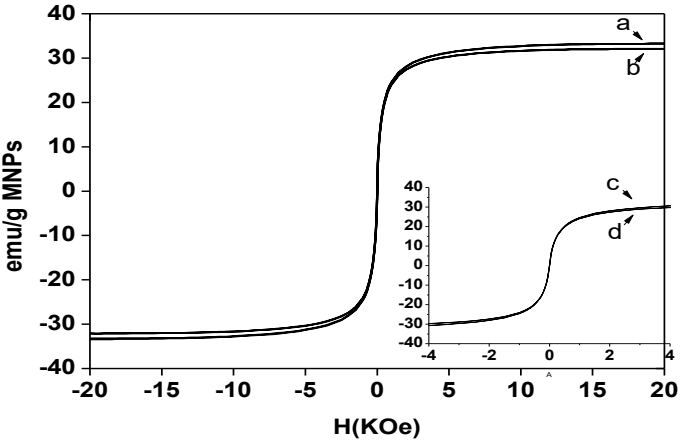

Figure 4.6 Magnetic properties with different concentrations of MNPs in PMMA (10% and 20%), magnetic field of 20 KOe (a)-(b) and magnetic field of 4 KOe (c)-(d), respectively.

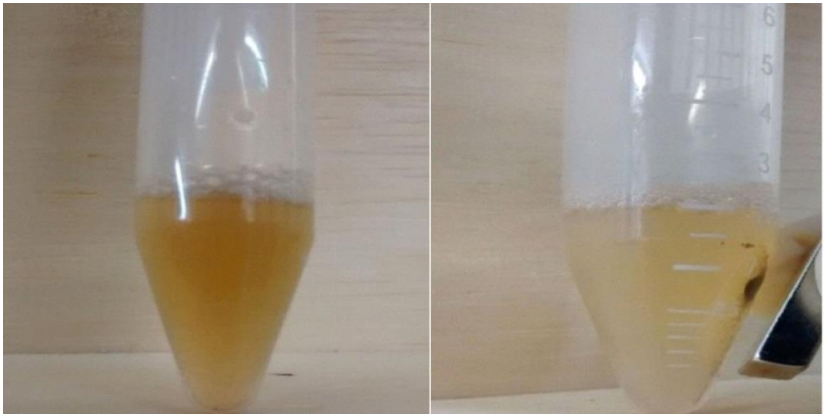

Figure7 MNPs-PMMA nanoparticles in PBS (7.4) without application of an external magnetic field and with application of an external magnetic field.

4.4.2 In vitro antitumor activity of MNPs-PMMA nanoparticles on L929 and U87MG cells

The cytotoxic effects of MNPs-PMMA nanoparticles on L929 cells were examined by the MTT assay. Figure 4.8 shows the cytotoxicity profile of L929 cells incubated with various concentrations of MNPs-PMMA nanoparticles. The nanoparticles did not show any cytotoxic effect on L929 cells. Cell viability of nearly 99% can be observed after treatment with the control group. This test with L929 cells is very important as it will facilitate innovative research using nanomaterials for hyperthermia based treatment and drug release systems (ABULATEEFH et al, 2011; SIMIONI et al, 2007).

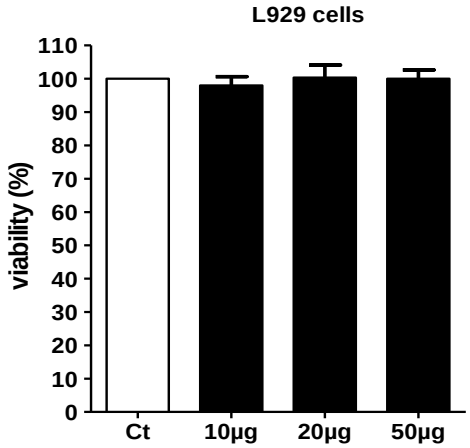

Figure 4.8 Cytotoxicity effects of different concentrations of MNPs-PMMA nanoparticles on L929 cells. $^{ns}p < 0.05$ compared to control group, using ANOVA followed by the Bonferroni post-hoc test.

The viability of U87MG cells treated with MNPs-PMMA nanoparticles under AC magnetic field activation is shown in Figure 4.9. The viability of U87MG cells decreased ($p < 0.05$) after AC magnetic field application, reaching 52% ($0.05\mu g.mL^{-1}$) and 54% ($0.1\mu g.mL^{-1}$). The temperature change caused by the AC magnetic field induced HPT. This observation can be attributed to the local heating caused by the

HPT process (DORNIANI et al, 2012; GUPTAab, 2005; ZHAO et al, 2013). The viability of U87MG cells with HPT for 1 min, 3 min and 6 min presented significant differences ($p<0.05$). However, different concentrations ($0.05\mu g.mL^{-1}$ and $0.1\mu g.mL^{-1}$) of MNPs used in the cytotoxicity assays did not present significant differences ($p<0.05$).

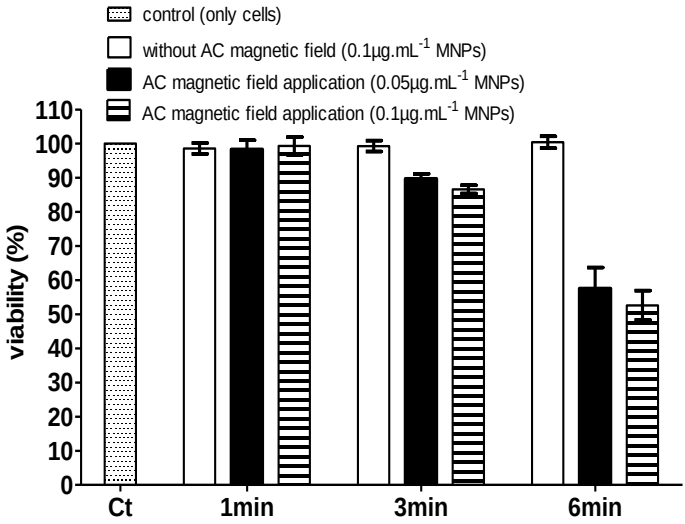

Figure 4.9 Cytotoxicity effect of two concentrations (0.05µg and 0.1µg of MNPs loaded in PMMA nanoparticles) on U87MG cells, 24 h after induced hyperthermia for 1, 3 and 6 min (40 Oe – 1 MHz) exposure. ***p <0.05 compared to control groups, using ANOVA followed by the Bonferroni post-hoc test.

The morphology of U87MG cells treated with MNPs-PMMA nanoparticles and the corresponding induction of hyperthermia is shown in Figure 4.10. Figure 4.10b shows that after 1 h, U87MG cells treated under AC magnetic field resulted in a region of hypoxia. According to Zee (2002), the architecture of the vasculature in solid tumors is chaotic, resulting in regions with hypoxia, which is not found in normal tissues in undisturbed conditions. The results of the MNPs-PMMA nanoparticles in the control group demonstrate that the superparamagnetic nanoparticles themselves (without AC magnetic field) do not have any treatment effect (Figure 4.10a). Figure10c show

the significantly reduced viability of U87MG cells, to 54% (0.1µg.mL^{-1}) after 24 hrs of U87MG cells treated under AC magnetic field for 6 min (40Oe / 1 MHz).

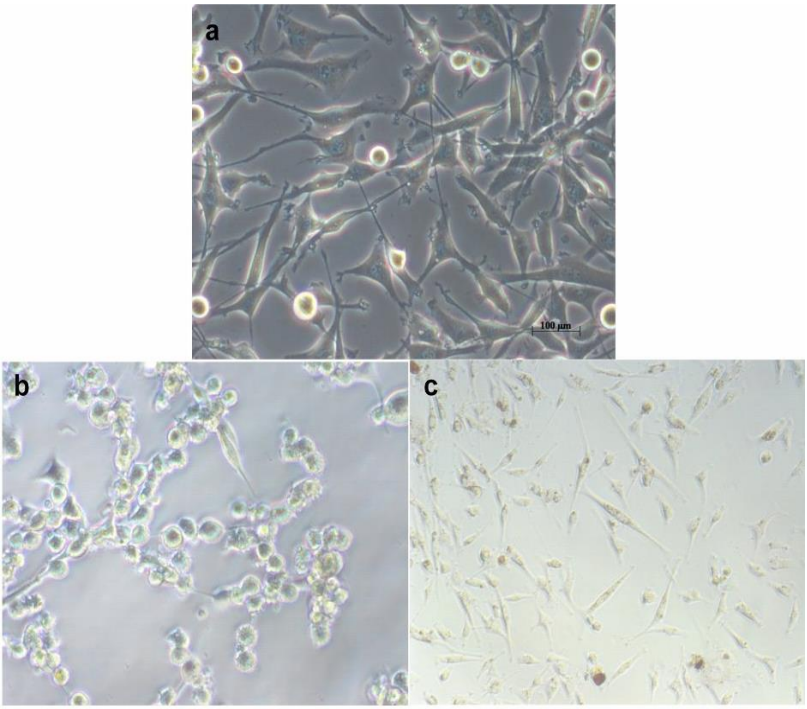

Figure 4.10 Morphology of U87MG cells treated for 6 minutes - hyperthermia treatment (40 Oe – 1 MHz) using MNPs-PMMA nanoparticles: Control: without application of magnetic field (a), one hour after hyperthermia (b) and 24 h after hyperthermia (c).

The impact of MNPs-PMMA nanoparticles on human red blood cells (RBCs) was evaluated by a hemolysis assay. The quantitation of hemoglobin in the supernatant of the nanoparticle-RBC mixture was done by recording the absorbance of hemoglobin at 540 nm. Treatment with 10 µl, 25 µl and 50 µl of MNPs-PMMA nanoparticles coated with 0.1µg.mL^{-1} of MNPs was not able to cause hemolysis of RBCs, suggesting that these systems do not have hemolytic capacity, even

when administered at high concentrations (Figure 4.11). These results reveal that these nanoparticle formulations have high blood biocompatibility, making them an alternative to carry drugs administered intravenously.

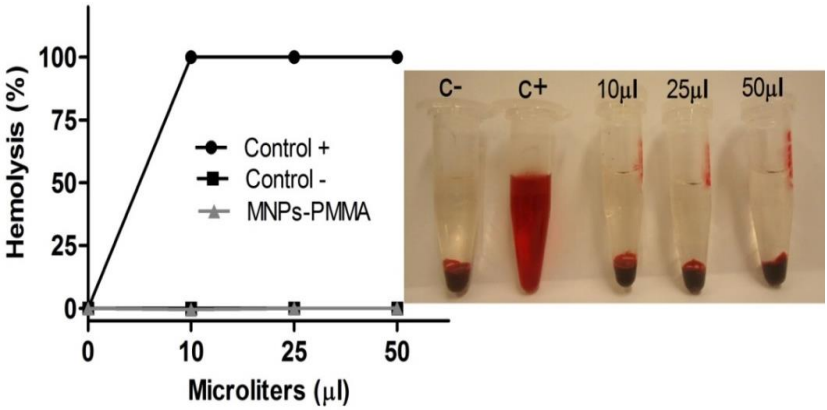

Figure 4.11 Hemolysis assay. Relative rate of hemolysis in human RBCs upon incubation with MNPs-PMMA nanoparticles at 10 µl, 25 µl and 50 µl volume. The presence of hemoglobin in the supernatant (red) was observed at 540 nm. Data are mean ± SD (n=3).

4. CONCLUSION

The encapsulation of MNPs loaded with PMMA by miniemulsion polymerization was efficient and resulted in stable MNPs-PMMA nanoparticles in aqueous dispersion, with narrow average size distribution, superparamagnetic properties and biocompatibility. The high value of Ms and superparamagnetic properties of MNPs-PMMA nanoparticles make them attractive for drug delivery to specific cells or tissues without damaging healthy cells. The *in vitro* result showed that AC magnetic field application in U87MG cells treated with MNPs-PMMA nanoparticles decreased the cells viability and resulted in a region of hypoxia. MNPs-PMMA nanoparticles presented high blood compatibility and have the potential to be used as carries of drugs in

cancer treatments, causing maximum tumor damage, with minimum side effects on healthy cells and tissues.

CHAPTER 5

SIMULTANEOUS ENCAPSULATION OF MAGNETIC NANOPARTICLES AND ZINC PHTHALOCYANINE IN POLY(METHYL METHACRYLATE) NANOPARTICLES BY MINIEMULSION POLYMERIZATION AND *IN VITRO* STUDIES

Abstract: The aim of this work was the simultaneous encapsulation of magnetic nanoparticles (MNPs) and zinc (II) phthalocyanine (ZnPc) in poly(methyl methacrylate) (PMMA) (MNPsZnPc-PMMA) nanoparticles (NPs) by miniemulsion polymerization and to evaluate the photobiological activity and/or hyperthermia (HPT) against human glioblastoma cells (U87MG). MNPsZnPc-PMMA NPs presented an average diameter of 104 ±2.5 nm with a polydispersity index (PdI) of 0.14 ±0.03 and negative surface charge - 47 ± 2.2 mV (pH 7.4 ±0.1). The encapsulation efficiency (EE%) of ZnPc was 85.7% ±1.30. The release of ZnPc from PMMA NPs was slow and sustained without the presence of burst effect, indicating a homogeneous distribution of the drug in the polymeric matrix. In the biological assay, MNPsZnPc-PMMA NPs showed considerable cytotoxic effect on U87MG cells only after activation with visible light at 675 nm (photodynamic therapy, PDT) or after application of an alternating magnetic field. The simultaneous encapsulation of MNPs and ZnPc in a drug delivery system with sustained release can be a new alternative for cancer treatment leading to significant tumor regression after minimum doses of heat dissipation and light.

Keywords: hyperthermia; miniemulsion polymerization; photodynamic therapy; polymeric nanoparticles.

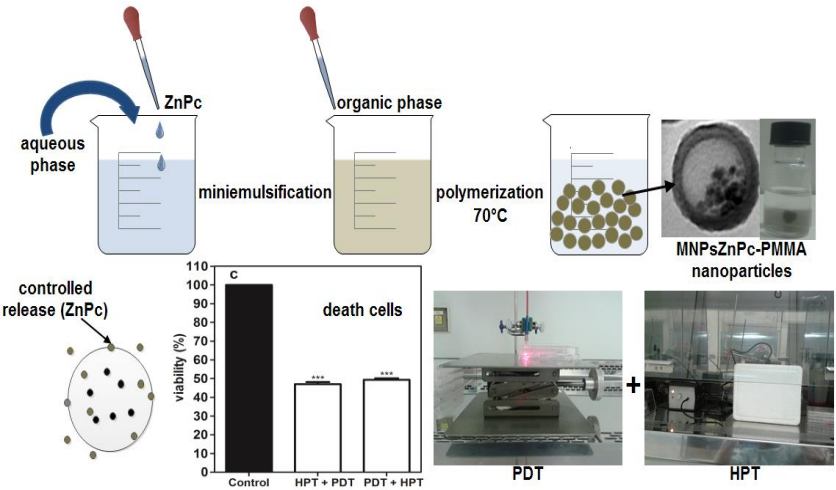

The manuscript was published in the Journal of Colloids and Surfaces B: Biointerfaces
doi: 10.1016/j.colsurfb.2015.07.067

5.1 INTRODUCTION

The development of polymeric nanoparticles (NPs) loaded with hydrophilic drugs has been attracting considerable interest in recent years for cancer treatment through targeted administration to specific tissues or cells, with controlled drug delivery (DANHIER et al, 2010; KUMARI et al, 2010). Miniemulsion polymerization allows the production of polymeric NPs with unique characteristics of great interest for biomedical applications (LANDFESTER et al, 2010). The miniemulsion polymerization technique may be an advantageous encapsulation method, including the ability to control the particle size, directly dispersing the hydrophobic inorganic particles in the monomer phase with the aid of a stabilizer, the ability to nucleate all the droplets containing inorganic particles, as well as presenting a faster polymerization and, depending on the formulation, resulting in biocompatible NPs dispersions (MAHDAVIAN et al, 2008; LANDFESTER and MAILANDER et al, 2013; QIU et al, 2007).

Poly(methyl methacrylate) (PMMA) is a biocompatible and non-biodegradable polymer prepared by miniemulsion polymerization that has been used for drug delivery (LANDFESTER et al, 2010; LANDFESTER and MAILANDER et al, 2013). Since it is non-biodegradable, it can increase the circulation time in bloodstream, reaching therapeutic index and reducing side effects of the encapsulated drugs (FU and KAO, 2010). NPs are promising delivery systems for use in photodynamic therapy (PDT) and hyperthermia (HPT). PDT consists of therapeutic approaches involving the activation of photosensitized drugs by a visible light source, always associated with the generation of cytotoxic reactive oxygen species (ROS) and other free radicals, by type I or Type II photochemistry pathaway (FOOTE, 1991), to promote the selective destruction of target tissues (MARANHO et al, 2009; NAWALANY et al, 2012; RICCI-JÚNIOR and MARCHETTI, 2006; TRIESSCHEIJN et al, 2006). An efficient photosensitizer should have a high absorption cross-section at a wavelength suitable for the desired application (SAVOLAINEN et al, 2008), normally close the maximum absorption wavelength of the drug in question, avoiding interference with natural endogenous molecules. PDT has been widely used to treat superficial tumors such as skin, head and neck tumors (PRIMO and TEDESCO, 2013; RAI et al, 2010; ROCHA et al, 2012). Zinc (II) phthalocyanine (ZnPc) is a promising second-generation photosensitizer for PDT that belongs to the phthalocyanine class due to its high optical absorption coefficient (in the range of 600-800 nm). These photosensitizers are insoluble in water, leading to self-aggregation in aqueous solutions, which drastically reduces the photosensitizing efficiency when used directly in biological fluids. To avoid these problems, an advanced drug delivery system is needed (FOOTE, 1991; NUNES et al, 2004). Several kinds of polymeric nanoparticles and polymerization methods have been used to encapsulate magnetic nanoparticles (MNPs) inside polymers (FEUSER et al, 2015; HE et al, 2009; HONG et al, 2008; LANDFESTER and MAILANDER, 2013). MNPs present low toxicity and are promising materials for cancer treatment (MUÑOS-BONILLA et al, 2012; DESHAYES and KASKO, 2013). Additionally, induced hyperthermia as a procedure for cancer treatment involves raising the temperature of tumor tissues to 40–43 °C (ABULATEEFEH et al, 2011; BASEL et al, 2012; Zee, 2002). Solid tumors have been shown to have increased susceptibility to small

temperature rises compared to healthy tissue due to their increased rate of cell cycling, increased hypoxia, reducing fluid exchange, increased acidity (pH 2-4) (BASEL et al, 2012; Zee, 2002). Therefore, the combination of hyperthermia with treatment methods like radiotherapy, chemotherapy and PDT turns these methods much more effective. The combination of HTP and PDT has produced promising results indicating synergistic interaction and significant tumor regression (BOLFARINI et al, 2012; PRIMO and TEDESCO, 2013; XU and SU, 2013). The heat released by HPT induces changes in cell cycle, causing faster denaturation of malignant cells through aggregation of nuclear proteins, thereby enhancing the sensitivity of cells denatured previously with PDT (KUMAR and MOHAMAD, 2011).

The simultaneous encapsulation of MNPs and ZnPc in the same system with controlled release is a promising new option for cancer treatment. Thus the objectives of this work were to encapsulate MNPs and ZnPc in PMMA NPs by miniemulsion polymerization and to evaluate their *in vitro* effect in the presence of alternating magnetic field and/or light on human glioblastoma cells (U87MG). These cells cause the most aggressive brain tumors, with low life cure rates after surgery associated with traditional therapies. Hence, this investigation can lead to promising new cancer treatments.

5.2 MATERIALS AND METHODS

5.2.1 Materials

For the synthesis of magnetic nanoparticles (MNPs) coated with oleic acid (OA) the following reagents were used: ferrous sulfate ($FeSO_4 \cdot 4H_2O$), iron (III) chloride hexahydrate ($FeCl_3 \cdot 6H_2O$), ammonium hydroxide (99%), and oleic acid (OA), all purchased from Vetec. For the synthesis of MNPsZnPc loaded PMMA NPs, the following reagents were employed: the monomer methyl methacrylate (MMA), purchased from Arinos; azobisisobutylonitrile (AIBN), sodium dodecyl sulfate (SDS), NaH_2PO_4 (sodium phosphate monobasic) and Na_2HPO_4 (sodium phosphate dibasic), purchased from Vetec; lecithin (Alpha Aesar); miglyol 812 (Sazol) and zinc (II) phthalocyanine (ZnPc) and n-methylpyrrolidone (NMP), both purchased from Sigma Aldrich. Distilled water was used throughout the experiments.

5.2.2 METHODS

5.2.2.1 Synthesis of magnetic nanoparticles coated with oleic acid (MNPs(OA))

MNPs(OA) were prepared by the co-precipitation method. $FeCl_3.6H_2O$ and $FeSO_4.7H_2O$ (molar ratio of 1:1) were dissolved in a beaker containing distilled water under mechanical stirring at 800 rpm. Then, ammonium hydroxide was rapidly added to the solution. After 1 hour, 20mL of OA was added and the stirring continued (800 rpm) for another 30 min. Finally the MNPs(OA) solution was centrifuged and washed with ethanol three times to remove excess OA.

5.2.2.2 Synthesis of PMMA nanoparticles

The preparation of PMMA nanoparticles via miniemulsion polymerization was the same as described by Feuser and collaborates (2014). The aqueous phase was composed of 20 mL distilled water and the organic phase contained: 2 g of MMA (monomer), 0.1 g of lecithin (surfactant), 0.1 g of miglyol (costabilizer) and 0.04 g of AIBN (initiator). The organic phase was added dropwise under high shear using sonication with amplitude of 70% (Fisher Scientific, Sonic Dismembrator, 500 W). Sonication was mantained for 5 min (10 s on, and 1 s off) in a beaker immersed in an ice bath to avoid the temperature increase during sonication. The miniemulsion was transferred to glass tubes (10 mL) at 70 °C where the polymerization took place for 3 hours under protection from light. Afterwards, the material was cooled, centrifuged and washed several times with phosphate buffered saline solution (PBS) at pH 7.4. Subsequently nanoparticles were transferred to glass vials, frozen in liquid nitrogen and lyophilized (Lyophilizer, FreeZone 4.5-L Benchtop Freeze Dry System; Labconco, Kansas City, MO). The lyophilized powder was stored at room temperature (25 °C) before analysis.

5.2.2.3 Simultaneous encapsulation of MNPs and ZnPc in PMMA NPs by miniemulsion polymerization (MNPsZnPC-PMMA)

MNPsZnPc in PMMA NPs were prepared by miniemulsion polymerization. For encapsulation of MNPs and ZnPc, initially 1 mL of

NMP containing 6 mg of ZnPc was added dropwise in a beaker containing 20 mL of distilled water (aqueous phase) under sonication with an amplitude of 70% (Fisher Scientific, Sonic Dismembrator, 500 W). Next, the organic phase (containing 2 g of MMA, 0.2 g of MNPs, 0.1 g of lecithin, 0.1 g of miglyol and 0.04 g of AIBN) was added dropwise under high shear to the previous aqueous ZnPc dispersion. The sonication was continued for 5 min (10 s on and 1 s off) in a beaker immersed in an ice bath to avoid temperature increase during sonication. The miniemulsion was transferred to glass tubes (10 mL) at 70 °C, where the polymerization took place for 3 hours under protection from light. Afterwards, the material was cooled, centrifuged and washed several times with PBS at pH 7.4. Subsequently, NPs were transferred to glass vials, frozen in liquid nitrogen and lyophilized (FreeZone 4.5-L Benchtop Freeze Dry System; Labconco, Kansas City, MO). The lyophilized powder was stored at room temperature (25 °C) before analysis.

5.3 Characterization

Monomer consumption was measured by gravimetric analysis of samples withdrawn from the polymerization medium at different times and the reaction was stopped with the addition of 1% (w/w) hydroquinone solution. The determination of the residual monomer concentration after the miniemulsion polymerization was performed by GC (Shimadzu GC2010AF). Particle size, polydispersity index (PdI) and surface charge were measured by dynamic light scattering (DLS) using a Malvern Zetasizer Nano ZS analyzer. All samples were analyzed five times, from which we calculated the average and standard deviation (SD). The NPs morphology was observed using a JEOL, JEM 2100F, transmission electron microscope (TEM) operated at 100 kV. For this analysis, several drops of the diluted sample were placed on a 200 mesh Formvar/carbon copper grid (Electron Microscopy Science). X-ray diffraction (XRD) experiments were performed to identify the crystallographic structure of free ZnPc, MNPs and MNPsZnPc-PMMA NPs. The crystalline phase of NPs was identified by XRD measurements using a XPert-Pro diffractometer, Cu-Kα radiation (45 kV/40 mA) in the 2θ range of 20-80^{o}. The average crystal size was calculated according to the Debye-Scherrer Eq. (1):

$$D = R\lambda/ß\cos\theta$$

(1)

where, D is the particle diameter, R is the Scherrer constant (0.89), λ is the wavenumber of incident X-ray beam, β is the half-maximum peak width, and θ is the diffraction angle). The average crystallite size is obtained from the most intense peak (311). MNPs(OA) and MNPsZnPc-PMMA NPs were characterized through thermogravimetric analysis (TGA) runs under nitrogen atmosphere at a heating rate of 10 °C/min. NPs chemical characterization was performed by Fourier transform infrared spectroscopy (FT-IR) using KBr pellets. A MicroSense model EV9 vibrating sample magnetometer (VSM) was used to measure the hysteresis loops of MNPs(OA) and MNPsZnPc-PMMA NPs. The encapsulation efficiency (EE) of ZnPc was determined by UV-Vis spectrophotometry. 10 mg of NPs was dissolved in NMP, the common solvent for both drug and polymer. ZnPc concentration was measured at 670 nm (visible region of the electromagnetic spectrum) using a calibration curve with different concentrations of ZnPc dispersed in NMP. The determination coefficient (R^2) exceeded 0.999, with excellent linearity (20 – 200 ng/mL). The EE% of ZnPc was calculated from Eq. (2):

$$EE\% = M_1/M_t\ x\ 100$$

(2)

where EE is the ZnPc encapsulation efficiency, M_1 is the mass of ZnPc in NPs and M_t is the mass of ZnPc used in the formulation. All samples were run in triplicate (n=3).

5.4 In vitro studies

5.4.1 Release profile

The *in vitro* release studies followed the procedure described by Ricci-Junior and Marchetti (2006). NPs (5 mg) were weighed and added to 30 mL of the receptor medium, composed of PBS (pH 7.4) and 2 wt.% SDS. The NPs suspension was continuously stirred (100 rpm) and the temperature was maintained at 37 ^{o}C in a thermostatically controlled water bath. At given time intervals, six samples (n = 6) of 3 ml were withdrawn and centrifuged at 10,000 × g for 30 min (Beckman J-25 centrifuge, USA). The precipitates were re-suspended in 3 ml of fresh medium and placed in the respective dissolution vessels.

The drug released in the receptor medium was quantified by spectrophotometry using the visible region of the spectrum (670 nm). The release profile was obtained by associating the percentage of drug released with time. The release data were fitted using the zero-order, first-order and Higuchi mathematical models, as described by Costa and Lobo (2002).

5.4.2 *In vitro* cytotoxicity assay - Cell culture

U87MG cells were seeded at $1x10^4$ cells/well in a 96-wells plate to assess the intrinsic cytotoxic effect of plain PMMA NPs and MNPsZnPc-PMMA NPs. After 24 h, U87MG cells were kept in the dark and incubated with a mixture of fresh medium and NPs at a final concentration of 50 µg of NPs, including 0.6 $\mu g.mL^{-1}$ of MNPs and 0.06 $\mu g.mL^{-1}$ of ZnPc (5% CO_2, 37 °C). After incubation, the medium containing the NPs was discarded and the cells were washed with PBS. Next, the cells were incubated with fresh medium for an additional 24 h, until the cell viability assay (MTT) was performed. Control cells were incubated with pure culture medium (untreated cells) or unloaded NPs mixed with medium, both in the dark. Cytotoxicity experiments in the dark were carried out in triplicate, with 36 wells for each condition. Murine fibroblast cells (L929) were cultivated in Dulbecco's Modified Eagle Medium (DMEM) (GIBCO, São Paulo, SP, Brazil). DMEM was supplemented with 10% fetal bovine serum (FBS) (GIBCO, São Paulo, SP, Brazil), 100 U/mL penicillin-streptomycin (GIBCO, São Paulo, SP, Brazil) and 10 mM HEPES (GIBCO, São Paulo, SP, Brazil). Cells L929 were treated with MNPsZnPc-PMMA NPs at the final concentration of 50 $\mu g.mL^{-1}$. Non-treated cells were considered as a control. Cells were incubated at 37 ^oC in a humidified atmosphere with 5% CO_2, in plastic culture flasks. The cytotoxic effect was evaluated by measuring cell viability using the MTT assay.

5.4.3 Photodynamic assay

In order to evaluate the treatment of U87MG cells *in vitro* with MNPsZnPc-PMMA NPs, the cells were seeded at $1x10^5$ cells/well in a 24-well plate. After 24 h, U87MG cells were treated with medium containing MNPsZnPc-PMMA NPs using 50 µg of NPs with 0.6$\mu g.mL^{-1}$ of MNPs and 0.06 $\mu g.mL^{-1}$ of ZnPc (5% CO_2, 37 °C). Following

incubation (3 h), the medium loaded with NPs was removed, after which the cells were rinsed with PBS (1X) and incubated with conditioned medium. After 24 h, the cells were irradiated with visible light at 0.5, 1, 3 and 5 J cm^{-2} in fresh medium without bovine serum. After the irradiation, U87MG cells were incubated (5% CO_2, 37 °C) in fresh conditioned medium for 24 h more, when the MTT cell viability assay was performed. Control cells were incubated with culture medium alone without encapsulated MNPsZnPc-PMMA NPs and PDT, or encapsulated MNPsZnPc-PMMA NPs mixed with medium (encapsulated control). The cytotoxicity assay was carried out in triplicate, with 36 wells for each condition.

5.4.4 Hyperthermia assay

To evaluate the hyperthermia treatment of U87MG cells with MNPsZnPc-PMMA NPs *in vitro*, the cells were seed at $1x10^5$ cells/well in a 24-well plate. After 24 h, the U87MG cells were treated with medium containing MNPsZnPc-PMMA NPs using 50 µg of NPs with 0.6µg.mL^{-1} of MNPs and 0.06 of ZnPc (5% CO_2, 37 °C). Following incubation (3 h), the media loaded with NPs were removed, the cells were rinsed with PBS (1X) and incubated with conditioned medium. After 24 h, the cells were treated for 3 min or 6 min with an alternating magnetic field operating at 1 MHz and 40 Oe amplitude, in the presence of fresh medium without bovine serum. The magnetohyperthermia (MHT) was carried out on a portable apparatus operating at 1 MHz with 40 Oe of field amplitude. The MHT system is composed by a metallic core with cylindrical cross-section (10.7 mm diameter) wounded by a coil of wire to concentrate the alternating magnetic flux. The solenoid core is linked to an adjustable support to apply the magnetic field in the targeted region (GUEDES et al, 2004;2005). The device details are described by patent INPI # PI 0204433-1 A2.

After the hyperthermic application, U87MG cells were incubated (5% CO_2, 37 °C) in fresh conditioned medium for an additional 24 h until the MTT cell viability assay was performed. Control cells were incubated with culture medium alone without encapsulated MNPsZnPc-PMMA NPs and magnetic field, or encapsulated MNPsZnPc-PMMA NPs mixed with medium (encapsulation control). The cytotoxicity assay was carried out in triplicate, with 36 wells for each condition.

5.4.5 Combined treatment – PDT and HPT

In order to evaluate the synergy of the PDT and HPT, the U87MG cells were treated under the same conditions described above for PDT and HPT using the MNPsZnPc-PMMA-NPs. The light dose chosen was 3 J/cm^2 and the magnetic field was applied for 6 min.

5.4.6 MTT viability assay

The cell MTT proliferation method was employed for assessment of cell viability after both the cytotoxic assays. Briefly, aliquots of 80 µl MTT solution (5 mg ml^{-1}) and 420 µl medium without phenol red were added to each well. The cells were then incubated for 4 h, at 37 °C and 5% CO_2 to allow the formazan formation reaction. Following incubation, the medium containing the MTT solution was removed and the formazan crystals were dissolved in 2-propanol. The optical density was measured at 570 and 690 nm using a Safire^2 microplate reader (Tecan Group Ltd.). Results are presented as percentage of survival, taking the control (untreated cells) as 100%.

5.5 Statistical analysis

Data are presented as the mean ± standard deviation of three determinations. One-way ANOVA followed by the Bonferroni post-hoc test were used to compare the cytotoxicity of the samples at different concentrations. Statistical analysis was performed using the Statistical Package for Social Sciences for Windows (SPSS Inc. version 13.0, USA). The statistical significance level was set at $p < 0.05$ for all analyses.

5.6 RESULTS AND DISCUSSION

5.6.1 Characterization of MNPs and ZnPc in PMMA NPs

The addition of MNPs and ZnPc in the reaction medium to prepare MNPsZnPc-PMMA NPs by miniemulsion polymerization caused a reduction in the reaction rate (Figure 5.1a). One of the reasons for the decrease in the polymerization rate was the increase of the

average particle diameter when MNPs and ZnPc were added (from 89 nm for PMMA NPs to 104 nm for MNPsZnPc-PMMA NPs), as it reduced the compartmentalization effect and the total number of free radicals present in the reaction medium (COSTA et al, 2013; FEUSER et al, 2014). Another reason was the reaction of the oxidizing initiator (AIBN) with part of the magnetite (Fe_3O_4) converting it to Fe_2O_3 reducing the concentration of AIBN from the reaction medium (COSTA et al, 2013; FEUSER et al, 2015; HONG et al, 2008). No residual monomer was detected by GC analysis after lyophilization of the MNPsZnPc-PMMA NPs, allowing application of these NPs in the biomedical field (AYDIN et al, 2002; PRADEEP et al, 2012).

Transmission electron microscopy images of the MNPs coated with oleic acid show particles with diameters between 5-13 nm (Figure 5.1b). The polymer particles formed during miniemulsion polymerization of MMA were analyzed by TEM in order to verify the encapsulation of MNPs. Since PMMA decomposes under exposure to a strong electron beam (OKUBO et al, 1999; TIARKS et al, 2001), it was possible to degrade the polymer to reveal the magnetite NPs that had been encapsulated being the MNPs attributed to the darker points in the image (Figure5.1c). The extent of degradation depends on exposure time and intensity of the electron beam resulting in the appearance of hollow PMMA nanoparticles when the TEM sample was covered with a carbon film that preserved the size and shape of the PMMA particles whereas lighter internal regions were formed during TEM analyses (STAUDT et al, 2013). As can be seen from the TEM images in Figure1C, PMMA particles contained several MNPs in most of the particles.

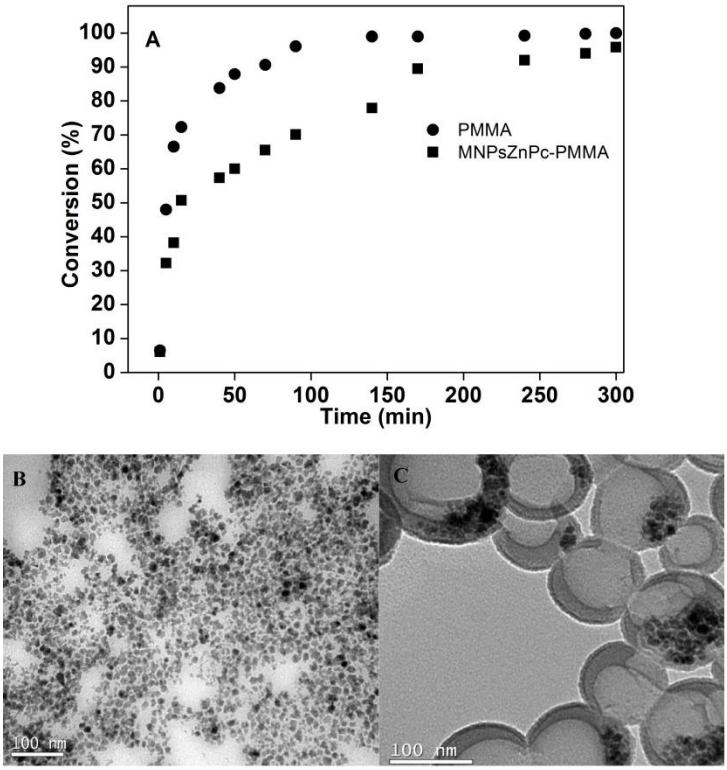

Figure 5.1 Gravimetric conversion of the PMMA and MNPsZnPc-PMMA NPs (a) and TEM images of MNPs(OA) (b) and MNPsZnPc-PMMA NPs (c).

The results of DLS analysis showed an intensity average diameter of 104nm ± 2.5 and polydispersity of 0.14 ± 0.03. The low PdI, around 0.1, indicates that the MNPsZnPc-PMMA NPs have narrow size distribution and that the osmotic pressure would be sufficient to prevent Ostwald ripening, increasing the stability of the small monomer droplets and of the miniemulsion (ASUA, 2002). TEM and DLS results show that the size distribution of the NPs is uniform, so it is likely that the dominant nucleation mechanism was the nucleation of the monomer droplets in preference to other possible mechanisms, such as micellar or homogeneous nucleation, as would be expected when employing a hydrophobic initiator (ASUA, 2002). Besides the size and morphology

of NPs, the zeta potential is another important characteristic of NPs, as it gives information about the colloidal stability and the possible interactions between NPs and the biological medium (HE et al, 2010; LANDFESTER and MAILANDER, 2010; PATIL et al, 2014;. The pH is a major factor affecting the zeta potential of a sample and therefore is an important parameter considered in the analysis. The empty PMMA NPs and MNPsZnPc-PMMA NPs exhibited negative zeta potential, -40 ± 4.3 mV and -47 ± 2.2 mV (pH 7.4 ± 0.1), respectively. The increase of the negative charge of MNPsZnPc-PMMA NPs is associated with the presence of surfactant (lecithin) and OA adsorbed on the nanoparticle surface (FEUSER et al, 2014).

X-ray powder diffraction (XRD) patterns for the naked MNPs(OA) and MNPsZnPc-PMMA NPs are shown in Figure 5.2. Figure 5.2a shows six characteristic peaks, observed at 2θ = (220), (311), (400), (422), (511) and (440) (FEUSER et al, 2015). These results demonstrate that the MNPs coated OA have the expected crystalline structure of Fe_3O_4 (FEUSER et al, 2015; PATIL et al, 2014; ZHENG et al, 2015). An additional broad peak for the ZnPcMNPs-PMMA NPs was observed at an angle between 10 and 20° due to amorphous polymer coating on the ZnPc and MNPs. Using the XRD results and Debye-Scherrer equation, the average crystallite size of MNPs was estimated at 10 nm. According to Mody and collaborates (2014), when MNPs have a critical diameter of about 5-10 nm it paves the way for them to become superparamagnetic NPs. XRD patterns of free ZnPc and PMMA are illustrated in Figure 5.2b. These data are useful in analyzing the degree of crystallinity of the MNPsZnPc-PMMA NPs. Free ZnPc exhibited a diffraction profile of crystalline material with several intense peaks. These results are similar to the results reported by Iwatsu and collaborates (1980) and Choi and collaborates (2014) for the polymorphic β-form of ZnPc. The XRD profile of free ZnPc shows a crystalline form related to β-phase of monoclinic structure. However, these peaks were not observed in the XRD patterns of MNPsZnPc-PMMA NPs. Therefore, the diffractograms of the MNPsZnPc-PMMA NPs indicate that the drug would be either molecularly dispersed in the polymers or distributed in an amorphous state or in very small crystals (LEKSHMI et al, 2010).

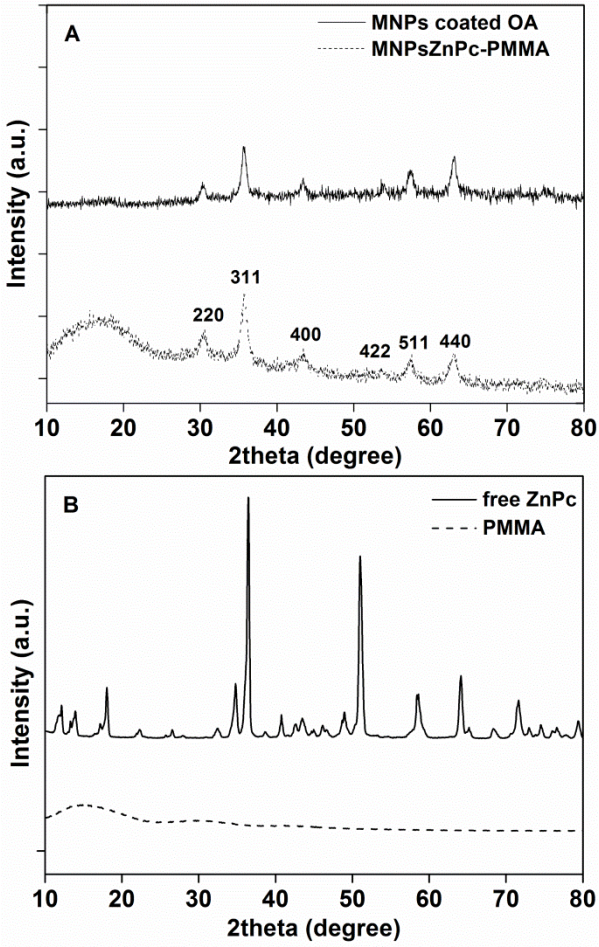

Figure 5.2 X-ray powder diffraction patterns of MNPs(OA) and MNPsZnPc-PMMA NPs (A) and free ZnPc and PMMA (B).

TGA analysis (Figure 5.3a) shows that there was no mass loss in the temperature range from 0 to 100 °C, indicating that the material is free of impurities (HONG et al, 2008). Two mass losses occurred in the MNPs(OA). The first, of 30%, occurred between temperatures of 200 and 280 ◦C, is related to free OA. The second mass loss, of about 13%,

was observed between 380 and 480 ◦C, corresponding to the OA adsorbed onto the MNPs (LANDFESTER and RAMIRES, 2013). In the case of MNPsZnPc-PMMA NPs, mass loss was gradual and it could be clearly seen that the PMMA NPs were completely degraded after reaching about 410 °C. The residual concentration of 11% corresponds to the MNPs. The other 89% correspond to the PMMA and AO present in MNPs. This analysis is very important to determine the total concentration of MNPs in the formulation. FT-IR spectrum of MNPsZnPc-PMMA NPs (Figure 5.3b) showed a band at 1736 cm^{-1} corresponding to C=O groups of PMMA. In addition, the bands in the 3000–2800 cm^{-1} region are attributed to the stretching of C–H bonds of the saturated alkane in PMMA. The peak at approximately 590 cm^{-1} corresponds to Fe-O, which is attributed to the MNPs (FEUSER et al, 2015; PATIL et al, 2014). The free ZnPc presented characteristics peaks (718, 747 and 783 cm^{-1}) of β-ZnPc (thermodynamically stable) (CHOI et al, 2014; HUSSEIN et al, 2011; IWATSU et al, 1980), corroborating with XRD analysis. The comparison between the FT-IR spectra of MNPsZnPc-PMMA NPs and free ZnPc confirmed that there is no significant interaction between ZnPc and the polymer showing that ZnPc was located in the polymeric matrix (molecularly dispersed) and not at the surface (LEKSHMI et al, 2010; ZHENG et al, 2005). These results also corroborate the XRD analysis.

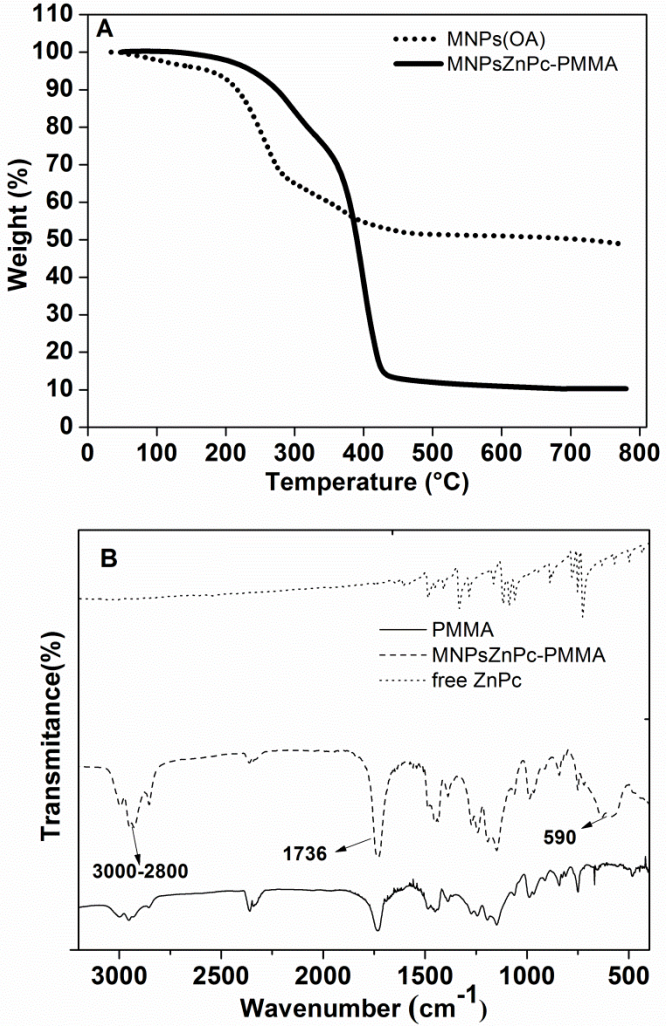

Figure 5.3 TGA analysis of MNPs(OA) and MNPsZnPc-PMMA NPs and FTIR spectrum of free ZnPc, PMMA and MNPsZnPc-PMMA NPs.

The magnetic properties of MNPs(OA) and MNPsZnPc-PMMA NPs were ascertained by VSM (Figure 5.4). Figure 5.4a shows the magnetization curves at room temperature. The MNPs coated with OA

and MNPsZnPc-PMMA NPs show typical superparamagnetic behavior at room temperature, with absence of hysteresis loop, and low value of the ratio remanent magnetization/saturation magnetization (Mr/Ms), $3.8x10^{-5}$ and $8x10^{-5}$ emu/g of MNPs and of the coercive field (Hc), 1.9 and 2.0 Oe. The superparamagnetic properties of NPs are very important for biomedical applications. In this way, without an external magnetic field, their overall magnetization value is randomized to zero, avoiding interactive behavior of the particles when there is no applied field (BATTLE and LABARTA, 2002). The Ms values in emu/g of MNPs were obtained considering the iron oxide mass determined by TGA (Figure 5.3a). The Ms value was 34 emu/g and 66 emu/g for MNPsZnPc-PMMA NPs and MNPs(OA), respectively. The decrease in Ms relative to the bulk value (Ms = 100 emu/g) may be due to oxidation processes during the sonication, leading to the formation of some nonmagnetic or low Ms iron oxide, since maghemite (γ-Fe_2O_3) has a lower Ms of 60–80 emu/g compared to 92-100 emu/g for magnetite (Fe_3O_4) (FEUSER et al, 2015; LANDFESTER and RAMIRES, 2003). MNPsZnPc-PMMA NPs presented a significant reduction of Ms compared with the bulk values, due to finite-size effects (BATTLE and LABARTA, 2002). However, this Ms value is enough for encapsulated MNPs to move quickly and be easily separated from the aqueous phase by the action of an external magnetic field gradient, as can be seen in Figure 5.4b and c. Hence, MNPsZnPc-PMMA NPs can be directed towards a specific target in the human body, with application of an external magnetic field.

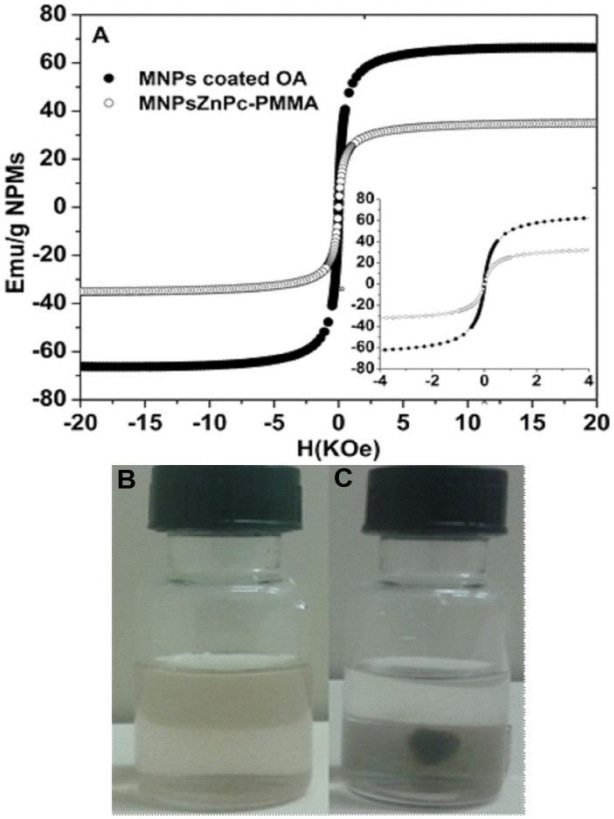

Figure 5.4 Magnetization curves of MNPs(AO) and MNPsZnPc-PMMA, for maximum applied field 20KOe and 4KOe (A). MNPsZnPc-PMMA NPs in PBS (7.4) without application of an external magnetic field (B) and with application of an external magnetic field (C).

The spectroscopic results are presented in Figure 5.5. ZnPc did not suffer changes in its basic photophysical properties after the encapsulation. The soret and Q bands remain in the same position (Figure5.5a). Free ZnPc and ZnPc simultaneously encapsulated with MNPs in PMMA nanoparticles have similar spectroscopic behavior, with maximum wavelength at 670 nm for the one of the Q bands and ZnPc presented high encapsulation efficiency (85.7 ± 1.3%). The fluorescence emission of the photosensitizers is sensitive in their

environment, yielding much information (CUCCOVIA et al, 1982). The fluorescence emission spectra shown in Figure5B, indicates the position of the maximum emission (675 nm) of the classic ZnPc emission maximum, after light excitation at 610 nm in NMP. A slight reduction in the fluorescence intensity of the MNPsZnPc-PMMA NPs was observed considering the fluorescence quenching by PMMA NPs complexes. Similar results were shown by Chen and collaborates (2006) and Maranho and collaborates (2009). However, this behavior did not change the photochemical pathway and the production of the ROS and cytotoxic free radicals as expected (ZHEN et al, 2013).

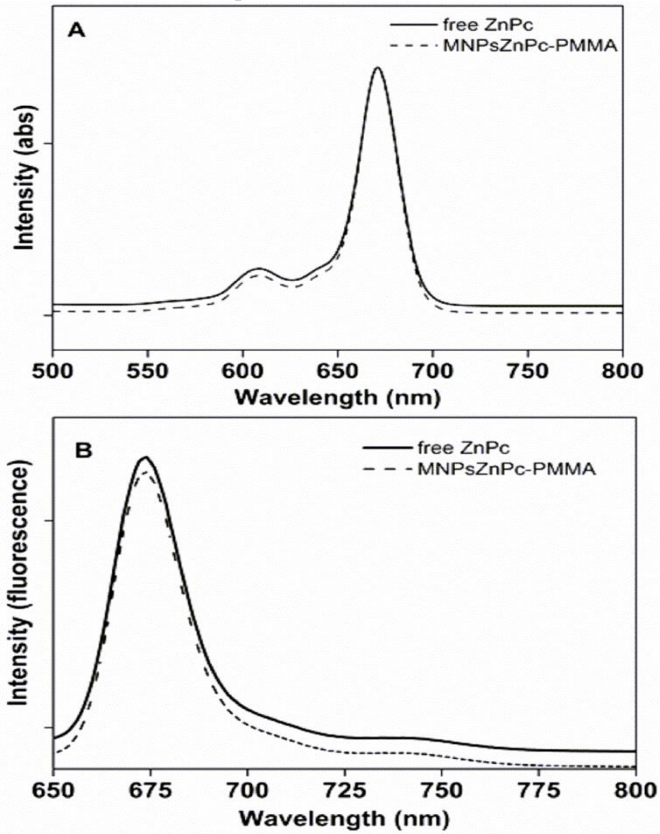

Figure 5.5 UV-Vis (a) and fluorescence spectrum (b): free ZnPc, MNPsZnPc-PMMA NPs

5.6.2 In vitro Studies

5.6.2.1 Release kinetics of ZnPc

The release kinetics of ZnPc from the PMMA NPs showed a slow and sustained release profile. The amount of ZnPc released from PMMA NPs increased from 12% after 24 hours, to 50% and 80% after, respectively, seven and twelve days (Figure 5.6). In addition, it was not detected any "burst" effect indicating that ZnPc was entrapped within the PMMA NPs and possibly homogeneously dispersed in the polymeric matrix of the NPs and not at the surface (KUMARI et al, 2010; HUANG, BRAZEL, 2001), corroborating the results previously evidenced by XRD and FTIR analyses. Thus, the results indicate that the drug release occurred by diffusion rather than desorption of the drug. The release of drugs from non-degradable polymeric delivery systems is more likely to be diffusion driven, which is associated with concentration gradient, diffusion distance and the swelling degree (FU and KAO, 2010).

The zero-order, first-order and Higuchi models were evaluated in this work. The choice of the model was made by linear correlation (R^2). The Higuchi model showed the highest values of R^2 (0.9378). This model is based on Fick's law, whereby the release occurs by the diffusion of drugs within the delivery system (MATHEW et al, 2007). These results suggest that the release of ZnPc from MNPs-PMMA NPs is controlled by diffusion.

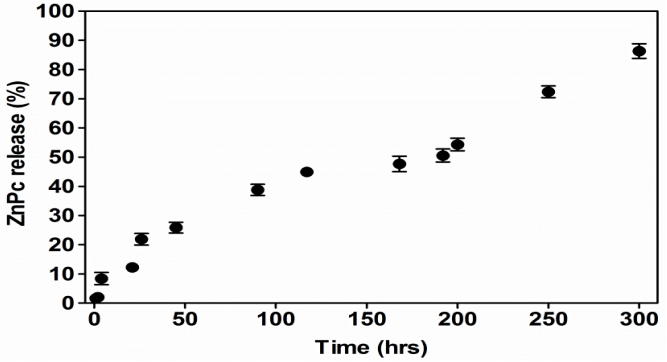

Figure 5.6 Release profiles of ZnPc in MNPs-PMMA NPs. The error bars represent the standard deviation (SD) from the mean for a triplicate experiment (n=3).

5.6.3 In vitro cytotoxicity

The biocompatibility of NPs was evaluated in L929 cells. The cells were treated with empty PMMA NPs and MNPsZnPc-PMMA NPs without magnetic field application and no light exposition, at a concentration of 50 $\mu g.mL^{-1}$ of NPs (Figure 5.7a). The NPs did not show any cytotoxic effect on L929 cells, when compared with the control group (only cells) ($p > 0.05$). These results demonstrate the biocompatibility of the NPs in the absence of both magnetic field and light, preventing toxic effects on the healthy cells (FEUSER et al, 2015; DESHAYES and KASKO, 2013).

Finally, cytotoxicity assays were performed on U87MG cells by HPT and PDT. HPT has been investigated in combination with PDT and the *in vitro* results show that HPT can act synergistically and have a photodynamic effect, which can be used for the treatment of solid tumors (BOLFARINI et al, 2012). The PDT is highly dependent on the photosensitizer's cellular uptake mechanism. In aqueous medium, free ZnPc is generally absorbed by diffusion across the plasmatic membrane leading to a low intracellular concentration. Moreover, lipophilic ZnPc tends to aggregate in aqueous medium with reduction of its photodynamic activity (DEDA et al, 2009; ISELE et al, 1995; LEVY et al, 2008). Therefore, encapsulation of ZnPc in NPs improves the phototoxicity (RIICI-JÚNIOR and MARCHETI 2006). The HPT is highly dependent on nanosize and superparamagnetic property (DEDA et al, 2009). In all *in vitro* studies of this work, the concentration was 50 µg of NPs with 0.6 $\mu g.mL^{-1}$of MNPs and 0.06 $\mu g.mL^{-1}$ of ZnPc. The *in vitro* synergic effect of both therapies and their separate application was investigated on U87MG cells. It is important to highlight that the MNPsZnPc-PMMA NPs without magnetic field application and no light exposition at a concentration of 50 $\mu g.mL^{-1}$ of NPs did not present cytotoxic effect on U87MG cells when compared with the control group (only cells). The *in vitro* cytotoxic effect of PDT was tested on U87MG cells incubated with MNPsZnPc-PMMA NPs. After incubation (3 h), the cells were irradiated using light doses of 0.5, 1.0, 3.0 and 5.0 Jcm^{-2} and a decrease in cell viability, from 76 ± 1.23 to 68 ± 0.68, with increasing light dose could be observed (Figure 5.7b). For 3.0 and 5.0 Jcm^{-2} light doses, the cell viability were very similar, therefore the lower light dose (3. 0 Jcm^{-2}) was chosen for the combined treatment. For

the HPT assay, U87MG cells were treated with MNPsZnPc-PMMA NPs under alternating (AC) magnetic field activation for 3 and 6 min (40Oe – 1 MHz). As can be seen from Figure 5.7c, the cell viability significantly decreased ($p < 0.05$) after AC magnetic field application for 3 min (72.0 ± 1.29%) and 6 min (64.8 ± 1.17%). The exposure time (3 or 6 min) to the alternating magnetic field caused a significant difference ($p < 0.05$). For the combined treatments, U87MG cells were incubated for 24 h with MNPsZnPc-PMMA NPs and exposed to light doses of 3 J/cm^2 followed by the application of the AC magnetic field for 6 min. In addition, the sequence of these treatments was also inverted, exposure to AC magnetic field followed by the application of the light doses. Figure 5.7d shows that cell viability decreased compared to that observed for the two therapies applied individually ($p < 0.05$). When the MNPsZnPc-PMMA NPs were exposed to light doses (3 J/cm^{-2}) followed the application of the AC magnetic field (6 min), the cell viability decreased to 48 ± 2.05. When the MNPsZnPc-PMMA NPs were exposed to alternating magnetic field (6 min) followed application of the light doses (3 J/cm^{-2}), the cell viability decreased to 51 ± 1.97. As can be observed, the order of the treatments (PDT and HPT or HPT and PDT) did not present a significant difference ($p < 0.05$).

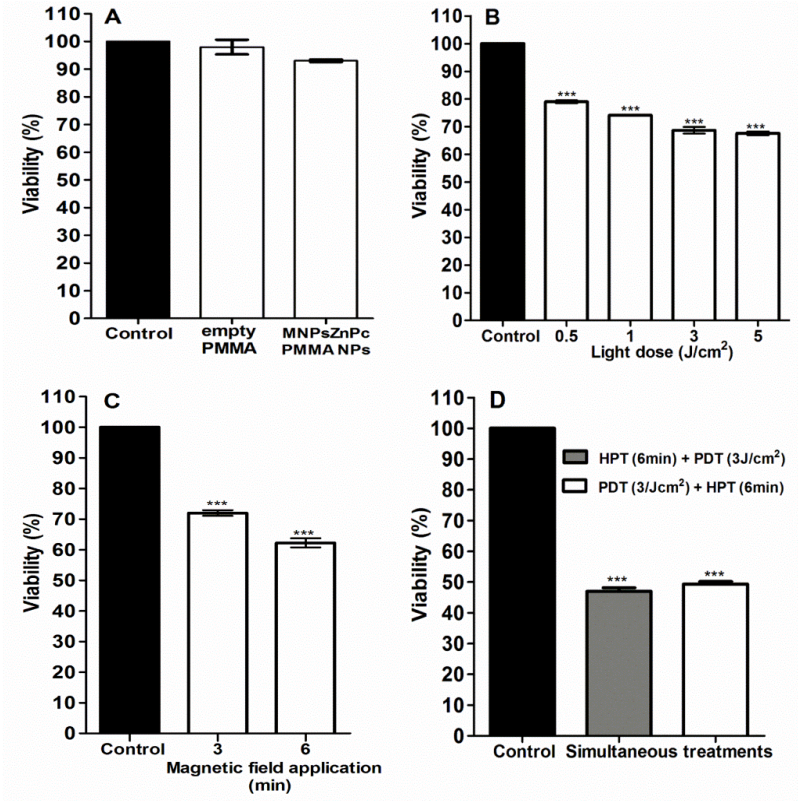

Figure 5.7 *In vitro* cytotoxicity assays in L929 cells (A). *In vitro* cytotoxicity assays of U87MG cells after treatment using MNPsZnPc-PMMA NPs irradiated with different light doses (B), after alternating (AC) magnetic field application (C) and combined therapies (D). ***$p < 0.05$ compared to control groups, using ANOVA followed by the Bonferroni post-hoc test.

5.7. CONCLUSION

The simultaneous encapsulation method of ZnPc and MNPs in PMMA NPs by miniemulsion polymerization resulted in stables MNPsZnPc-PMMA NPs, with an average size around 104 nm, superparamagnetic properties and high encapsulation efficiency of

ZnPc. The dissolution profile test shows that the release of ZnPc from PMMA NPs is slow (12 days) and the mathematical models suggest that this release is controlled by diffusion, maintaining drug release for extended periods and allowing better treatment compliance. Therefore, MNPsZnPc-PMMA NPs can be applied to PDT and HPT for sustained drug delivery. The *in vitro* results showed that the application of light dose and AC magnetic field together can be more effective than each of the two treatments applied separately. The synergistic action of PDT and HPT in a drug delivery system can lead to a significant tumor regression after minimum doses of heat dissipation and/or photosensitization by light, in contrast to conventional treatments like chemotherapy and radiotherapy, where repeated administration of high drug doses is necessary to achieve a desired pharmacokinetic profile.

CHAPTER 6

SUPERPARAMAGNETIC POLY(METHYL METHACRYLATE) NANOPARTICLES SURFACE MODIFIED WITH FOLIC ACID PRESENTING CELL UPTAKE MEDIATED BY ENDOCYTOSIS

Abstract

The encapsulation of superparamagnetic nanoparticles (MNPs) in polymeric nanoparticles (NPs) with modified surfaces can improve targeted delivery and induce cell death by hyperthermia. The goals of this study were to synthesize and characterize surface modified superparamagnetic poly(methyl methacrylate) with folic acid (FA) prepared by miniemulsion polymerization (MNPs-PMMA-FA) and to evaluate their *in vitro* cytotoxicity and cellular uptake in non-tumor cells, murine fibroblast (L929) cells and tumor cells that overexpressed folate receptor (FR) β, and chronic myeloid leukemia cells in blast crisis (K562). Lastly, hemolysis assays were performed on human red blood cells. MNPsPMMA-FA presented an average mean diameter of 135 nm and a saturation magnetization (Ms) value of 37 emu/g of iron oxide, as well as superparamagnetic behavior. The MNPsPMMA-FA did not present cytotoxicity in L929 and K562 cells. Cellular uptake assays showed a higher uptake of MNPsPMMA-FA than MNPsPMMA in K562 cells when incubated at 37 °C. On the other hand, MNPsPMMA-FA showed a low uptake when endocytosis mechanisms were blocked at low temperature (4 °C), suggesting that the MNPsPMMA-FA uptake was mediated by endocytosis. High concentrations of MNPsPMMA-FA showed hemocompatibility when incubated for 24 h in human red blood cells. Therefore our results suggest that these carrier systems can be an excellent alternative in targeted drug delivery via FR.

Keywords: superparamagnetic; nanoparticles; poly(methyl methacrylate); folic acid; cell uptake

The manuscript was was published in the Journal of Nanoparticles Research

6.1 INTRODUCTION

Due to their unique physical properties, magnetic nanoparticles (MNPs), have been widely used in various biomedical applications, such as, targeted drug delivery (ZHAO et al, 2011; ZHENG et al, 2005), hyperthermia (FEUSER et al, 2015a; KUMAR et al, 2011 SIMIONI et al, 2007), and magnetic resonance imaging (MRI) (ABULATEEFEH et al, 2011; GUPTA and GUPTA, 2005). For these applications, MNPs must have combined properties of high magnetic saturation, superparamagnetic properties and biocompatibility (KUMAR et al, 2011; ZHENG et al, 2005). MNPs represented by magnetite (Fe_3O_4) are often made in sizes smaller than 15 nm in diameter and their supepraramagnetic properties are sufficient to cause tumor cell death by hyperthermia (FEUSER et al, 2015a and 2015b). However, the use of pure MNPs for these applications are challenging due to the high surface to volume ratio and strong dipole–dipole interaction between the particles, which makes MNP agglomeration possible (KUMAR et al,. 2014; TANG et al, 2013). The agglomeration of MNPs can be attenuated with the encapsulation of MNPs in polymeric nanoparticles (NPs). The encapsulation of MNPs in polymeric NPs improves their chemical and physical stability, solubility, biological stability, target delivery and reduces the side effects of the encapsulated material (AKBARZADEH et al, 2012; FAN et al, 2009; ZHANG et al, 2011). A large number of strategies have been proposed in the literature to encapsulate MNPs in polymeric colloidal particles including, inverse miniemulsion polymerization (ROMIO et al, 2013) and direct miniemulsion polymerization (FEUSER et al, 2015a; HE et al, 2009; YAN et al, 2011).

Polymeric NPs can be prepared from natural or synthetic polymers (LANDFESTER and MAILANDER, 2013). They have been studied extensively as drugs carriers, where the main advantages are the protection of the drug, controlled release and the possibility of drug delivery within the targeted cell or tissue (LANDFESTER and MUSYANOVYCH, 2010; LANDFESTER and MAILANDER, 2013). Miniemulsion polymerization allows the production of polymeric NPs with unique characteristics of great interest for biomedical application, producing stable aqueous dispersions of droplets (50-500 nm) containing monomer, surfactant, ultrahydrophobe, initiator and water

insoluble compounds (e.g., hydrophobic MNPs) by applying high shear stress (ASUA, 2014; CRESPY and LANDFESTER 2010; HIGUCHI and MIRA, 1962; LANDFESTER 2009). The main advantage of the miniemulsion polymerization process is the ability to produce complex nanostructures, including inorganic nanoparticle encapsulation, in a single reaction step with fast polymerization rates (MAHDAVIAN et al, 2008; QUIU et al, 2007).

The NP surface modification with folic acid (FA) can increase drug uptake in tumor cells that express high levels of type α or β folate receptors (FR). The FR-α is significantly overexpressed on the surface of tumor cells, while the FR-β is overexpressed in leukemic cells and macrophages. FRs exhibit limited expression on non-tumor cells and tissues, where one of the main advantages is the targeted drug delivery by folate receptors (BHATTACHARYA et al, 2007; JIA-JYUN et al, 2009; LEE et al, 2015; WIBOWO et al, 2013; YANG et al, 2014). FR-mediated drug delivery is facilitated by endocytosis, which may enable drug delivery (CHEN et al, 2013; PENGCHENG et al,. 2009; SUDIMACK and LEE, 2000). The NPs can be internalized across a plasmatic membrane (passive diffusion) and through endocytosis (NPs are engulfed by endocytic vesicles) (WANG et al, 2012). Several *in vitro* studies have demonstrated that the modified surface of nanoparticles with FA increases the cellular uptake in tumor cells that overexpressed FR (DUAN et al, 2012; SAHOO et al, 2013; YANG et al,. 2014; ZHANG et al, 2009). However, the functionalization or adsorption of the ligands cannot ensure drug delivery when it is intravenously administered (*in vivo*). When the functionalized nanoparticles enter the bloodstream they need to cross the blood vessel endothelial cells, which do not express FR, in order to reach the interstitial space of tumor sites (CHIN and FERREIRA, 1999; ANDHARIYA et al, 2013). To overcome this, a drug delivery system with superparamagnetic properties was proposed that could be guided by external magnetic field and uptake *in vivo* by FR mediated by endocytosis (XU et al,. 2014; ZHENG et at 2005). Furthermore, MNPs can also induce cell death by hyperthermia, when external alternating magnetic fields are applied (FEUSER et al,. 2015a and 2015b; MODY et al, 2014; XU et al, 2014). In a previous study, Feuser and collaborates (2015a) showed that superparamagnetic poly(methyl methacrylate) nanoparticles obtained by miniemulsion polymerization induced

glioblastoma (U87MG) cell death when alternating magnetic fields were applied for six minutes.

The goal of this study was to synthesize and characterize superparamagnetic poly(methyl methacrylate) (PMMA) NPs obtained by miniemulsion polymerization surface modified with folic acid. *In vitro* cytotoxicity and cellular uptake assays were performed with the surface modified superparamagnetic poly(methyl methacrylate) (PMMA) with FA (MNPsPMMA-FA) and without FA (MNPsPMMA) on non-tumor cells, murine fibroblast cells (L929), cells that overexpressed FR-β, and chronic myeloid leukemia (K562) cells at two different temperatures (4 °C and 37 °C). Lastly, hemolysis assays was performed on human red blood cells.

6.2 MATERIALS AND METHODS

6.2.1 Materials

For synthesis of magnetic nanoparticles coated with oleic acid (MNPsOA), the following reagents were used (high purity grade): ferrous sulfate ($FeSO_4 \cdot 4H_2O$), iron (III) chloride hexahydrate ($FeCl_3 \cdot 6H_2O$), ammonium hydroxide (99%), and oleic acid (OA), all purchased from chemistry Vetec. For the preparation of surface modified superparamagnetic PMMA NPs with FA (MNPsPMMA-FA), the following reagents were used: methyl methacrylate (MMA) obtained from chemistry Arinos, azobisisobutyronitrile (AIBN) and folic acid (FA) purchased from chemistry Vetec, lecithin obtained from Alpha Aesar, and Crodamol GTCC (as co-stabilizer) purchased from Croda. Distilled water was used throughout the experiments.6.2.2 Methods

6.2.2.1 Synthesis of MNPsOA

MNPsOA were prepared by co-precipitation in aqueous phase methods as described by Feuser and collaborates (2015a). Momentarily, $FeCl_3.6H_2O$ and $FeSO_4.7H_2O$ (mole ratio of 1:1.2) were dissolved in a beaker containing distilled water under mechanical stirring in the range of 800 rpm. Afterwards an ammonium hydroxide solution (11 mL) was rapidly added to the solution. After 1 h, 30 mL was added to the OA and the stirring process was continued (800 rpm) for 1 h. The MNPsOA

produced was centrifuged and washed three times with ethanol to remove the unreacted OA.

6.2.2.2 Preparation of MNPsPMMA-FA by miniemulsion polymerization

For encapsulation of MNPsOA by miniemulsion polymerization, an organic phase containing 2 g of MMA with 0.4 g of MNPsOA, 0.1 g of lecithin, 0.1 g of crodamol and 0.04 g of AIBN were added to a beaker containing 20 mL of distilled water and 0.02 g of FA (aqueous phase). The organic phase was added dropwise under higher shear with an amplitude of 70% (Fisher Scientific, Sonic Dismembrator, 500 W). The high shear was maintained for 5 min (10 s on and 1 s off) in an ice bath immersed beaker to avoid an increased temperature during sonication. The miniemulsion product was transferred to glass tubes (10 mL) at 70 °C for polymerization during 3 h. Afterwards the material was cooled, centrifuged and washed three times with phosphate buffered saline (PBS) at pH 7.4. Subsequently, NPs were resuspended in 20 mL of PBS buffer. The magnetic fluid concentration used to produce the FA-MNPsPMMA was about $7x10^{16}$ particles.mL^{-1}. For a comparative study, MNPs were prepared without folic acid (MNPsPMMA). The method of preparation was the same already described by Feuser and collaborates (2105a).

6.2.2.3 Preparation of MNPsPMMA-FA by miniemulsion polymerization labeled with 6-coumarin

A highly fluorescent molecule, 6-coumarin, was dissolved in Miglyol to form a uniform solution (0.5mg.mL^{-1}). This solution (6-coumarin/Miglyol) was used in the preparation of NPs to assess cellular uptake by fluorescence microscopy. In a beaker containing 20 mL of distilled water and 0.02 g of FA (aqueous phase) the organic phase was added (10 g of MMA with 0.5 g of MNPsOA, 0.1 g of lecithin, 0.1 g of solution Miglyol/6-coumarin and 0.04 g of AIBN) dropwise under higher shear. The following steps are the same as previously described.

6.3 Characterization

Monomer consumption was monitored by gravimetric analysis of samples withdrawn from the polymerization medium at different

times and the reaction was stopped with addition of a 1 % hydroquinone (w/w) solution. The determination of the concentration of residual monomer after the polymerization reaction in miniemulsion was performed by GC (Shimadzu GC2010AF). Particle size and surface charge were measured by dynamic light scattering (DLS) using a Malvern Zetasizer Nano ZS analyzer. The NPs morphology was observed using a JEM 2100F transmission electron microscope (TEM) operating at 80 kV. Average particle size and polydispersity index (PdI) were also measured by dynamic light scattering and the surface charge of the NPs was investigated through zeta potential measurements (in both cases using the same Zetasizer). All samples were analyzed three times, from which the average and standard deviation (SD) were calculated. Chemical characterization was performed by Fourier transform infrared spectroscopy (FT-IR) using KBr pellets. X-ray diffraction (XRD) experiments were performed to identify the crystallographic structure of MNPs and MNPsPMMA-FA NPs. The crystalline phase of NPs was identified by XRD measurements using an XPert-Pro diffractometer, Cu-Kα radiation (45 kV/40 mA) in the 2θ range of 20-80^{o}. Thermogravimetric analysis (TGA) was performed. The MNPs(OA) and MNPsPMMA-FA NPs were measured through TGA runs under nitrogen atmosphere at a heating rate of 10 °C/min. A MicroSense model EV9 vibrating sample magnetometer (VSM) was used to measure the hysteresis loops of MNPs(OA) and MNPsPMMA-FA NPs. All analyses were performed at room temperature.

6.4 In vitro studies

6.4.1 Cell culture and maintenance

K562 cells were cultured in Roswell Park Memorial Institute Medium (RPMI) (GIBCO, São Paulo, SP, Brazil) supplemented with 10 % heat-inactivated fetal bovine serum (FBS), 100 U/ml penicillin, 100μg/ml streptomycin and 10 mM HEPES under 5 % CO_2 humidified atmosphere in 75 cm^2 flasks at 37 °C. Cell lines were purchased from American Type Culture Collection (ATCC, Rockville, MD, USA). L929 cells were cultured in Dulbecco's Modified Eagle's Medium (DMEM) (GIBCO, São Paulo, SP, Brazil) supplemented with 10% heat-inactivated fetal bovine serum (FBS), 100 U/ml penicillin, 100 μg/ml streptomycin and 10 mM HEPES under 5 % CO_2 humidified

atmosphere in 75 cm^2 flasks at 37 °C. Cell lines were purchased from American Type Culture Collection (ATCC, Rockville, MD, USA).

6.4.2 Viability assay (MTT assay)

The MTT cell proliferation assay was employed to assess cell viability after the cytotoxic assay. Briefly, 150µl of medium was removed and 50µl of MTT solution (5 $mg.ml^{-1}$) was added to each well. The cells were then incubated for 4 h, at 37 °C and 5% CO_2 to allow the formazan-formation reaction. Following incubation, the medium containing the MTT solution was removed, and the formazan crystals were dissolved in 2-propanol. The optical density was measured at 570 nm and 690 nm using a *Safire2* microplate reader (Tecan Group Ltd.). The results are presented as survival percentage, where the control (untreated cells) was 100%.

6.4.3 Cellular uptake by fluorescence microscopy

The intracellular fate of carrier systems marked with 6-coumarin (MNPsPMMA and MNPsPMMA-FA) were evaluated with fluorescence microscopy. L929 and K562 cells were cultured at a density of $5x10^5$ cells/mL, 200 mL/well. MNPsPMMA and MNPsPMMA-FA NPs were incubated at a low temperature (4°C), blocking receptor-mediated endocytosis mechanisms (LEAMON and LOW, 1991; GARCÍA-DÍAS et al, 2011), and at 37 °C with a concentration of 100 µg/mL. After 2 h of incubation, L929 were washed with PBS and the coverslips covering the bottom of the plate were removed and placed on a glass slide. The K562 cells were washed with PBS and placed on a glass slide. Cells were analyzed under a fluorescence microscope (Olympus BX41). Cell morphology and cellular uptake were evaluated by optical microscopy and the fluorescence of NPs was monitored by fluorescence microscopy. Cell images were acquired using emission mode with 20x objective after exciting the sample from 450 nm to 490 nm using barrier filters. Fluorescence imaging at a wavelength of 505 nm was collected. In order to quantify the 6-coumarin fluorescence, image analysis was performed using ImageJ software.

6.4.3 Hemolysis assay

In order to analyze the effect of MNPsPMMA-AF in normal red blood cells (RBC), five human blood samples were collected according to the ethics committee requirements (CEPSH n° 913/2010). Briefly, 4 mL of whole blood was added to 8 mL of a sterile solution of sodium chloride in water (saline) and the RBCs were isolated from serum by centrifugation at 10,000 × g for 5 min. The RBCs were further washed five times with saline solution, after that, the RBCs were diluted in 2 mL of saline. Then 120 µL of the diluted RBC suspension was added to 880 µL of water or saline. Samples were treated with MNPsPMMA-AF at a concentration of 50 and 100 µg.mL^{-1}. All samples were prepared in triplicate and the suspension was briefly vortexed before undergoing a gentle stirring at 37 °C for 60 min. Afterwards, the mixture was briefly vortexed again and centrifuged at 10.000 × g for 5 min. 100 µL of supernatant was transferred to a 96-well plate. The absorbance value of hemoglobin at 570 nm was measured with the reference wavelength at 540 nm. 120 µL of the diluted RBC suspension incubated with 880µL of water and saline were used as the positive and negative control, respectively (Yu et al,. 2011; Wang et al, 2009). Hemolysis percentage was calculated according to Eq. 2:

$$Hemolysis\ (\%) = \frac{\text{Sample absorbance} - \text{negative control}}{\text{positive control} - \text{negative control}}\ x\ 100$$

Eq. (2)

6.5 RESULTS AND DISCUSSION

The polymerization kinetics of NPs with and without FA obtained by miniemulsion polymerization was verified by gravimetric conversion. Analysis of residual monomer is an important parameter to be evaluated, since the total conversion of the monomer to polymer avoids possible toxic effects of the residual monomer, allowing application of the PMMA NPs in the biomedical field (BETTENCOURT and ALMEIDA, 2010; GOSAVI et al, 2010). The gravimetric conversion presented in Figure 6.1, showed that around 200 min of reaction the conversion of MNPsPMMA and MNPsPMMA-FA reached approximately 98%. As can be observed in Fig. 6.1, the

final conversion did not reach 100%, probably due to the loss of monomer (MMA) by evaporation during the emulsification and polymerization stages. Monomer evaporation can occur due to high vapor pressure of the MMA. It is important to mention that FA did not interfere in the polymerization rate.

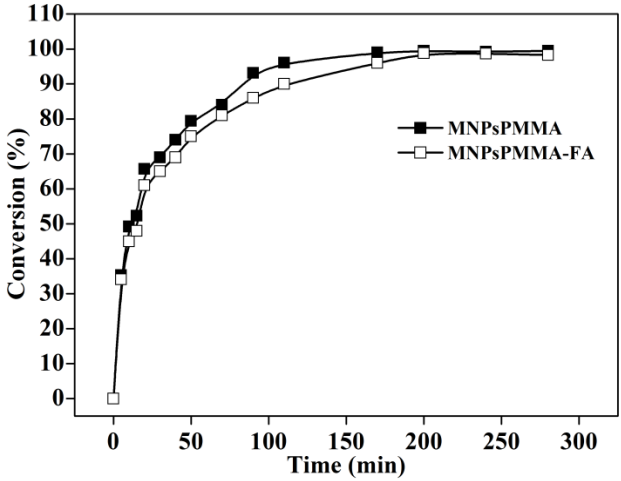

Figure 6.1 Gravimetric conversion analyses of the MNPsPMMA and MNPsPMMA-FA NPs obtained by miniemulsion polymerization.

The results of the DLS and TEM analyses are presented in Fig. 6.2. DLS analyses (Figure 6.2a and 2c) showed that the MNPsPMMA and MNPsPMMA-FA NPs have intensity average particle diameters of 104 ± 3.9 nm and 134 ± 3.5 nm, and a polydispersity index of 0.11 ± 0.02 and 0.14 ± 0.02, respectively. The FA adsorption on NPs surface increased the average size by approximately 30 nm, when compared to NPs without FA. The broadening of the particle size distribution and the increase in particle size can be attributed to the adsorption of FA on the NP surface. TEM images of MNPsPMMA-FA showed dark regions (black arrow) (Figure 6.2b and d), which are attributed to the presence of MNPs (5-13 nm in diameter) encapsulated in PMMA NPs. The MNPsPMMA-FA obtained by miniemulsion polymerization presented a sub micrometric size with a spherical morphology and unimodal size distribution. Other important factors in

the preparation of NPs for biomedical application is the zeta potential, since particle size can influence their ability to interact with cells. At pH 7.4 the zeta potential of MNPsPMMA (-37mV± 4.8) and MNPsPMMA-FA NPs (-38 mV ± 4.5) are not significantly different. The negative zeta potential can be attributed to the carboxylic groups of oleic acid and folic acid on the nanoparticle surface. The high negative values of zeta potential are related to the good colloidal stability of NPs and their possible interactions with biological medium (HE et al, 2010).

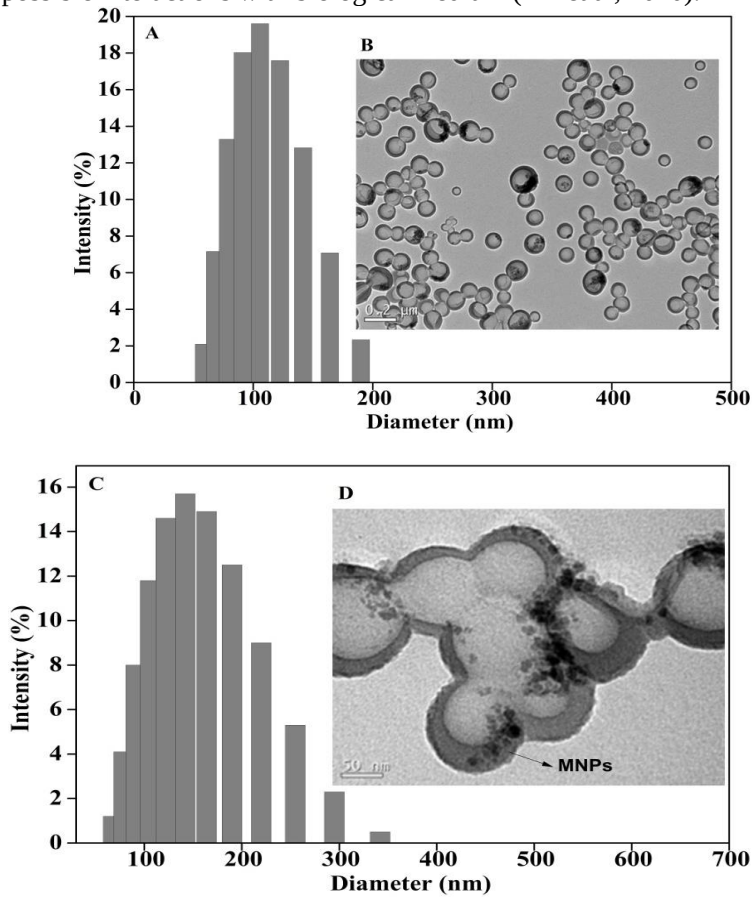

Figure 6.2 a and c Dynamic light scattering; b and d transmission electron microscopy images of MNPsPMMA and MNPsPMMA-FA NPs, respectively.

The FTIR analyses (Figure 6.3) were performed, in order to evaluate possible chemical interactions of MNPs and FA on PMMA NPs. FTIR spectrum (Figure 6.3a) showed a band at 1736 cm^{-1} corresponding to C=O groups of PMMA. In addition, the bands in the 3000–2800 cm^{-1} region are attributed to the stretching of C-H bonds of the saturated alkane in PMMA. The peak at approximately 580 cm^{-1} corresponds to asymmetric stretching vibrations of Fe-O ligands, which is attributed to the MNPs (ANDHARIYA et al, 2013; FEUSER et al, 2015a). The absorption bands at 1694 (amide I), 1603 (amide II) and 1482 cm^{-1} (ring phenyl) are characteristic peaks of FA (DUAN et al, 2012; PAN et al, 2013; SAHOO et al, 2013; YOO et al, 2013; ZHANG et al, 2007). The FTIR spectrum of MNPsPMMA-FA NPs suggested an adsorption of FA onto NPs due to the appearance of an additional band at 1694 cm^{-1}, as can be seen in Fig. 6.3b.

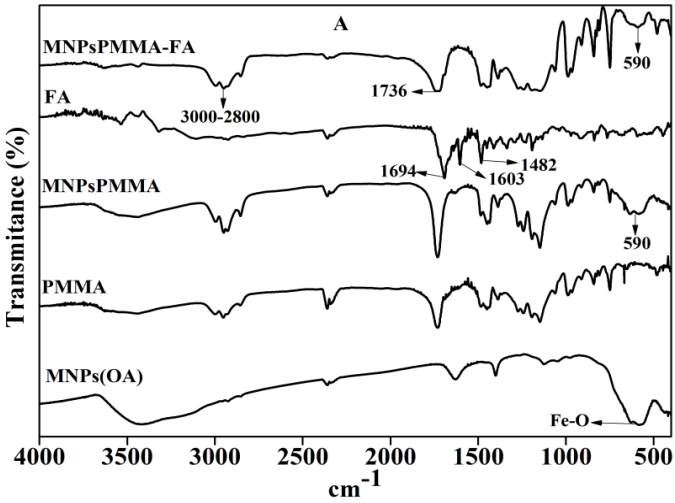

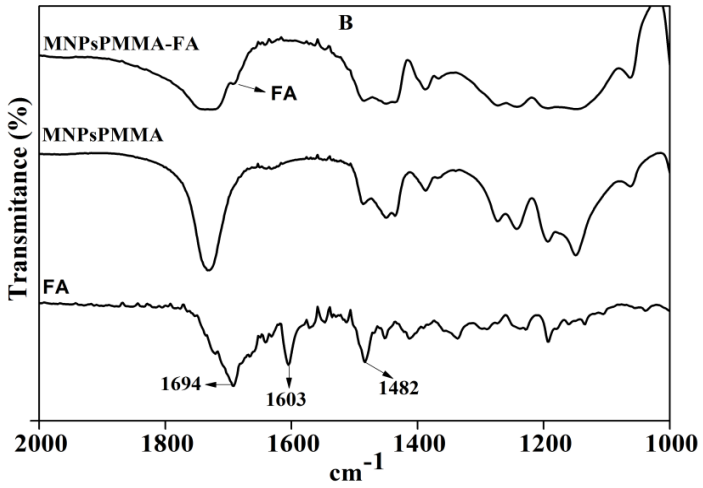

Figure 3 A FTIR spectrum: a MNPs(AO), PMMA, FA, MNPsPMMA and MNPsPMMA-FA and b FTIR spectrum at low scale: FA and MNPsPMMA-FA NPs.

X-ray diffraction (XRD) patterns for the naked MNPs(OA) and MNPsPMMA-FA NPs are shown in Figure 6.4. Figure 6.4 shows six characteristic peaks from the cubic inverse spinel structure of bulk magnetite/maghemite, observed at 2θ = (220), (311), (400), (422), (511) and (440) (DORNIANI et al, 2012; YANG et al, 2014). These results demonstrate that the MNPsPMMA-FA have the expected crystalline structure of magnetite/maghemite. An additional broad peak for the MNPsPMMA-FA NPs was observed at an angle between 10 and 20°, which are characteristic of amorphous polymers. (FEUSER et al, 2015a; SAHOO et al, 2013).

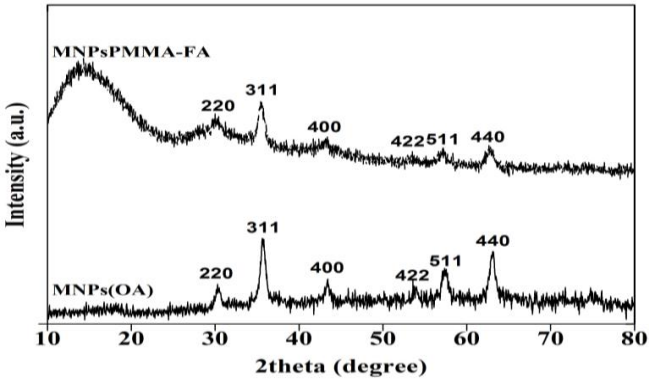

Figure 6.4 XRD powder diffraction patterns of MNPs(OA) and MNPsPMMA-FA NPs

TGA analysis was performed estimating the total concentration of MNPs in formulation. Figure 6.5 showed mass loss in the temperature range from 20 to 220 °C, which can be attributed to the evaporation of water. (NAN et al, 2013). The weight loss between 230 and 420 °C correspond to the polymer PMMA, which are completely degraded when reaching approximately 410 °C, co-stabilizer (Crodamol), OA and FA contribute to the major portion of the total weight. (FEUSER et al, 2015a ; LANDFESTER and RAMIRES 2003; MOHAPATRA et al, 2007). The residual weight of 16% corresponds to the encapsulated MNPs.

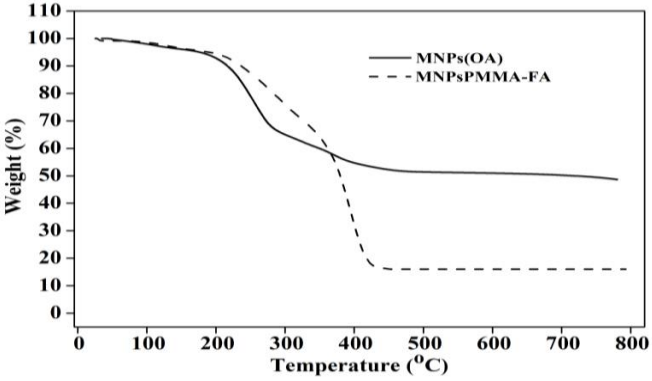

Figure 6.5 TGA analyses of MNPsOA and MNPsPMMA-FA NPs.

The magnetic properties of MNPs(OA) and MNPsPMMA-FA NPs were ascertained by VSM (Figure 6.6). The encapsulation of MNPs in PMMA NPs with FA modified surface showed typical superparamagnetic behavior at room temperature (Figure 6a and b), with the absence of hysteresis loop and a low remanent magnetization/saturation magnetization (Mr/Ms) ratio value, and a coercive field (Hc) of $5.0x10^{-2}$ and 0.4, respectively (CHANDRASEKHARANA et al, 2011; MODY et al, 2014; NAN et al, 2013; YANG et al, 2014). The superparamagnetic properties are very important for biomedical field. Thus, when an external magnetic field is not applied, their overall magnetization value is randomized to zero, avoiding the interactive behavior of the nanoparticles (Mody et al, 2014). The value of magnetization saturation (Ms) in emu/g of MNPs was obtained considering the iron oxide mass determined by TGA (Figure 5). The Ms value was 37 emu/g and 66 emu/g for MNPsPMMA-FA NPs and MNPs(OA). The decrease in Ms value can be attributed to the dense coating of PMMA, as well as oxidation processes during the sonication, leading to the formation of some nonmagnetic or low Ms iron oxide, since maghemite (γ-Fe_2O_3) has a lower Ms of 60–80 emu/g compared to 92-100emu/g for magnetite (CHANDRASEKHARANA et al,. 2011; FEUSER et al,. 2015b; LANDFESTER and RAMIRES 2003). However, this Ms value was enough to move encapsulated MNPs quickly and can be easily separated from the aqueous phase by the action of an external magnetic field gradient, which can be seen in Fig. 6.6c and 6d. Hence, MNPsPMMA-FA NPs can be directed towards a specific target in the human body, with application of an external magnetic field.

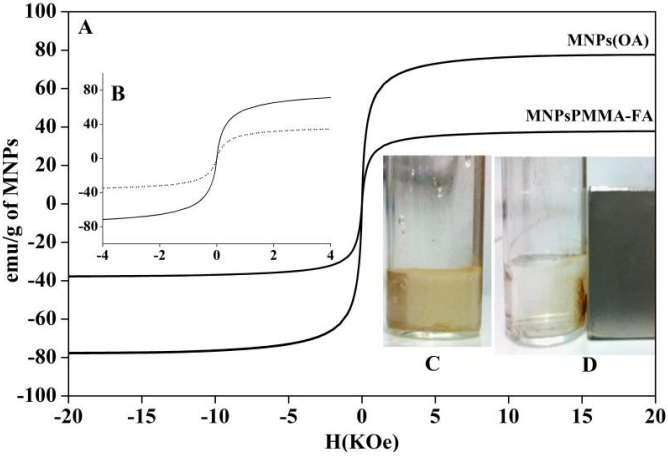

Figure 6.7 Cytotoxicity assay. Cytotoxicity effects of different concentrations of MNPsPMMA-FA on L929 and K562 cells exposed 24h. The cell viability was monitored through MTT assay. ($p>0.05$) using one-way ANOVA followed by post-test Bonferroni's.

Fluorescence microscopy assay was performed in order to evaluate the morphology and cellular uptake on L929 (non-tumor) and K562 (tumor) cells overexpressing FR-β (SHI et al, 2013). The cells were treated with 13 ug.mL^{-1} of MNPsPMMA-FA and MNPsPMMA at two different temperatures (4°C and 37°C). As can be seen in Figure 8, L929 and K562 cells incubated for 24 h at 37 °C and 4 °C, and did not present significant changes in their morphology. The cellular uptake assays showed a higher internalization of MNPsPMMA-FA than MNPsPMMA at 37°C in K562 cells, which can be shown by their bright fluorescence (Figure 6.8). These results were corroborated with the quantification of fluorescence, which showed a significant increase in fluorescence intensity of MNPsPMMA-FA when compared with MNPsPMMA. These increases in cellular uptake suggested that MNPsPMMA-FA entered into cancer cells by folate receptor-mediated endocytosis (GARCÍA-DÍAS et al, 2011; KAM et al, 2005; ZHENG et al, 2014). On the other hand, when folate receptor-mediated endocytosis was blocked by low temperature at 4 °C, there was no significant difference in cellular uptake, as can be seen in Figure 6.8 and Figure 6.9. However, when L929 cells were used, similar results were observed for

L929 cells at 37 °C and 4 °C (Fig. 6.8 and Fig. 6.9). These results were expected for L929 cells, since they do not express FR, suggesting that the NPs entered into cells by energy-independent mechanisms (KAM et al, 2005; ZHENG et al, 2014). All endocytosis pathways are energy and temperature dependent mechanisms, which involve the uptake of NPs in small invaginations of membrane vesicles (RASTOGI et al, 2014). Finally, our results showed that the superparamagnetic PMMA NPs with an FA modified surface are possibly an attractive target for cancer selective delivery by FR (MORIYAMA et al,. 1986; MOULIN et al, 2007; QI AND RATNAM, 2006; VAN DER HEIJDEN et al, 2009; WIBOWO et al, 2013).

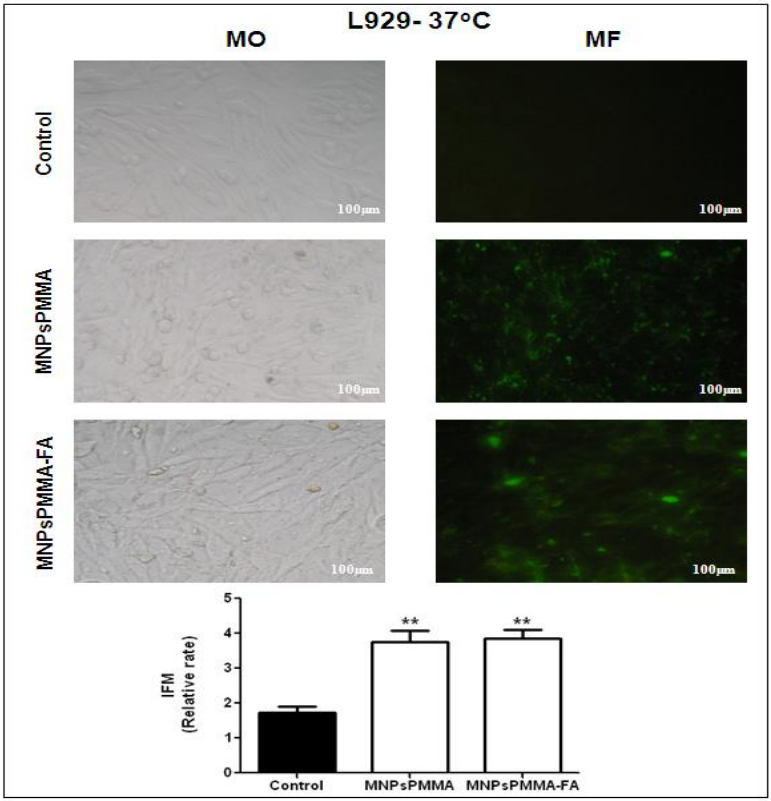

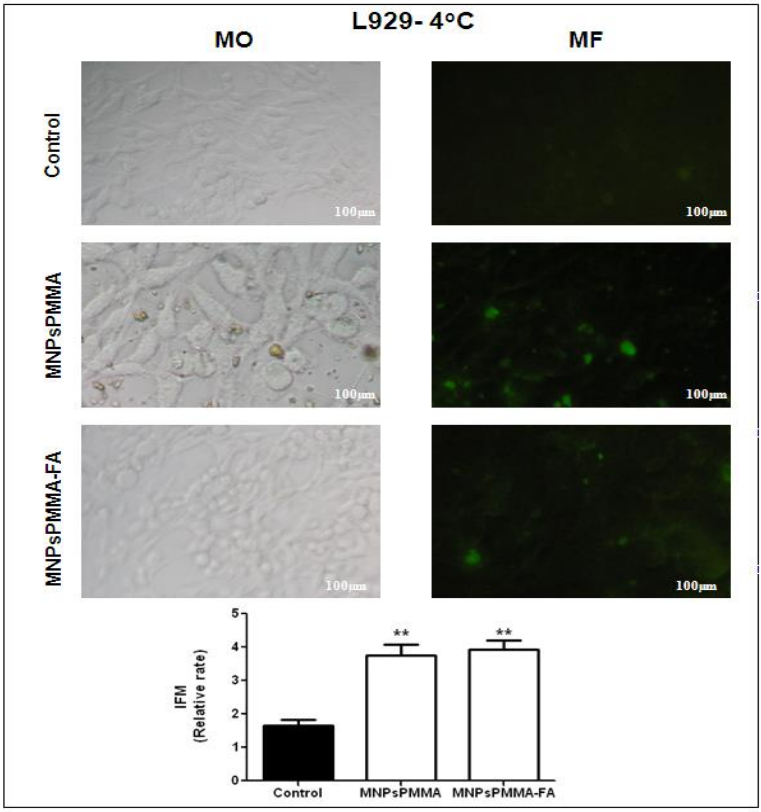
L929- 4°C
MO
MF
Control
MNPsPMMA
MNPsPMMA-FA
100μm
IFM
(Relative rate)
0
1
2
3
4
5
**
**
Control
MNPsPMMA
MNPsPMMA-FA

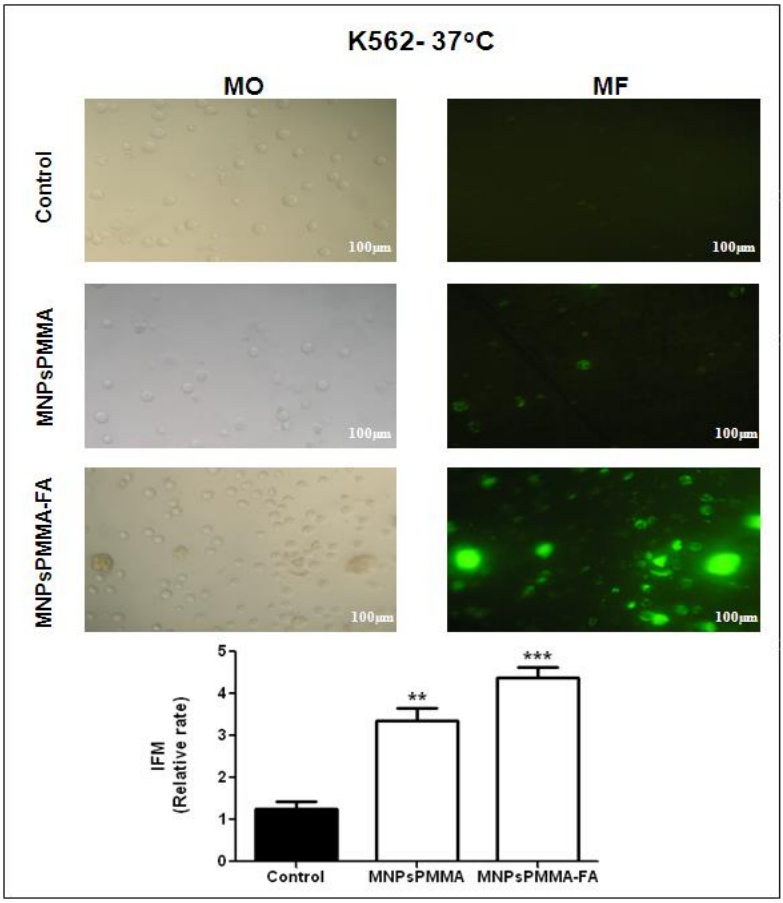
K562- 37°C
MO
MF
Control
MNPsPMMA
MNPsPMMA-FA
100µm
IFM
(Relative rate)
0
1
2
3
4
5
**
***
Control
MNPsPMMA
MNPsPMMA-FA

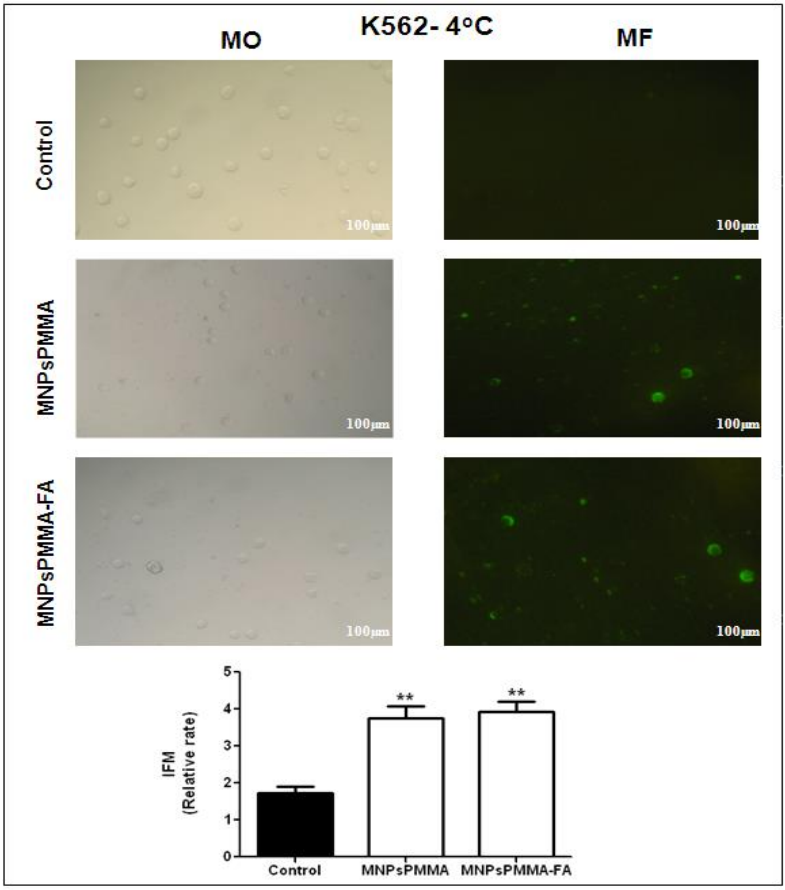

Figure 6.8 Optical and fluorescence microscopy images of L929 and K562 cells. The cells were treated with MNPsPMMA or MNPsPMMA-FA at concentration of 100 µg.mL^{-1} and incubated at 37 °C or at 4 °C for 2 h, after this period the cell morphology was evaluated by optical microscopy and the fluorescence of NPs was monitored by fluorescence microscopy (Olympus BX41).

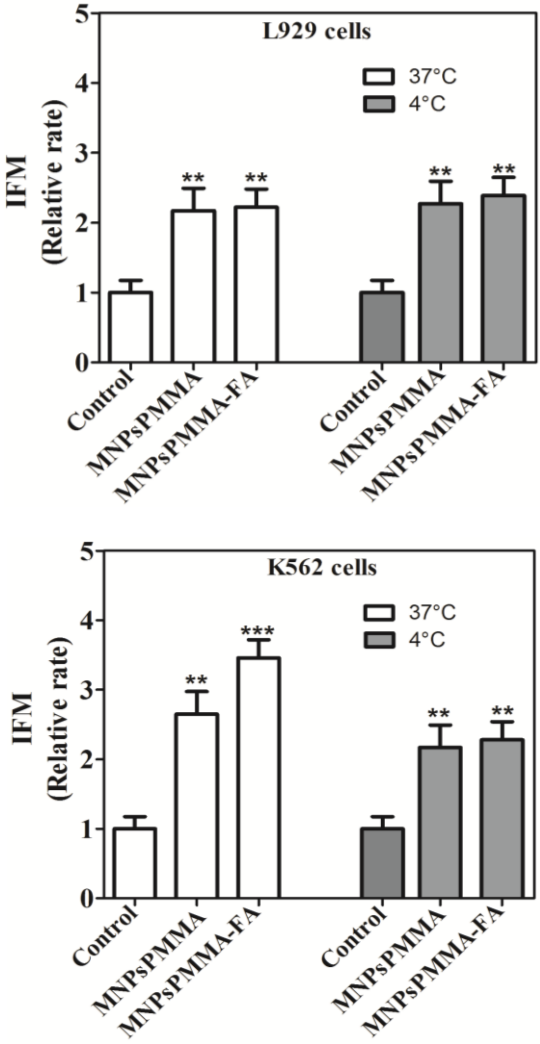

Figure 6.9 Quantification of fluorescence intensity by ImajeJ software. Cells (K562 and L929) were incubated with MNPsPMMA and MNPsPMMA-FA NPs at 37 °C and 4 °C for 2 h, labeled with 6-coumarin at concentration of 100 μg/mL. (**$p < 0.01$, ***$p < 0.001$) using one-way ANOVA followed by Bonferroni's post-test.

In order, to evaluate the biocompatibility on human red blood cells, hemolysis assays were carried out, which can be seen in Figure 6.10. The hemolysis assay is an important test to assess cytotoxicity in red blood cells (CHEN et al, 2012; ZHOU et al, 2011). According to the criterion of Standard Test Method for Analysis of Hemolytic Properties of Nanoparticles (ASTM E2524-08), a percentage hemolysis > 5% indicates that the test material causes damage. As can be seen in Figure 10, high concentrations of MNPsPMMA-FA incubated for 24 h with human red blood cells, did not exceed 5%. The non-hemolytic character confirms the hemocompatibility of NPs obtained by miniemulsion polymerization, which can be an alternative for drug delivery systems administered systemically for leukemic treatment.

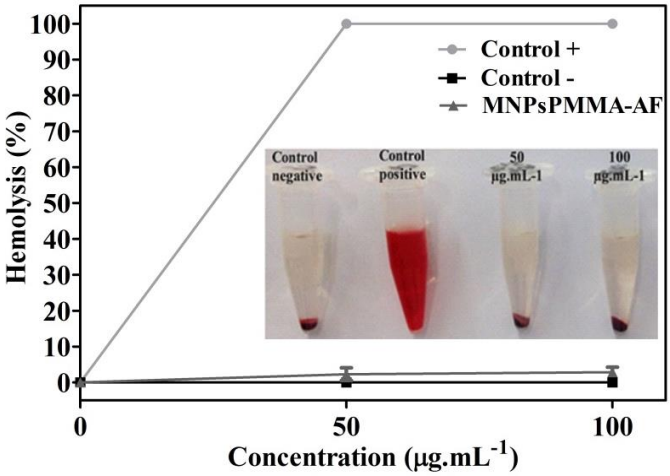

Figure 6.10 Hemolysis Assay of MNPsPMMA-FA. Relative rate of hemolysis in human RBCs upon incubation with MNPsPMMA-FA at concentration of 50 and 100 µg.mL^{-1}. The presence of hemoglobin in the supernatant (red) was observed at 540 nm. Data are mean ± SD (n=3).

6.6 CONCLUSION

The synthesis of surface modified superparamagnetic PMMA with FA obtained by miniemulsion polymerization resulted in a stable

polymeric system in aqueous dispersion, with good polydispersity index and biocompatibility. MNPsPMMA-FA presented a significant increase in the K562 cell uptake at 37°C, when compared with the MNPsPMMA, suggesting that it enters into cancer cells by folate receptor-mediated endocytosis. When the MNPsPMMA-FA were incubated at 4°C, there was a reduction in cellular uptake, demonstrating that the mechanism of entering into K562 cells is energy dependent (endocytosis). The hemolysis assay demonstrated the hemocompatibility of MNPsPMMA-FA, which can be administered at 100 µg/mL without causing any damage to human red blood cells. Moreover, other studies are being performed, such as, drug encapsulation for cancer treatment and cellular uptake assays to improve and understand the entering mechanism of these NPs in cells overexpressing FR-α and FR-β.

CHAPTER 7

SYNTHESIS OF FOLIC ACID-SUPERPARAMAGNETIC POLY(METHYL METHACRYLATE) NANOPARTICLES LOADED WITH LAURYL GALLATE BY MINIEMULSION POLYMERIZATION AND *IN VITRO* STUDIES

Abstract: The goals of this study were to synthesize and characterize superparamagnetic poly(methyl methacrylate) (PMMA) nanoparticles (NPs) loaded with G12 (MNPsG12PMMA) and folic acid (FA) adsorbed on NPs (FA-MNPSG12PMMA) obtained by miniemulsion polymerization (MNPsG12PMMA-FA). *In vitro* cytotoxicity assay on L929 (murine fibroblast), HeLa (uterine colon cancer), and human red blood cells were performed. Lastly, an uptake cellular assay was performed, in order to verify the uptake of MNPsG12PMMA and FA-MNPsG12PMMA NPs into HeLa cells. FA-MNPsG12PMMA and MNPsG12PMMA presented an average mean diameter of 129 nm and 105 nm, respectively, with a saturation magnetization value of 38 emu/g of iron oxide and superparamagnetic behavior. FA-MNPsG12PMMA and MNPsG12PMMA did not present any cytotoxicity effects on L929 and human red blood cells at the doses used, but significantly inhibited HeLa cell growth with a biphasic release profile. However, free G12 presented cytotoxic effects on non-tumor cells and red blood cells. Cellular uptake assays demonstrated a higher uptake of FA-MNPsG12PMMA than MNPsG12PMMA when HeLa cells were incubated at 37 °C. On the other hand, when the NPs were incubated at low temperature (4 °C) no cellular uptake was observed, suggesting that the NPs are internalized by energy-dependent mechanism. The higher cellular uptake of FA-MNPsG12PMMA (2 times) after 24h of incubation in HeLa cells, suggests that those targeted Folate receptor-mediated endocytosis. Therefore our results suggest that these carrier systems prepared with NPs can be an excellent alternative in targeted drug delivery by FR and in protection drugs, preventing possible toxic effects of free drug.

Keywords: folic acid, lauryl gallate, polymeric nanoparticles, superparamagnetic, folate receptor.

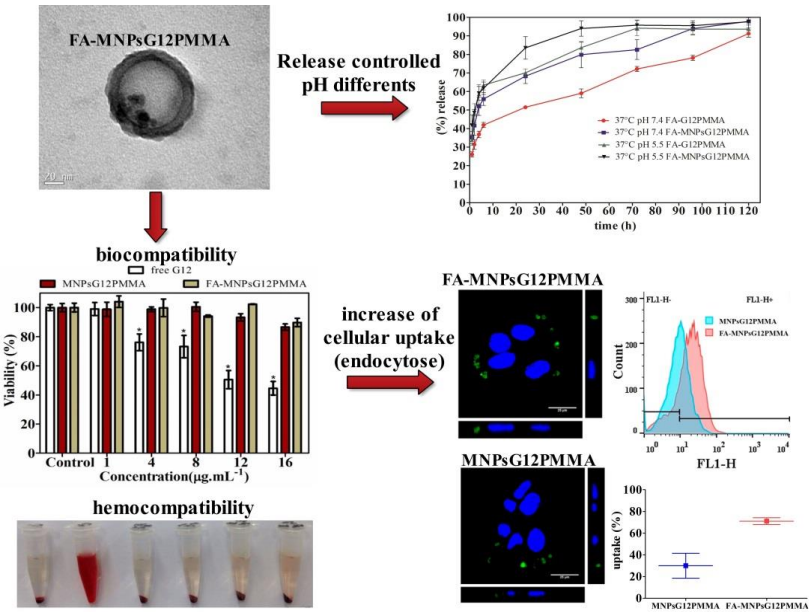

The manuscript was submitted

7.1 INTRODUCTION

Folic acid (FA) is a water-soluble vitamin and it has been *targeted* for therapy *drugs* in oncology (SCOMPARIN et al, 2015; SAHOO et al, 2013). The folate receptor is significantly overexpressed on the surface of different human cancer cells (DONG et al, 2014; LICCIARDI et al, 2005; SALTAN et al, 2011; SCOMPARIN et al, 2015). Folate receptor-mediated drug delivery is based on conjugation with FA, which is internalized by folate receptor-mediated endocytosis (CHEN et al, 2012; ANDHARIYA et al, 2013; PENGCHENG et al, 2013). The main advantage of FA adsorption or functionalization in polymeric nanoparticles (NPs) is their absent expression on non-tumor cells (LICCIARDI et al, 2005; SALTAN et al, 2011). However, the functionalization cannot ensure the delivery of the drug when it is

intravenously administered (*in vivo*). When the drug is administered in the bloodstream, the following occurs: distribution in the vascular space; penetration through the microvascular wall; movement through the interstitial space; interaction with the cell surface, and lastly cellular uptake (CHIN and FERREIRA, 1999). However, the transfer of bloodstream to the interstitial space of tumor sites is done through blood vessel endothelial cells that do not express the tumor-specific antigens (ANDHARIYA et al, 2013). In order to overcome these difficulties the preparation of a drug delivery system with superparamagnetic properties can be an attractive option in cancer treatment, in which the drug could be guided by an external magnetic field and internalized *in vivo* by receptor-mediated endocytosis (SALTAN et al, 2011, XU et al, 2013). Furthermore, the application of an external magnetic field can also induce cell death by hyperthermia (GUPTA and GUPTA 2005; XU et al, 2013; FEUSER et al, 2015b, 2015c). Magnetic nanoparticles (MNPs) have been widely used in various biomedical applications, due their excellent biocompatibility (GUPTA and GUPTA 2005; LAURENT et al, 2010; TEJA et al, 2009). For medical field applications, MNPs must have combined properties of high magnetic saturation, superparamagnetic properties and biocompatibility (KUMAR 2011; ZHENG et al, 2005).

Several strategies have been proposed in the literature to encapsulate MNPs in NPs via *in situ* polymerization (CHIARADIA et al, 2015; He et al, 2009; FEUSER et al, 2015b). Miniemulsion polymerization allows the production of polymeric NPs with unique characteristics, which is of great interest in biomedical applications (LANDFESTER and MAILANDER, 2010). The miniemulsion polymerization technique may be an advantageous encapsulation method, which can control particle size, directly dispersing the hydrophobic inorganic particles into the monomer phase with the aid of a stabilizer, it has the ability to nucleate all the droplets containing inorganic particles, faster polymerization rate and biocompatibility (LANDFESTER, MUSYANOVYCH, MAILANDER, 2010; MAHDAVIAN et al, 2008; QUIU et al, 2007).

The encapsulation of anticancer drugs in polymeric NPs with superparamagnetic properties can be an excellent strategy in cancer treatment, ensuring selective drug delivery and reducing side effects (DONG et al, 2014; LAPINA et al, 2013; MODY et al, 2014). Gallic

acid (GA) is a natural antioxidant, which is obtained from the hydrolysis of natural plant polyphenols (OW and STUPANS, 2003; WANG et al, 2007). GA and its ester derivatives, such as octyl (G8) and lauryl gallate (G12), have been shown to be involved in a wide variety of biological actions. The biological activity of GA and its derivatives has been described in the literature as antimalarial (KLEIN and WEBER 2001), antioxidant (GRUNDHOFER and NIEMETZ, 2007; OW and STUPANS, 2003), anticancer (Zhao and Hu, 2013) and antibacterial (MANNA and KUO, 1999). The only difference among the ester derivatives is found in the number of carbon atoms in the aliphatic side chain, giving them different physicochemical characteristics, especially lipophilicity evaluated by the partition coefficient value (LOCATELLI et al, 2013; OW and STUPANS, 2003; ROSSO et al, 2006). These ester derivatives, especially those with eight or more carbon atoms in the side-chain, were more efficient than GA in antiviral, antifungal, antioxidant and antitumoral activities (CORDOVA et al, 2011; LOCATELLI et al, 2013). These many biological activities have been correlated to the amphipathic character by increasing the cell membranes affinity and permeability (SAEKI et al, 2000; LOCATELLI et al, 2013). Although some of these ester derivatives showed a high cytotoxic activity, the chemical derivatization decreased their water solubility, constituting a disadvantage for intravenous administration (STELLA et al, 2007). According to Ximenes and collaborators (2010), GA and ester derivatives could interact and disrupt the erythrocyte membrane, another disadvantage for systemic administration. Another disadvantage involving *in vivo* administration of GA is poor pharmacokinetic profile (low bioavailability) (ALVES et al, 2016). Therefore the encapsulation of G12 in superparamagnetic polymeric nanoparticles (NPs) can increase site-specific drug concentration (increased bioavailability), reduce toxic effects on non-tumor cells or tissues, protecting and preventing possible aggregation of encapsulated drugs (DANHIER et al, 2012; SULISTIO et al, 2011). In addition, NPs can improve intravenous administration, when it is dispersed in an aqueous medium, providing an excellent strategy for cancer treatment (ORTEAG et al, 2011; SULISTIO et al, 2011).

With the aim of improving target drug delivery, we synthetized and characterized superparamagnetic poly(methyl methacrylate) (PMMA) nanoparticles loaded with G12 (MNPsG12PMMA) and FA

adsorbed in NPs (FA-MNPsG12PMMA) by miniemulsion polymerization. The nanocarriers were developed and their polymeric structure characterized as: morphology by transmission electron microscopy; average particle size and polydispersity index; zeta potential; Fourier-transform infrared spectroscopy; thermogravimetric analysis; and determination of the superparamagnetic properties. A release study was performed to evaluate the profile and release kinetics. I*n vitro* cytotoxicity, biocompatibility and uptake assays were performed.

7.2 MATERIALS AND METHODS

7.2.1 Materials

For synthesis of magnetic nanoparticles coated with oleic acid (MNPsOA), the following reagents were used (high purity grade): ferrous sulfate ($FeSO_4 \cdot 4H_2O$), iron (III) chloride hexahydrate ($FeCl_3 \cdot 6H_2O$), ammonium hydroxide (99%), and oleic acid (OA), all purchased from Vetec. For the preparation of NPs, the following reagents were used: methyl methacrylate (MMA), obtained from Arinos Química Ltda, azobisisobutyronitrile (AIBN) and FA purchased from Vetec. G12 obtained from sigma-aldrich, lecithin obtained from Alpha Aesar and Crodamol (as co-stabilizer) purchased from Croda. Distilled water was used throughout the experiments.

7.2.3 Methods

7.2.3.1 Synthesis of magnetic nanoparticles coated with oleic acid (MNPs-OA)

MNPs-OA nanoparticles were prepared by co-precipitation as described by Feuser and collaborators (2015b). Briefly, $FeCl_3.6H_2O$ and $FeSO_4.7H_2O$ (mole ratio of 1:1.2) were dissolved in a beaker containing distilled water under mechanical stirring in the 800 rpm range. Then an ammonium hydroxide solution (11 mL) was rapidly added to the solution. After 1 h, 30 mL was added to the OA and the stirring process continued (800 rpm) for 30 min. The MNPs-OA produced were

centrifuged and washed three times with ethanol to remove unreacted OA.

7.2.3.2 Preparation of MNPSG12PMMA nanoparticles

MNPsG12PMMA nanoparticles were prepared through miniemulsion polymerization. The simultaneous encapsulation of MNPs and G12 was the same as described by Feuser and collaborators (2015c). Initially 1 mL of NMP containing 40 mg of lauryl gallate was added dropwise into a beaker containing 20 mL of distilled water (aqueous phase) under sonication with an amplitude of 70% (Fisher Scientific, Sonic Dismembrator, 500 W). Then, the organic phase containing 2 g of MMA (monomer) coated with 0.2 g of MNPs (magnetic nanoparticles), 0.1 g of lecithin (surfactant), 0.1 g of miglyol (costabilizer) and 0.04 g of AIBN (initiator) was added dropwise under higher shear to the previous aqueous lauryl gallate dispersion. The sonication was continued for 5 min (10 s on and 1 s off) in a beaker immersed in an ice bath to avoid a temperature increase during sonication. The miniemulsion was transferred to glass tubes (10 mL) at 70 °C, where polymerization took place for 3 hours under light protection. Afterwards, the material was cooled, centrifuged and washed several times and ressupended with phosphate buffered saline (PBS) at pH 7.4. The polymeric NP suspension was stored at room temperature.

The process for the preparation of NPs loaded with G12 (G12PMMA) was similar to the method described for MNPsG12PMMA (described above), however, MNPs were not added in the organic phase.

7.2.3.3 Preparation of FA-MNPsG12PMMA nanoparticles

FA-MNPsG12PMMA nanoparticles were prepared by miniemulsion polymerization. Initially 1 mL of NMP containing 40 mg of lauryl gallate was added dropwise into a beaker containing 20 mL of distilled water and 0.002 g of FA (aqueous phase) under sonication with an amplitude of 70% (Fisher Scientific, Sonic Dismembrator, 500 W). Next, the organic phase (containing 2 g of MMA (monomer) coated with 0.2 g of MNPs, 0.1 g of lecithin (surfactant), 0.1 g of miglyol (costabilizer) and 0.04 g of AIBN (initiator) was added dropwise under higher shear to the previous aqueous lauryl gallate dispersion. The next steps are the same as previously described. For the preparation of G12

loaded in PMMA NPs with FA adsorbed in NPs (FA-G12PMMA) the procedure was the same (without the addition of MNPs in the organic phase).

The preparation of FA adsorbed in PMMA NPs (FA-PMMA) was similar to that described by Feuser and collaborators (2014). The difference is the addition of FA (0.002 g) in the aqueous phase.

7.2.4 Characterization

The NPs morphology was observed using a JEM 2100F transmission electron microscope (TEM) operating at 100 kV. For TEM analysis, several drops of the diluted sample (1:10) was placed on a 200 mesh Formvar/carbon copper grid (Electron Microscopy Science). After drying, samples were sputter-coated with a thin layer of carbon film to avoid the degradation of the PMMA under the electron beam and observed at 80 kV. Average particle size and polydispersity index (PdI) were also measured by dynamic light scattering and the surface charge of the NPs was investigated through zeta potential measurements (in both cases using the same Zetasizer). All samples were analyzed three times, from which we calculated the average and standard deviation (SD). Fourier-transform infrared spectroscopy (FT-IR) was used to confirm the chemical structure of the NPs using a KBr pellet. Ultraviolet-visible (UV-vis) spectrum was performed to verify the FA adsorption in NPs. The NPs were measured through TGA runs under a nitrogen atmosphere at a heating rate of 10 °C/min. A MicroSense model EV9 vibration sample magnetometer (VSM) was used to measure the hysteresis loops of NPs. For FTIR, TGA and VSM analyses the samples were centrifuged (13.400rpm) and lyophilized (Lyophilizer, FreeZone 4.5-L Benchtop Freeze Dry System; Labconco, Kansas City, USA)

7.2.4.1 Encapsulation efficiency of G12 (EE)

The EE of G12 was analyzed using UV-Vis spectrophotometry, where 10 mg of NPs were dissolved in NMP, the common solvent for both drug and polymer. The determination coefficient (R^2) exceeded 0.997, with excellent linearity (0.2 – 2µg/mL). The G12 concentration was measured at 273 nm (ultraviolet region of the electromagnetic spectrum) using a calibration curve with different concentrations of

lauryl gallate dispersed in NMP. The EE% of G12 was calculated from Eq. (1):

$$EE(\%) = {}^{M_1}/_{M_t} \times 100 \quad (1)$$

where EE is the G12 encapsulation efficiency, M_1 is the mass of G12 in NPs and M_t is the mass of G12 used in formulation. The experiments were run in triplicate (n=3). The NPs were measured through TGA runs under nitrogen atmosphere at a heating rate of 10 °C/min. A MicroSense model EV9 vibrating sample magnetometer (VSM) was used to measure the hysteresis loops of MNPs and superparamagnetic NPs.

7.5 In vitro studies

7.5.1 Controlled and kinetic release

The release was carried out in the diffusion cell. NPs (15 mg) were weighed and placed in the donor compartment of the diffusion cell. A cellulose acetate membrane (cellulose membrane tubing Dialysis, Follow-Aldrich, Ref D9652-100TF) was used for separating donor compartments containing the nanoparticles of the receptor compartment that contained 20 ml of PBS pH 7.4 with 0.5 % SDS or PBS pH 5.5 with 0.5 % SDS. A release study with acidic medium receptor (PBS pH 5.5 with 0.5 % SDS) was carried out to simulate the medium lysosomal of tumor cells. The membrane is thin and porous allowing free diffusion of the solvent and drug. Receptor medium was continuously stirred (100 rpm) and the temperature was maintained at 37 ^{o}C in a thermostatically controlled water bath. The release studies followed the sink conditions. At 1, 2, 4, 6, 24, 48, 72, 96 and 120 h, an aliquot was withdrawn from the receptor medium of the release studies. The release study was performed in triplicate (n=3 determinações). The drug released in the receptor medium was quantified by spectrophotometry using the visible region of the spectrum (273 nm). The analytical curve was made in the concentration range from 1.6 to 8.8 µg.mL^{-1} with a determination coefficient of 0.999. The release profile was obtained by associating the percentage of drug released with time. The release data were fitted using the mathematical models of zero order ($Qt = Q_0 + K_0 t$), first order ($\ln Qt = \ln Q_0 + K_1 t$) and Higuchi ($Qt = K_H t^{1/2}$) described by Costa and Lobo (2002), and the determination coefficient

(R^2) and straight line equation were determined using the software Excel. The mathematical model with best fit is the model that provides the highest value of determination coefficient.

7.5.2 Biocompatibility assay on L929 (murine fibroblast) cells

The L929 cell lines were selected to evaluate cytotoxicity as a direct contact test, as recommended by ISO 10993 for *in vitro* toxicity. The cells were cultured in Dulbecco's Modified Eagle's medium (DMEM) supplemented with 10% fetal bovine serum, penicillin (100 units/ml), streptomycin (100 mg/mL), and 4 mM/L of glutamine at 37 °C in tissue culture flasks with 5 % CO_2. For experimental purposes, trypsinized cells were adjusted to a concentration of $1x10^4$ cells/well and plated in a 96 well flat bottom culture plate. After 24 h, the cells were treated with a medium containing G12 dissolved in DMSO (0.1%), MNPsG12PMMA, and FA-MNPsG12PMMA NPs dissolved in PBS 7.4 at five concentrations: 1, 4, 8, 12 and 16 $\mu g.mL^{-1}$ (5% CO_2, 37 °C). After of incubation time (24h) the NPs were washed three times with PBS and cell viability was assessed using the classical MTT assay (Sigma, MO, USA).

7.5.3 In vitro cytotoxicity assay on HeLa (human cervical cancer cells) cells

HeLa cell lines were obtained from the Adolfo Lutz Institute (São Paulo). HeLa cells were grown in MEM medium containing 7.5% fetal bovine serum and maintained at 37 °C in a humidified incubator containing 5% CO_2. The HeLa cells were seeded at $1x10^4$ cells/well in 96-well plate. After 24 h, the cells were treated with a medium containing G12 dissolved in DMSO (0.1%), MNPsG12PMMA, and FA-MNPsG12PMMA NPs dissolved in PBS 7.4 at five concentrations: 10, 11, 12, 13 and 14 $\mu g.mL^{-1}$ (5% CO_2, 37 °C). After 24 h of incubation the cells were washed three times with PBS (7.4) and the MTT cell viability assay was performed. The cytotoxicity assay was carried out in triplicate, with three wells for each condition.

7.5.4 MTT viability assay

The MTT cell proliferation assay was employed to assess cell viability after both the cytotoxic assays. Briefly, 200µl aliquots of MTT solution (5 $mg.ml^{-1}$) were added to each well and incubated for 3 h (37 °C and 5% CO_2), to allow the formazan-formation reaction. Following incubation, the medium containing the MTT solution was removed, and the formazan crystals were dissolved in DMSO. The absorbance was measured at 550nm using an Infinite 200 TECAN microplate reader. The results are presented as survival percentage (100%), where the control group contained 1% DMSO (v/v).

7.5.5 Hemolysis assay

This study was approved by the medical ethics committee of Polydoro Ernani de São Thiago University Hospital (Florianopolis, Brazil). Citrate-stabilized human blood was freshly collected and used within 3 h of being drawn. 4 mL of whole blood was added to 8 mL of a sterile solution of sodium chloride in water (saline) and the human red blood cells (RBCs) were isolated from serum by centrifugation at 10.000 × *g* for 5 minutes. The RBCs were further washed five times with saline solution. Following the last wash, the RBCs were diluted in 2 mL of saline solution and then 120 µL of the diluted RBC suspension was added to 880µL of water or saline. The G12, MNPsG12PMMA and FA-MNPsG12PMMA samples were treated at concentration 10, 25 and 50$\mu g.ml^{-1}$. All samples were prepared in triplicate and the suspension was briefly vortexed before gentle stirring at 37 °C for 60 minutes. After that, the mixture was briefly vortexed again and centrifuged at 10,000 × *g* for 5 minutes. 100 µL of supernatant from the sample tube was transferred to a 96-well plate. The absorbance value of hemoglobin at 570 nm was measured with the reference wavelength at 540 nm. The 120 µL of diluted RBC suspension incubated with 880 µL of water and saline was used as the positive and negative control, respectively. The hemolysis percentage (%) was calculated using Equation 1:

$$\text{Hemolysis } (\%) = \frac{(\text{sample absorbance-negative control})}{(\text{positive control-negative control})} \times 100\% \quad (1)$$

7.5.6 Cellular uptake assay by laser scanning confocal microscopy

HeLa cells (5x104) were cultured on 13 mm diameter glass coverslips in 24 well plates for three days. Cells were then treated with 10µg/mL of MNPsG12PMMA or FA-MNPsG12PMMA and incubated for 1 hour, at 37 ºC. In order to block the endocytotic pathways, NPs were also incubated for 1 h at 4 ºC (ZHENG et al, 2014). After the incubation, cells were washed 3 times with PBS, fixed with 2% paraformaldehyde (Electron Microscopy Science) in PBS for 20 minutes at 22 ºC, then mounted using Prolong Gold with DAPI (Thermo Fisher) and examined using laser scanning confocal microscopy A1RSi+MP (Nikon Corp). For images the 405 laser for DAPI excitation was used and 488 laser for NP excitation was used. For the study of cellular uptake by confocal microscopy, the polymeric NPs were marked with 6-coumarin, a highly fluorescent molecule (green).

7.5.7 Cellular uptake assay by flow cytometry

HeLa cells (10^3) were cultured in 12 well plates for 24h. Cells were then treated with 10 µg/mL of MNPsG12PMMA or FA-MNPsG12PMMA, both incorporated with 6-coumarin, and incubated for 24 hours, at 37 ºC. Cells were collected by trypsinization and washed twice with PBS. Cellular uptake efficacy was evaluated by flow cytometry using a BD FACScalibur cytometer and analyzed using Flowing software.

7.6 RESULTS AND DISCUSSION

FA-MNPsG12PMMA nanoparticles were obtained successfully by miniemulsion polymerization. This technique showed a high EE of G12 (87 ± 2 %). TEM analysis (Figure 7.1) showed that the incorporation of G12 and MNPs didn't affect the morphology and size of NPs. The NPs presented a mean size of 100nm approximately, a relatively narrow size distribution and spherical morphology. The superparamagnetic NPs presented some darker regions of very small size, around 5-14 nm in diameter, which are attributed to the core formed by MNPs, as can be observed in Fig 7.1B, E and F (FILIPPOUSI et al, 2013; ZHENG et al, 2005). DLS analyses

(Table 7.1) showed that the FA adsorption on polymeric NPs surface increased the average size by approximately 25 nm, when compared to polymeric NPs without FA. The broadening of the particle size distribution and the increase in particle size can be indicative of adsorption of FA on the NP surface. Observing Figure 7.1C, D, E and F, we can suggest that the FA was adsorbed on the surface of polymeric NPs (black arrow). Zeta potential analysis (Table 7.1) showed a negative surface charge, contributing to good colloidal stability (He et al, 2010). The negative surface charge of NPs can be attributed to the carboxylic groups (OA and PMMA) and the surfactant (lecithin) on the nanoparticle surface (FEUSER, 2015b).

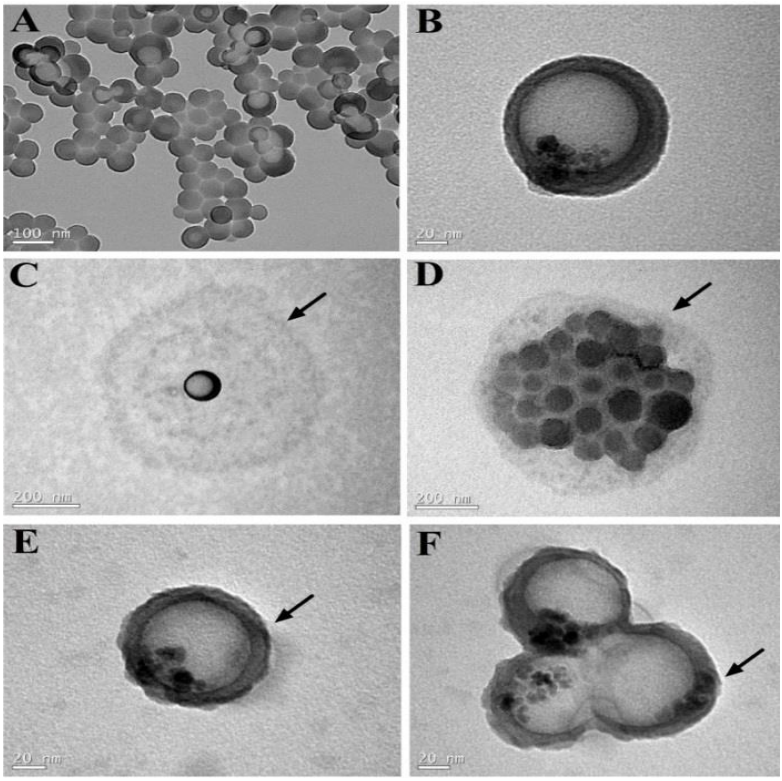

Figure 7.1 TEM analysis of NPs obtained by miniemulsion polymerization: (A) G12PMMA; (B) MNPsG12PMMA; (C and D) FA-G12PMMA; (E and F) FA-MNPsG12PMMA.

Table 7.1 Analysis of average droplet (Dg) and particle (Dp) diameter, initial and final polydispersity index (PdI_g and PdI_p) and zeta potential of NPs obtained by Zetasizer

Samples	**Dg (nm)**	**Dp (nm)**	**PdI_g**	**PdI_p**	**Zeta Potential (mV)**
PMMA	90 ± 3	98 ± 3	0.08 ± 0.0.1	0.11 ± 0.0.1	-37 ± 3
G12PMMA	103 ± 4	106 ± 4	0.13 ± 0.02	0.13 ± 0.02	-38 ± 4
MNPsG12PMMA	98 ± 3	105 ± 3	0.14 ± 0.02	0.18 ± 0.03	-42 ± 6
FA-PMMA	112 ± 2	121 ± 3	0.14 ± 0.02	0.13 ± 0.01	-36 ± 2
FA-G12PMMA	116 ± 3	126 ± 4	0.13 ± 0.02	0.16 ± 0.02	-34 ± 5
FA-MNPsG12PMMA	117 ± 4	129 ± 4	0.19 ± 0.02	0.19 ± 0.02	-38 ± 4

The XRD patterns of free G12, FA-PMMA, FA-MNPsG12PMMA and MNPsG12PMMA are shown in Figure 7.2. The XRD profile of free G12 exhibited several characteristic peaks at diffraction angles of 15.94°, 18.91° and 22°, confirming the crystalline form of G12. However, these peaks were not observed in the diffractograms when the G12 was encapsulated in PMMA NPs, indicating that the drug (G12) can be molecularly dispersed in the polymeric matrix in its amorphous state (FEUSER et al, 2015c; ALVES et al, 2016). The peaks observed at 2θ: (220), (311), (400), (422), (511) and (440) in samples of MNPsG12PMMA and FA-MNPsG12PMMA are characteristic of magnetite (Fe_3O_4) encapsulated in PMMA NPs (DALLAS et al, 2006; FEUSER et al, 2015b; SAHOO et al, 2013). An additional broad peak for the FA-PMMA, FA-MNPsG12PMMA and MNPsG12PMMA was observed at an angle between 10 and 20°, which is characteristic of an amorphous polymer (LEKSHMI et al, 2010).

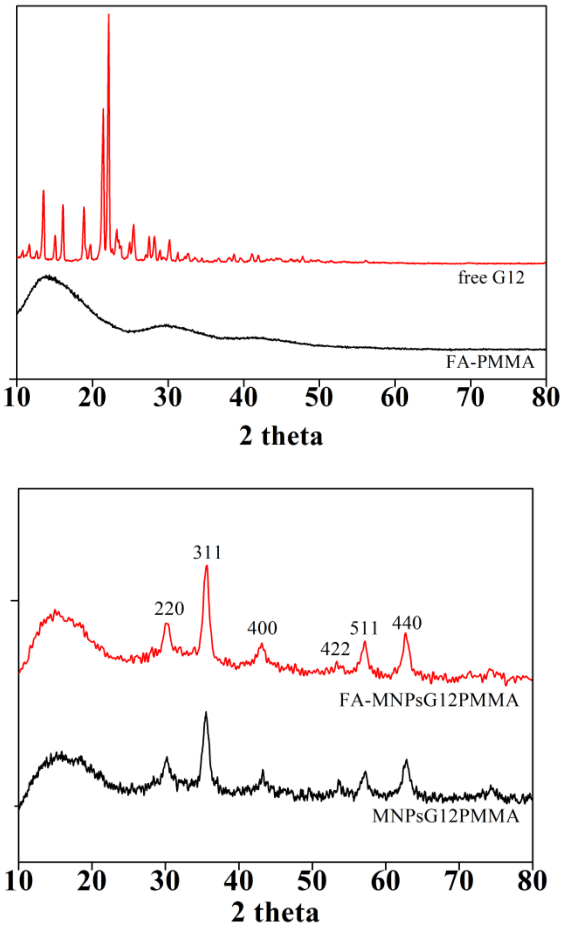

Figure 7.2 X-ray powder diffraction patterns of free G12, FA-PMMA (left), FA-MNPsG12PMMA and MNPsG12PMMA (right)

FTIR analyses were performed to verify the incorporation of G12 and MNPs in the PMMA nanoparticles. In addition, the FTIR technique can indicate FA adsorption. In Figure 7.3A, the peaks at 1736 cm^{-1} and 3000 – 2800 cm^{-1} correspond to C=O groups and stretching of C-H bonds, characteristic of PMMA nanoparticles (FEUSER et al, 2014). The peak at 577cm^{-1} is related to the vibration of the Fe-O bond, which matches well with the characteristic peak of

MNPs (CHIARADIA et al, 2015; GAO et al, 2010; SAHOO et al, 2013). Comparing the FTIR spectra of PMMA nanoparticles and MNPsG12PMMA nanoparticles we confirmed that there is no significant interaction between drug (G12) and polymer, and the G12 is embedded into a polymeric matrix, corroborating with XRD analysis. FTIR spectrum of FA presented peaks at 1680, 1590, 3540, 3423 and 3315cm^{-1} corresponding to amide I, amide II, ring O–H, NH_2 and secondary NH groups (ANDHARIYA et al, 2012; MOHAPATRA et al, 2007). The appearance of bands at 3400cm^{-1} and 1688cm^{-1} as can be seen in Figure 3B and D (small scale), can be indicative of FA adsorption, due to the interaction of hydrogen bonds (DONG et al, 2014; ZHANG et al, 2007). It is worth mentioning that the NPs without FA (Figure 7.3C) didn't present bands at 3400 and 1688 cm^{-1}. To confirm these results a UV spectrum (Figure 7.3E) was performed. The bands at 284 nm reference the absorption of FA in UV spectrum (LICCIARDI et al, 2005; YANG et al, 2014; YOO et al, 2013), and confirms the FA adsorption onto the surface PMMA nanoparticles.

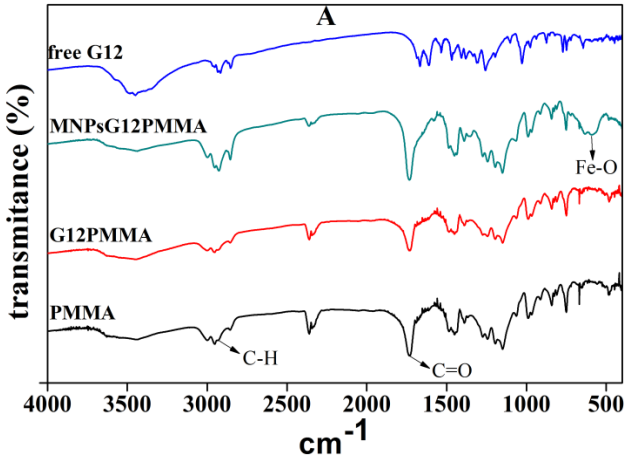

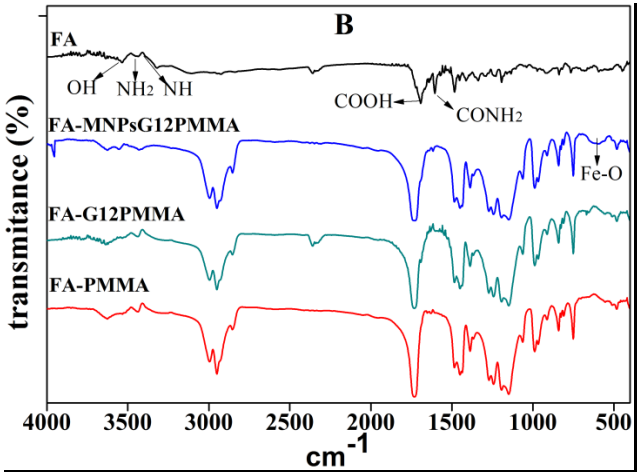
B
FA
OH
NH2
NH
COOH
CONH2
FA-MNPsG12PMMA
Fe-O
FA-G12PMMA
FA-PMMA
transmitance (%)
4000
3500
3000
2500
2000
1500
1000
500
cm-1

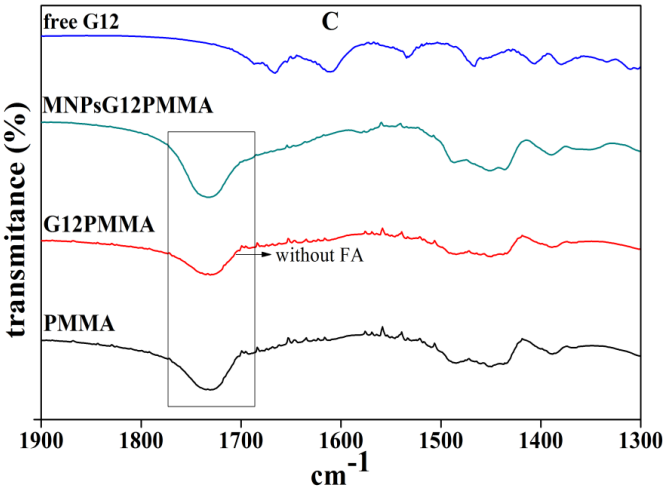
C
free G12
MNPsG12PMMA
G12PMMA
without FA
PMMA
transmitance (%)
1900
1800
1700
1600
1500
1400
1300
cm-1

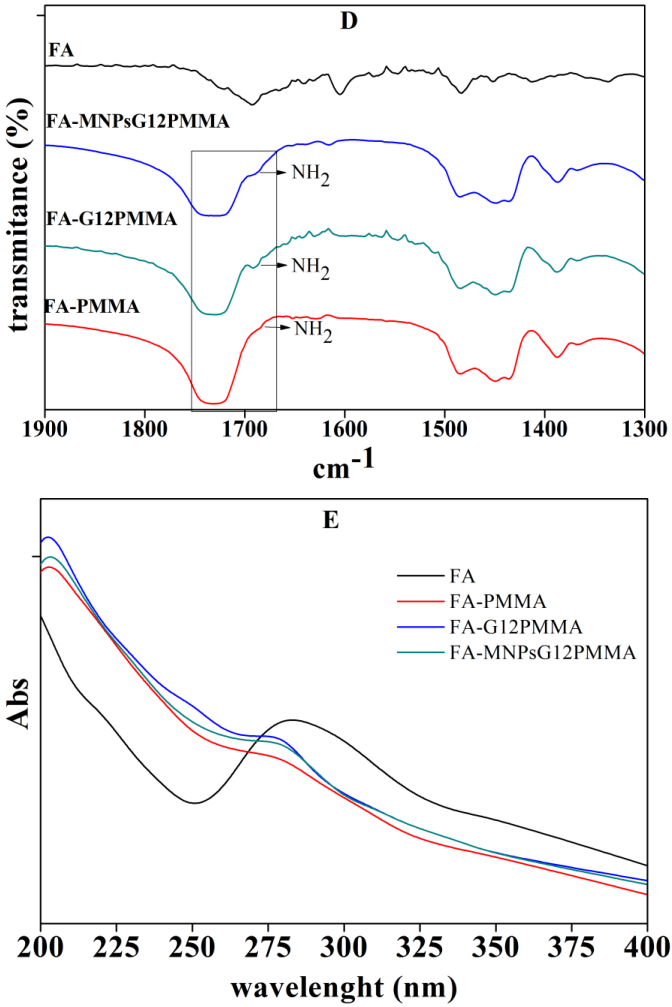

Figure 7.3 FTIR spectra of NPs without FA (A and C); FA adsorbed on NPs (B and D) and UV-vis spectra of FA adsorbed on NPs (E).

TGA analyses (Figure 7.4) were performed to determine the total concentration of MNPs in the formulation (GAO et al, 2010). The MNPs-OA presented a weight loss at around 200 and 440 °C (40 %), attributed to the OA on the surface of MNPs (RAMIRES and

LANDFESTER, 2003). The total concentration of MNPs obtained by the co-precipitation method was of 60%. In the case of MNPsG12PMMA and FA-MNPsG12PMMA mass loss is gradual and it can be clearly observed that the polymer is completely degraded when reaching about 430 °C (Feuser et al, 2014). The residual concentration of approximately 19 %, corresponds to the MNPs. The other 81% corresponds to the PMMA and AO on the surface of MNPs.

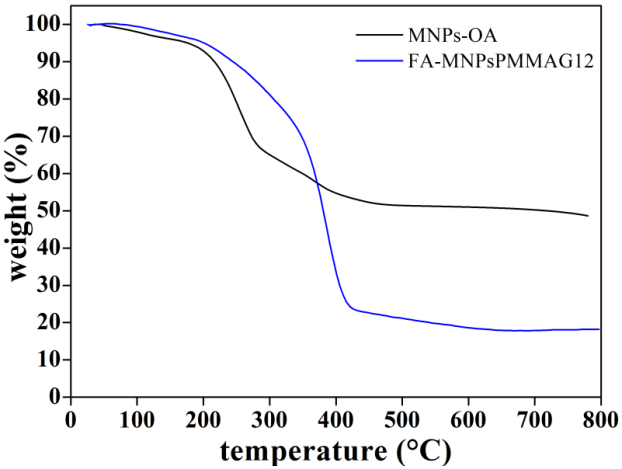

Figure 7.4 TGA analyses of MNPs-OA (FEUSER et al, 2015b) and FA-MNPsG12PMMA

The magnetic properties of NPs were studied by VSM. Figure 7.5 shows that all NP coated MNPs presented a high value of saturation magnetization. The samples presented a saturation magnetization value of approximately 38 emu/g of iron oxide (Figure 7.5A). The FA adsorbed onto NPs and the incorporation of G12 didn't affect the saturation magnetization value. However, the saturation magnetization decrease of values bulks (90-100emu/g of Fe_3O_4 and 60-80 emu/g of maghemite (γ-Fe_2O_3) when MNPs are encapsulated in NPs. This decrease of saturation magnetization can be attributed to the dense coating of the non-magnetic polymer, or because during polymerization, some of the Fe_3O_4 convert to another type of iron oxide, like γ-Fe_2O_3, due to the presence of the oxidizing initiator fragments (CHANDRASEKHARAN et al, 2011; DALLAS et al, 2006; FEUSER

et al, 2015b; RAMIRES and LANDFESTER, 2003). All analyzed samples showed superparamagnetic behavior at room temperature, with an absence of hysteresis loop, low remanent magnetization/saturation magnetization ratio and small coercive field values (Figure 7.5B) (CHANDRASEKHARAN et al, 2011). The superparamagnetic properties of NPs are very important for biomedical applications, which, without an external magnetic field their overall magnetization value is randomized to zero, preventing active behavior of the particles when there is no applied field (GAO et al, 2010; XU and SU, 2013), resulting in an excellent strategy to drug delivery by influence of an external magnetic field (Mody et al, 2014).

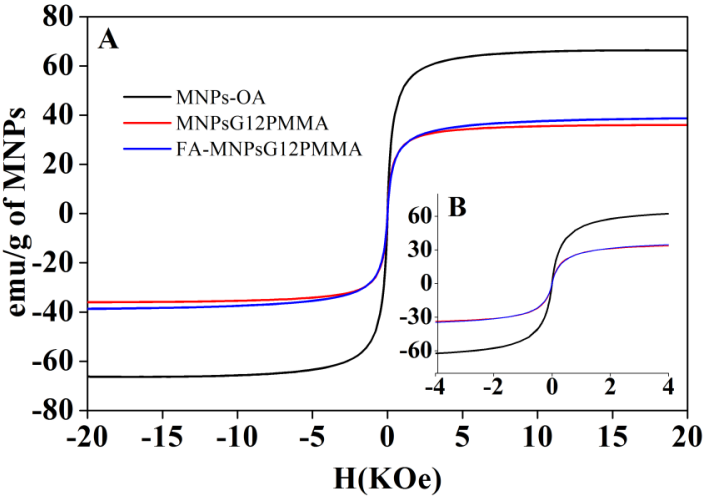

Figure 7.5 VSM analyses of magnetic properties of FA-MNPsG12PMMA and MNPsG12PMMA nanoparticles, with magnetic field of 20 KOe and 4 KOe.

7.6.2 In vitro studies

7.6.2.1 Release kinetics of G12 from FA-superparamagnetic PMMA NPs

A release study was performed at both physiological and lysosomal pH conditions (tumor cells are slightly acidic) (NOWICKA et al, 2013; SAHOO et al, 2013) at 37 ^{o}C, in order to evaluate the release

profile of G12 incorporated into NPs with AF. The release profiles for pH 7.4 and 5.5 exhibited rapid release with initial burst effect from 0 to 1 h. At 1 h, the release profile followed a biphasic pattern in both samples (FA-G12PMMA and FA-MNPsG12PMMA) and pH conditions (7.4 and 5.5): release was slow and linear from 1 to 6 h and very slow and sustained from 24 to 120 h (Figure 7.6). The release of G12 from NPs was accelerated in pH 5.5 that simulates the lysosomal medium of the tumor cells (Sahoo et al, 2013) in comparison with physiological pH (pH 7.4). Results also indicated that G12 was released more quickly from FA-MNPsG12PMMA NPs in comparison with FA-G12PMMA NPs (Figure 7.6). Thus, the polymer matrix resistance to diffusion G12 was lower in FA-MNPsG12PMMA NPs. The biphasic pattern can be an excellent strategy in the development of targeted drug systems, where the drug is released during two periods: (I) immediate drug release to maintain the constant drug concentration in the blood plasma for a prolonged period, followed by a slow and sustained release in the target tissue, consequently improving patient compliance (decreases the number of daily administrations) and therapeutic efficacy (LI et al,. 2014; YU et al,. 2013; GAO et al, 2011; HUANG and BRAZEL 2001).

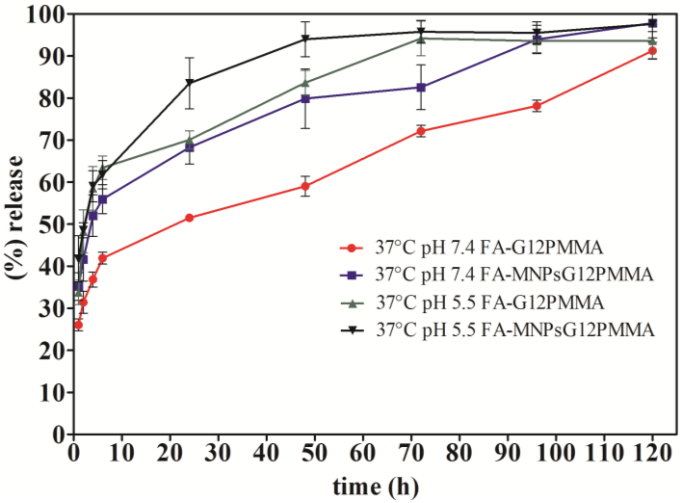

Figure 7.6 Release profiles of G12 loaded in NPs with FA. Data refers to mean ± standard deviation (n = 3) in different experiments at 37 °C with differing pH (pH 7.4 and pH 5.5).

The zero order, first order, and Higuchi mathematical models were used in this study to evaluate the release kinetics. Mathematical models were applied to the release data. The choice of model was based on the highest coefficient of determination (r^2). The kinetics of release was best explained by Higuchi model followed by the zero-order model and finally the first order model. The Higuchi model describes the release drugs from a solid matrix by diffusion based on Fick's law (COSTA and LOBO, 2001; LEKSHMI et al, 2010). Generally, diffusion is the mechanism that controls the drug release in delivery systems produced with non-biodegradable polymers such as PMMA, and consequently, factors such as concentration gradient, location of the drug in the polymer matrix, diffusion distance, and the degree of swelling can influence the profile and the release rate (FU and KAO 2010, GAO et al, 2011; RAO and GECKELER, 2011). Thus, we can conclude that the release of G12 from the nanocarriers followed the Higuchi model and the mechanism that controls the release is diffusion.

7.6.2.2 *In vitro* cytotoxicity on L929 cells and hemolys is assay

Mouse fibroblast (L929) is a popular cell line recommended by ISO 10993-5 in many experimental aspects for polymer cytotoxicity testing. In this study the biocompatibility of free G12 and NPs was evaluated in L929 cells. The cells were treated with five different concentrations (1, 4, 8, 12 and 16 $\mu g.mL^{-1}$ of G12). As shown in Figure 7.7, free G12 significantly inhibited L929 cell growth in a dose-dependent manner when these cells were treated for 24 h. Cell viability was 76% and 44% when the cells were treated with 4 and 16 $\mu g.mL^{-1}$, respectively. Other studies also have demonstrated the cytotoxic effect of GA derivatives on L929 cells (LOCATELLI et al, 2013; SERRANO et al,; 1998). However, when the G12 was encapsulated in superparamagnetic PMMA NPs with and without FA no cytotoxic effects were observed on L929 cells at the same doses. Therefore we can conclude that the encapsulation of G12 into the polymer matrix provides a decrease in cytotoxic effects on L929 non-tumor cells at the used doses (DANHEIR et al, 2012).

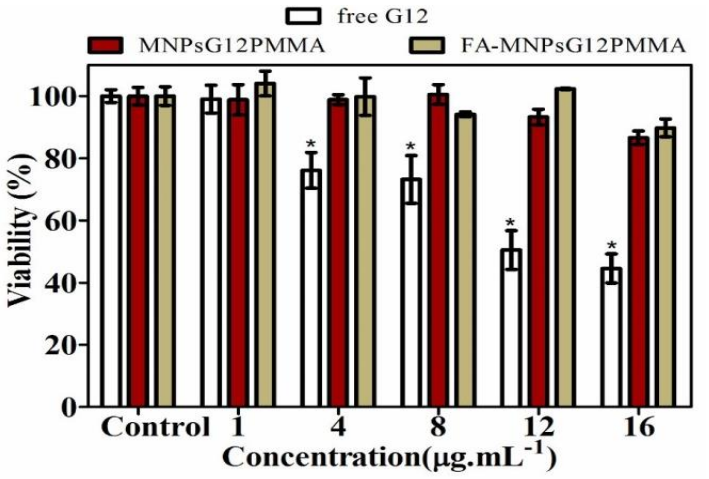

Figure 7.7 *In vitro* cytotoxicity assays of free G12, MNPsG12PMMA and FA-MNPsG12PMMA in L929 cells at different concentrations ($1 - 12 \mu g.mL^{-1}$). Values represent the mean ± SD of the percentage of viable cells in comparison with the DMSO control considered as 100%. Data represent three independent experiments, each being performed in triplicate. Significant differences: * $p < 0.05$.

In order, to evaluate the biocompatibility of red blood cells, hemolysis assays were carried out, as can be seen in Figure 7.8. The hemolysis assay is an important test for assessment of cytotoxicity on red blood cells (CHEN et al, 2012; ZHOU et al, 2011). According to the criterion of Standard Test Method for Analysis of Hemolytic Properties of Nanoparticles (ASTM E2524-08), a percentage hemolysis > 5% indicates that the test material causes damage. Hemocompatibility assays of free G12 on human red blood cells demonstrated a high hemolytic percentage at all tested concentrations. The hemolytic percentage reached 16, 25, 33 and 99 % when the red blood cells were treated with 10, 20, 40 and 80 $\mu.mL^{-1}$. On the other hand, G12 encapsulated in FA-superparamagnetic PMMA NPs did not exceed 5% at concentrations of 10 (3.5 %) 20 (4.2 %), and 40 $\mu g.mL^{-1}$ (4.8 %). When the red blood cells were exposed to high concentrations the hemolytic percentage reached 17%. The results obtained corroborate with the cytotoxicity assay. The non-hemolytic character confirms the hemocompatibility of NPs, which ensure the protection of G12 when

encapsulated in PMMA NPs. In others words FA-MNPsG12PMMA are similar to the original plasma, which indicates that the NPs have no obvious activation or coagulation factors and thrombin generation (ZHOU et al, 2011). The good biocompatibility of NPs on human red blood cells is due main their negative surface charge. Recent studies reported in literature have demonstrated that the preparation of NPs with positive surface charges tend to cause hemolysis (JONG and BORM, 2008; FORNAGUERA et al, 2015). Lastly, we can affirm that the encapsulation of the G12 into the polymer matrix provides protection to the drug, which can decrease cytotoxic effects on non-tumor cells and offer possibility of specific targeting (cancer) when intravenously administered with a sustained release.

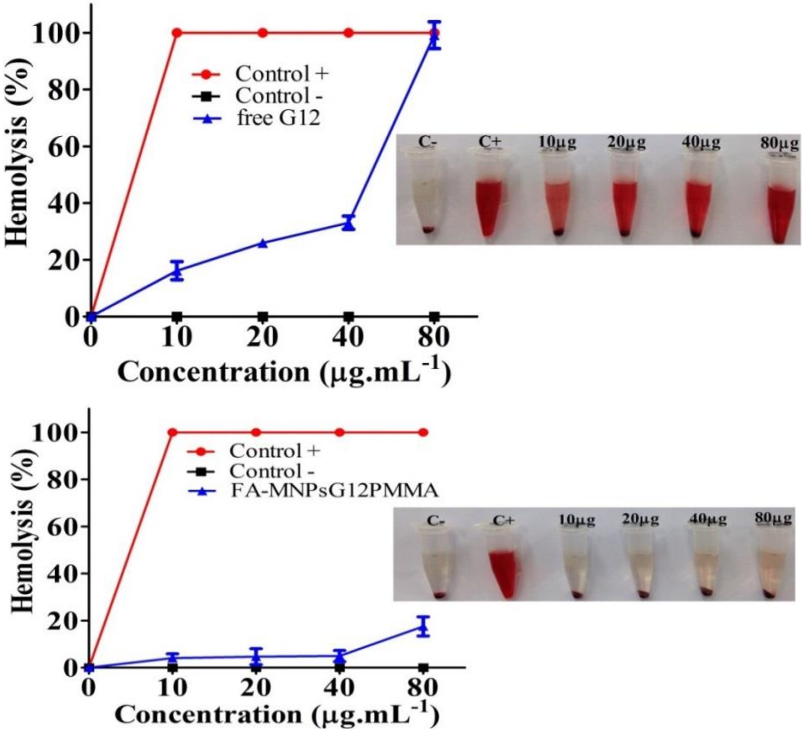

Figure 7.8 Hemolysis assay. Relative rate of hemolysis in human RBCs upon incubation with Free G12 and FA- MNPsG12PMMA at concentrations: 10, 20, 40 and 80µg.mL^{-1}. Data represent mean ± SD (n = 3). (* p < 0.05) one way ANOVA followed by Tukey's test.

7.6.2.3 In vitro anticancer activity of G12 on HeLa cells

The cytotoxic effects of free G12, MNPsG12PMMA and FA-MNPsG12PMMA NPs were evaluated on HeLa cells and examined through the MTT assay. The aim of this study was to compare the cytotoxic effects of free G12 and NPs with and without FA. As can be seen in Figure 7.9 the free G12 did not present any cytotoxic effects on HeLa cells at concentrations of 10 and 11 $\mu g.mL^{-1}$. MNPsG12PMMA NPs, induced a decrease in cell viability (19%) at a concentration of 11 $\mu g.mL^{-1}$. The cytotoxic effect using 10 and 11 $\mu g.mL^{-1}$ of G12 was more pronounced in FA-MNPsG12PMMA NPs, which promoted significant reduction in cell viability, 14% and 30%, respectively. The free G12 induced cell death from concentrations of 12 $\mu g.mL^{-1}$, with a reduction in cell viability of 18% (12 $\mu g.mL^{-1}$) to 39% (14 $\mu g.mL^{-1}$). However, a higher reduction in cell viability was observed when FA-MNPsG12PMMA was exposed to HeLa cells at concentrations of 12, 13 and 14 $\mu g.mL^{-1}$, which decreased cell viability to 59%, 48% and 41%, respectively. FA-MNPsG12PMMA NPs, presented a higher cytotoxic effect than MNPsG12PMMA NPs at concentrations of 11 - 14 $\mu g.mL^{-1}$. The optical microscopy analysis of FA-MNPsG12PMMA NPs (13 $\mu g.mL^{-1}$) incubated at 24 h on HeLa cells, showed a significant change in cell morphology (Figure 7.9C), when compared with the control group (Figure 7.9B), resulting in a loss of cell membrane integrity (white arrow) and inducing cell death. Lastly, our results suggest that the higher cytotoxic effect of the FA-MNPsG12PMMA NPs can be related with an increase in cellular uptake due to the interaction between the folate groups adsorbed on NPs and FR of HeLa cells (LAPINA et al, 2013; SABHARANJAK and MAYOR, 2004; WIBOWO et al, 2013).

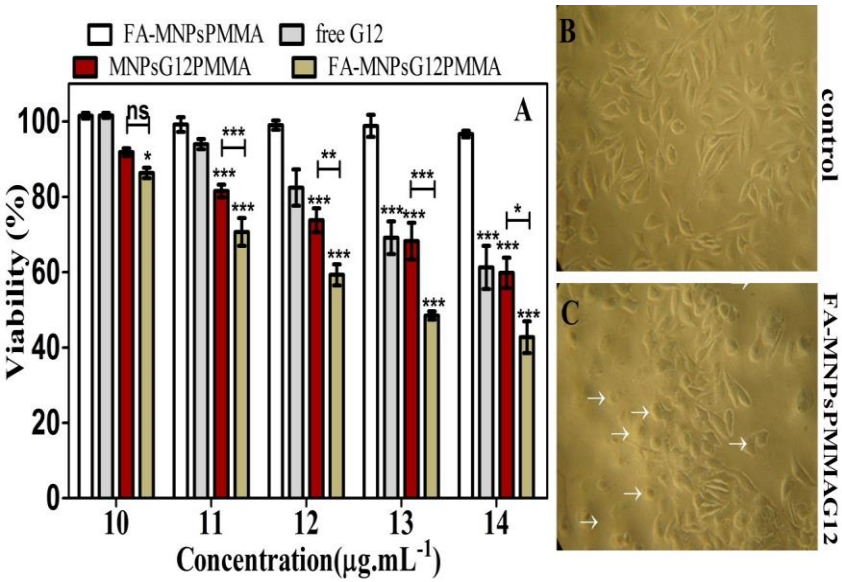

Figure 7.9 *In vitro* cytotoxicity of free G12, MNPsG12PMMA and FA-MNPsG12PMMA at different concentrations (10 - 14µg.mL^{-1}) (A). Optical microscopy analysis (100x) of HeLa cells: Control (B) and FA-MNPsPMMA (IC_{50}) (C) after 24 h of incubation. Values represent the mean ± SD of the percentage of viable cells in comparison with the DMSO control considered as 100%. Data represent three independent experiments, each being performed in triplicate. Significant differences: ***p< 0.0001; **p< 0.0001 and *p< 0.0001.

7.6.2.4 Cellular uptake study by confocal microscopy and flow cytometry

To evaluate binding to the cell surface or uptake of MNPsG12PMMA and FA-MNPsG12PMMA NPs, HeLa cells were treated with NPs marked with 6-coumarin at 37 ºC or 4 ºC (Figure 7.10A). Assuming that at 4 ºC endocytosis is inhibited (TRINDADE et al, 2008; ZHENG et al, 2014), the diffusion capacity was evaluated across the plasmatic membrane. As can be observed in Figure 7.10, both NPs were not able to diffuse at 4 ºC, suggesting that some energy-dependent process in endocytotic pathways internalized the NPs (PANARITI et al, 2012; ZHANG et al, 2009; ZHENG et al, 2014). When NPs were incubated at 37ºC, a higher cellular uptake was

observed in NPs with FA, as can be seen in Figure 7.10. The orthogonal images of MNPsG12PMMA and FA-MNPsG12PMMA NPs uptake by cells at 37 ºC (Fig 7.10B and C) show that those NPs were at same level as the nucleus of cells (observed in blue), which indicates that NPs were internalized, and not just binding on the cell surface. Lastly, the flow cytometry assay showed that FA improved the internalization of NPs into HeLa cells (Fig 7.10 D and E), suggesting that those were targeted HeLa cells by FR-mediated endocytosis, corroborating with data previously described.

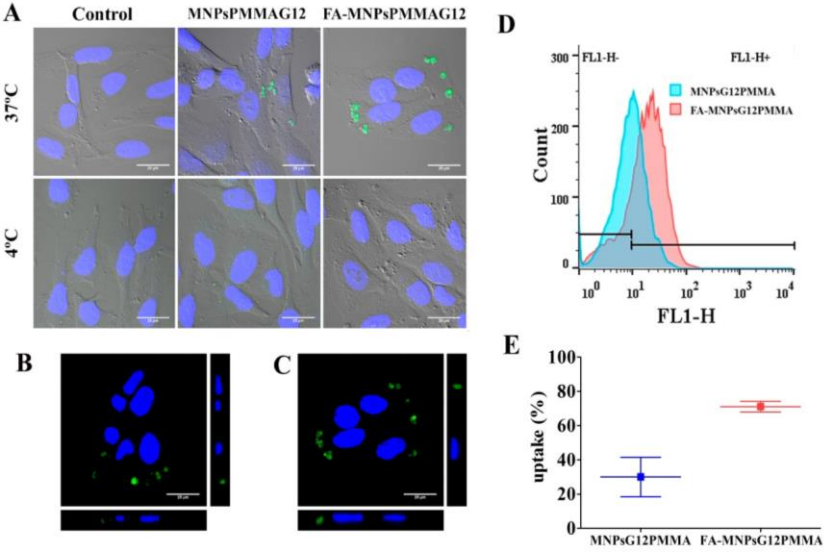

Figure 7.10 Cellular uptake of MNPsG12PMMA and FA-MNPsG12PMMA NPs. (A) Cells treated with MNPsG12PMMA or FA-MNPsG12PMMA, at 4ºC or 37ºC. (B) Orthogonal view of cells treated with MNPsG12PMMA at 37ºC, (C) Orthogonal view of cells treated with FA-MNPsG12PMMA at 37ºC. Observe the nuclei in blue and the compounds in green. (D) Histogram of fluorescence of HeLa cells treated with MNPsG12PMMA and FA-MNPsG12PMMA NPs. (E) Quantification of cells that uptake MNPsG12PMMA and FA-MNPsG12PMMA NPs.

7.7 Conclusion

In conclusion this work has demonstrated that FA-MNPsG12PMMA NPs are suitable for encapsulation and controlled release of G12. The NPs were able to reduce cytotoxicity of encapsulated G12 in non-tumor L929 cells and red blood cells, protecting the drug inside the polymeric matrix, as shown in DRX and FTIR analysis. The FA adsorption on NPs increased the cellular uptake suggesting that those were targeted HeLa cells by FR-mediated endocytosis. Lastly, our studies demonstrated that the FA adsorption in PMMA NPs obtained by miniemulsion polymerization could be an excellent alternative in cancer treatment with targeted drug delivery and controlled release of encapsulated drugs.

CHAPTER 8

8. GENERAL CONCLUSION

The synthesis of PMMA NPs loaded with drugs and MNPs obtained by miniemulsion polymerization technique, resulted in stable NPs, with nanometric size, superparamagnetic properties, high encapsulation efficiency, prolonged drug release drug protection and biocompatibility on tumor and non-tumor cells. The encapsulated drugs, ZnPc and G12, were more effective than free drugs. The incorporation of MNPs in PMMA NPs was effective against U87MG cells when AC magnetic field was applied resulting in cells death by HPT. Similar results were observed when ZnPc and MNPs were simultaneously encapsulated in PMMA NPs. In this study the synergic effect was demonstrated by simultaneous treatment of PDT and HPT. The FA adsorption on PMMA NPs presented biocompatibility in non-tumor cells and a higher cellular uptake on cells that overexpress FR type β (K562). The simultaneous encapsulation of G12 and MNPs in PMMA NPs with FA-modified surface, presented a higher cytotoxic on HeLa cells than NPs without FA. Finally, uptake assay shown that the higher cytotoxic effect of G12 and MNPs loaded in PMMA NPs with FA-modified surface on HeLa cells was due to uptake cellular by FR-mediated endocytosis.

BIBLIOGRAPHIC REFERENCES

ABULATEEFEH S. R, SPAIN S. G, THURECHT K. J, AYLOTT J. W, CHAN W. C, GARNETT M. C, ALEXANDER C. Thermoresponsive polymer colloids for drug delivery and cancer therapy. Macromolecular Bioscience, v. 1, p.434–442, 2011.

AL-GHAMDI, G.H., SUDOL, E.D., DIMONIE, V.L., EL-AASSER, M.S., Encapsulation of Titanium Dioxide in Styrene/n-Butyl Acrylate Copolymer by Miniemulsion Polymerization. J. Appl. Polym. Sci., 2006, v. 101, pp. 3479-3486.

ALVES A. C. S, MAINARDES R. M, KHALIL N. M. Nanoencapsulation of gallic acid and evaluation of its cytotoxicity and antioxidant activity. *Materials and Engineering C*, v. 60, p.126-134, 2016.

ANDHARIYA N, UPADHYAY R, MEHTA R, CHUDASAMA B. Folic acid conjugated magnetic drug delivery system for controlled release of doxorubicin. *Journal of Nanoparticles Research*, v. 15, p.1416, 2013.

ANTONIETTI M, LANDFESTER K. Polyreactions in miniemulsion *Program Polymer. Science*, v.27, p.689-700, 2002.

AROSIO P, ORSINI F, PIRAS AN, SANDRESCHI S, CHIELLINI F, CORTI M, MASA M, MÚČKOVÁ M, SCHMIDTOVÁ L, RAVAGLI C, BALDI G, NICOLATO E, CONTI G, MARZOLA P, LASCIALFARI A. MR imaging and targeting of human breast cancer cells with folate decorated nanoparticles. ***RSC Advance*, v. 5, p.**39760-39770, 2015.

ASUA J. M. Mapping the Morphology of Polymer–Inorganic Nanocomposites Synthesized by Miniemulsion Polymerization. *Macromolecular Chemical and. Physical*, v. 215, p.458−464, 2014.
ASUA M. J. Miniemulsion Polymerization. *Program of Polymer Science*, v. 27, p. 1283-1346, 2002.

AYDIN O, ATTILA G, DOGAN A, AYDIN M. V, CANACANKATAN N, KANIK A, *Toxicologic Pathololy*, v. 30, p.350-366, 2002.

BARTH B. M, ALTINOGLU E. I, SHANMUGAVELANDY S. S, KAISER J. M, CRESPO-GONZALEZ D, DIVITTORE N. A, MCGOVERN , GOFF T. M, KEASEY N. R, ADAIR J. H, LOUGHRAN T. P, CLAXTON D. F, KESTER M, Targeted indocyanine-green-loaded calcium phosphosilicate nanoparticles for in vivo photodynamic therapy of leukemia. *ACS Nano*, v. 5(7), p.5325-5337, 2011.

BASEL M. T, BALIVADA S, WANG H, SHRESTHA T. B, SEO G. M, PYLE M, ABAYAWEERA G. Cell-delivered magnetic nanoparticles caused hyperthermia-mediated increased survival in a murine pancreatic cancer model. *International Journal of Nanomedicine*, v. 7, p.297-306, 2012.

BATLLE X, LABARTA A. Finite-size effects in fine particles: magnetic and transport properties. *Journal of Physical* D, v. 35, p.15-42, 2002.

BERNARDY N, ROMIO A. P, BARCELOS E. I, DAL PIZZOL C, DORA C. L, LEMOS-SENNA E, ARAÚJO P. H. H, SAYER C. Nanoencapsulation of Quercetin via Miniemulsion Polymerization. Journal of Biomedical Nanotechonoly, v. 6, p.181-186, 2010.

BETTENCOURT A, ALMEIDA A. J. Poly(methyl methacrylate) particulate carriers in drug delivery. *Journal of Microencapsulation*, v. 29, p.353-367, 2012.

BICALHO L. S, LONGO J. P, CAVALCANTI C. E. O, SIMIONI A. R, BOCCA A. L, SANTOS M. D. M. D, TEDESCO A. C, AZEVEDO R. B. Photodynamic Therapy Leads to Complete Remission of Tongue Tumors and Inhibits Metastases to Regional Lymph Nodes. *Journal of Biomedical Nanotechnology*, v.9, p.811-818, 2013.

BOLFARINI B. C, SIQUEIRA-MOURA M. P, DEMETS G. J. F, MORAIS P. C, TEDESCO A. C. Journal of Photochemistry and Photobiology B : Biology In vitro evaluation of combined hyperthermia and photodynamic effects using magnetoliposomes loaded with cucurbit [7] uril zinc phthalocyanine complex on melanoma. *Journal of Photochemistry and Photobiololy A*, v. 115, p.1-4, 2012.

BOURGEOUT-LAMI E, LANSALOT M. Organic/Inorganic Composite Latexes: The Marriage of Emulsion Polymerization and Inorganic Chemistry. *Advance Polymer Technology*, v. 233, p.53-123, 2010.

BRETAGNOL F, RAUSCHER H, HASIWA M, KYLIAN O, CECCONE G, HAZELL L, PAUL A. J, LEFRANC O, ROSSI F. The effect of sterilization processes on the bioadhesive properties and surface chemistry of a plasma-polymerized polyethylene glycol film: XPS characterization and L929 cell proliferation tests *Acta Biomateralia*, v. 4, p.1745-1751, 2008.

CALVO P, VILA JATO J. L, ALONSO M. J. Effect of lysozyme on the stability of polyester nanocapsules and nanoparticles: Stabilization approaches *Journal of Pharmaceutical. Science*, v. 85, p.530, 1996.

CARTWRIGHT M, MARTIN S, D'MELLO S, HEINRICH G. The human nerve growth factor gene: structure of the promoter region and expression in L929 fibroblasts. *Molecular Brain Research*, v. 15, p.67-75, 1992.

CHANDRA S, DIETRICH S, LANG H, BAHADUR D. *Journal of Materials Chemical*, v. 21, p. 5729-5737, 2011.

CHANDRASEKHARANA P, MAITY D, YONGC CX, CHUANG K-H, DING, J, FENG S-S. Vitamin E (D-alpha-tocopheryl-co-poly(ethylene glycol) 1000 succinate) micelles-superparamagnetic iron oxide nanoparticles for enhanced thermotherapy and MRI. *Biomaterials*, v. 32, p.5663-5672, 2011.

CHANDRASEKHARANA P, MAITY D, YONGC C. X, CHUANG K-H, DING, J, FENG S-S. Vitamin E (D-alpha-tocopheryl-co-poly(ethylene glycol) 1000 succinate) micelles-superparamagnetic iron oxide nanoparticles for enhanced thermotherapy and MRI. *Biomaterials*, v. 32, p.5663-5672, 2011.

CHARTTEJEE D. K, FONG L. S, ZHANG Y. Nanoparticles in photodynamic therapy: An emerging paradigm, *Advances Drug Delivery Reviews*, v. 60, p.1627-1337, 2008.

CHELLAT F, MERHI Y, MOREAU A, YAHIA L. H. Therapeutic potential of nanoparticulate systems for macrophage targeting *Biomaterials*, v. 26, p.7260-7275, 2005.

CHEN D, TANG Q, LI X, ZHOU X, ZANG J, XUE W-Q, XIANG J-Y, GUO, C-Q. Biocompatibility of magnetic Fe3 O4 nanoparticles and their cytotoxic effect on MCF-7 cells. *Journal of Nanomedicine*, v. 7, p.4973-4985, 2012.

CHEN J, SHEN Y, ZHANG J, GU F, ZHU J, XIA Y. Photoelectric Properties of Soluble ZnPc-Epoxy Derivative Doped with C 60. *Journal of Materials Science Technolology*, v. 22, p. 549- 2006.

CHEN M. L, HE Y. J, CHEN X. W, WANG J. H. Quantum dots conjugated with Fe3O4-filled carbon nanotubes for cancer-targeted imaging and magnetically guided drug delivery. *Langmuir*, v. 28, p.16469–16476, 2012.

CHERTOK B, MOFFAT B. A, DAVID A. E, YU F, BERGEMANN C, ROSS B. D, YANG V. C. Iron Oxide Nanoparticles as a Drug Delivery Vehicle for MRI Monitored Magnetic Targeting of Brain Tumors. *Biomaterials*, v. 29, p.487-496, 2008.

CHIARADIA V, VALÉRIO A, FEUSER P. E, OLIVEIRA D, ARAÚJO P. H. H, SAYER C. Incorporation of superparamagnetic nanoparticles into poly(urea-urethane) nanoparticles by step growth interfacial polymerization in miniemulsion. *Colloids and Surfaces A: Physicochem. Eng. Aspects*, v. 482, p.596–603, 2015.

CHIN, C. M, FERREIRA E. The latentiation process in drug design. *Química Nova*, v. 22, p.75-84, 1999.

CHOI H. C, MOON H. K, LEE S. H. Alpha-form zinc-phthalocyanine nanowires having enhanced water solubility and water dispersibility, composite of an alpha-form zinc-phthalocyanine nanowire/phenothiazine, and method for preparing same. *Patent 0371192*, Dec. 18, 2014.

COLLINS T. J. ImageJ for microscopy. *Biotechniques*, v. 43, p.S25-S30, 2007.

COSTA C, TIMMERMAN S. A. S, ARÁUJO P. H. H, SAYER C. Compartmentalization effects on miniemulsion polymerization with oil-soluble initiator. *Macromolecular Reaction Engineering*, v.7, p.221-231, 2013.

COSTA, P.; LOBO, J. M. S. Modeling and comparison of dissolution profiles. *European Journal of Pharmaceutical Sciences*, v. 13, p. 123-133, 2001.

CRESPY D, LANDFESTER K. Miniemulsion polymerization as a versatile tool for the synthesis of functionalized polymers. *Beilstein Journal Organic Chemistry*, v. 6, p.1132–1148, 2010.

CUCCOVIA M, QUINA F. H, CHAIMOVICH H. Singlete oxygen-mediated damage to proteins and its consequences. *Tetrahedron*, v. 38, p.187-195, 1982.

DALLAS P, GEORGAKILAS V, NIARCHOS D, KOMNINOU P, KEHAGIAS T. Synthesis, characterization and thermal properties of polymer/magnetite nanocomposites. *Nanotechnology*. v. 17(8):2046-2053, 2006.

DANHIER, F.; FERON, B.; PRÉAT, V. To exploit the tumor microenvironment: Passive and active tumor targeting of nanocarriers for anti-cancer drug delivery. *Journal of Controlled Release*, v.148, p.135–146, 2010.

DE JONG W. H, BORM P. J. A. Drug delivery and nanoparticles: Applications and hazards. *International Journal of Nanomedicine*, v. 3(2), p.133-149, 2008.

DEDA D. K, UCHOA A. F, CARITÁ E, BAPTISTA M. S, TOMA H. E, ARAKI K, A newmicro/nanoencapsulated porphyrin formulation for PDT treatment. *International Journal of Science Pharmaceutical*, v. 376, p.76-83, 2009.

DESHAYES S, KASKO A. M. Polymeric biomaterials with engineered degradation. *Journal of Polymer Science* A, v. 51, p.3531-3566, 2013.

DIEZ B, ERNSTC G, TEIJOA M. J, BATLLEA A, HAJOSC S, FUKUDA H. Combined chemotherapy and ALA-based photodynamic therapy in leukemic murine cells. *Leukemia Research*, v. 36, p.1179-1184, 2012.

DOLMANS D. E. J. G. J, FUKUMURA D, JAIN R. K. Photodynamic therapy for cancer. *Nature Review Cancer*, v. 3, p.380-387, 2003.
DONG S, CHO H. J, LEE W. Y, ROMAN M. Synthesis and cellular uptake of folic acid-conjugated cellulose nanocrystals for cancer targeting. *Biomacromolecules*, v. 15, p.1560-1567, 2014.

DORNIANI D, HUSSEIN M. Z. B, KURA A. U, FAKURAZI S, SHAARI A. H, ZALINAH A. Preparation of Fe_3O_4 magnetic nanoparticles coated with gallic acid for drug delivery. *International Journal of Nanomedicine*, v. 7, p.5745–5756, 2012.

ELMORE S. Apoptosis: a review of programmed cell death. *Toxicology Pathololy*, v. 35(4), p.495-516, 2007.

FABRIS C, VALDUGA G, MIOTTO G, BORSETTO L, JORI G, GARBISA S, REDDI E. Photosensitization with Zinc (II) Phthalocyanine as a Switch in the Decision between Apoptosis and Necrosis Photosensitization with Zinc (II) Phthalocyanine as a Switch in the Decision between Apoptosis and Necrosis. *Cancer Research*, v. 61, p.7495-7500, 2001.

FARIA G, CARDOSO C. R., LARSON R. E, SILVA J. S, ROSSI M. A. Chlorhexidine-induced apoptosis or necrosis in L929 fibroblasts: A role for endoplasmic reticulum stress. *Toxicology Applied and Pharmacology*, v. 234, p.256-265, 2009

FELICE B, PRABHAKARAN M. P, RODRÍGUEZ A. P, RAMAKRISHNA S. Drug delivery vehicles on a nano-engineering perspective. *Materials and Science Engineering C*, v. 41, p.178–195, 2014.

FERREIRA G. L, SEGURA T, SOUZA JUNIOR F. G, UMPIERRE A. P, MACHADO F. Synthesis of poly(vinyl acetate)-based magnetic polymer microparticles. *European Journal Polymer*, v. 48, p.2050-2069, 2012.

FEUSER P. E, BUBNIAK L. S, BODACK C. N, VALÉRIO A, SANTOS-SILVA M. C, RICCI-JÚNIOR E, SAYER C, ARAÚJO P. H. H. *In Vitro* Cytotoxicity of Poly(Methyl Methacrylate) Nanoparticles and Nanocapsules Obtained by Miniemulsion Polymerization for Drug Delivery Application. *Journal of Nanoscience and Nanotechnology*. in press, 2015.

FEUSER P. E, BUBNIAK L. S, SANTOS-SILVA M. C, CAS VIEGAS A, CASTILHO-FERNANDES A, NELE M, RICCI-JÚNIOR E, TEDESCO A. C, SAYER C, ARAÚJO P. H. H. Encapsulation of magnetic nanoparticles in poly(methyl methacrylate) by miniemulsion and evaluation of hyperthemia in U87MG cells. *European Journal Polymer*, v. 68, p.355-365, 2015.

FEUSER P. E, FERNADES A. C, NELE M, CAS VIEGAS A, TEDESCO A. C, RICCI-JÚNIOR E, SAYER C, DE ARAÚJO, P. H. H. Simultaneous encapsulation of magnetic nanoparticles and zinc phthalocyanine in poly(methyl methacrylate) nanoparticles by miniemulsion polymerization and in vitro studies. *Journal of Colloids and Surfaces B*, v. 135, p.357-364, 2015.

FEUSER, P. E, GASPAR P. C, NELE M, SILVA M. C. S, RICCI E, SAYER C, ARAUJO P. H. H. Synthesis and Characterization of

Poly(Methyl Methacrylate) PMMA and Evaluation of Cytotoxicity for Biomedical Application. *Macromolecular. Symposia*, v. 343, p.65-69, 2014.

FEUSER P. E, GASPAR, P. C, JACQUES A. V, TEDESCO A. C, SANTOS-SILVA M. C, RICCI-JÚNIOR E, SAYER C, ARAÚJO P. H. H. Synthesis of ZnPc loaded poly(methyl methacrylate) nanoparticles via miniemulsion polymerization for photodynamic therapy in leukemic cells. *Materials and Engineering C*, v.60, p.458-466, 2016.

FILIPPOUSI M, ALTANTZIS T, STEFANOU G, BETSIOU M, BIKIARIS D. N., ANGELAKERIS M, PAVLIDOU E, ZAMBOULIS D, VAN TENDELOO G. Polyhedral iron oxide core–shell nanoparticles in a biodegradable polymeric matrix: preparation, characterization and application in magnetic particle hyperthermia and drug delivery. *RSC Advances*, v. 3, 24367–24377, 2013.

FISCHERA D, LIB Y, AHLEMEYERC B, KRIEGLSTEINC J, KISSEL T. *In vitro* cytotoxicity testing of polycations: influence of polymer structure on cell viability and hemolysis. *Biomaterials*, v. 24(7), p.1121-1131, 2003.

FOOTE C. S. Definition of Type I and Type II photosensitized oxidation. *Photochemistry and. Photobiology*, v. 54, p.659-665, 1991.

FORNAGUERAA C, CALDERÓA G, MITJANSB M, VINARDELLB M. P, SOLANSA C, VAUTHIERC C. Interactions of PLGA nanoparticles with blood components: protein adsorption, coagulation, activation of the complement system and hemolysis studies. *Nanoscale*, v. 7(14), p.6045-6058, 2015.

FU Y, KAO W. J. Drug Release Kinetics and Transport Mechanisms of Non-degradable and Degradable Polymeric Delivery Systems. *Expert Opinion of Drugs Delivery*, v. 7(4), p.429–444, 2010.

FURRE I. E, SHAHZIDI S, LUKSIENE Z, MOLLER M. T. N, BORGEN E, MORGAN J, TKACZ-STACHOWSKA K, NESLAND J. M, PENG Q. Targeting PBR by hexaminolevulinate-mediated

photodynamic therapy induces apoptosis through translocation of apoptosis-inducing factor in human leukemia cells. *Cancer Research*, v. 65, p.11051-11060, 2005.

GAO F, CAI Y, ZHOU J, XIE X, OUYANG W, ZHANG Y, WANG X, ZHANG X, WANG X, ZHAO L, TANG J. Pullulan Acetate Coated Magnetite Nanoparticles for HyperThermia: Preparation, Characterization and In Vitro Experiments. *Nanoscale*, v. 3, p.23-31, 2010.

GAO P, NIE X, ZOU M, SHI Y, CHENG G. Recent advances in materials for extended-release antibiotic delivery system. *The Journal of Antibiotics*, v. 64, p.625-634, 2011.

GOSWAMI T. K, GADADHAR S, BALAJI B, GOLE B, KARANDE A. A, CHAKRAVARTY A. R. Ferrocenyl-L-amino acid copper(II) complexes showing remarkable photo-induced anticancer activity in visible light. *Dalton Transations*, v. 23, p.11988-11999, 2014.

GRUNDHOFER P, NIEMETZ R, Schilling G, Gross G. G. Biosynthesis and subcellular distribution of hydrolyzable tannins. *Phytochemistry*, v. 57, p.915–927, 2007.

GUEDES M. H. A, SADEGHIANI N, PEIXOTO D. L. G, COELHO J. P, BARBOSA L. S, AZEVEDO R. B, KUCKELHAUS S, DA SILVA M. D, MORAIS P. C, LACAVA Z. G. M. "Effects of AC magnetic field and carboxymethyldex- tran-coated magnetite nanoparticles on mice peritoneal cells. *Journal of Magnetism and Magnetic Materials*, v. 293, p.283-286, 2005.

GUPTA A. K, GUPTA M. Synthesis and surface engineering of iron oxide nanoparticles for biomedical applications. *Biomaterials*, v. 25, p.3995-4021, 2005.

GUTERRES S. S, ALVES M. P, POHLMANN A. R. Polymeric nanoparticles, nanospheres and nanocapsules, for cutaneous applications. *Drugs target insights*, v. 2, p.147-157, 2007.

GYERGYEKA S, MAKOVECA D, MERTELJ A, HUSKI M, DROFENIK M. Superparamagnetic nanocomposite particles synthesized using the mini-emulsion technique. *Colloids and Surfaces A*, v. 366, p.113-119, 2010.

HAUSER A. K, WYDRA R. J, STOCKE N. A, ANDERSON K. W, HILT J. Z. Magnetic nanoparticles and nanocomposites for remote controlled therapies. *Journal of Controlled Release*, v. 219, p. 76-94, 2015.

HE C, HU Y, YIN L, TANG C, YIN C. Effects of particle size and surface charge on cellular uptake and biodistribution of polymeric nanoparticles. *Biomaterials*, v. 31(13, p.:3657-3666, 2010.

HE L, LI Z, FU J, DENG Y, HE N, WANG Z, WANG H, SHI Z, WANG Z. Preparation of SiO2/(PMMA/Fe3O4) from monolayer linolenic acid modified Fe3O4 nanoparticles via miniemulsion polymerization. *Journal of Biomedical Nanotechnology*, v. 5(5), p.596-601, 2009.

HE, C.; HU, Y.; YIN, L.; TANG, C.; YIN, C. Effects of particle size and surface charge on cellular uptake and biodistribution of polymeric nanoparticles. Biomaterials, v. 31, p.3657–3666, 2010.

HE, Z. LI, J. FU, Y. DENG, N. HE, Z. WANG, H. WANG, Z. SHI, Z. Wang, Preparation of SiO2/(PMMA/Fe3O4) from monolayer linolenic acid modified Fe3O4 nanoparticles via miniemulsion polymerization. *Journal Biomedical Nanotechnology*, v.5 (5) p.596–601, 2009.

HIGUCHI W. I, MISRA J. Physical degradation of emulsions via the molecular diffusion route and the possible prevention thereof. *Journal of Pharmaceutical Science*, v. 51, p.459-466, 1962.

HONG R. Y, FENG B, CAI X, LIU G, LI H. Z, DING J, ZHENG Y, WEI D. G. Double-Miniemulsion Preparation of Fe 3 O 4 / Poly (methyl methacrylate) Magnetic Latex. *Journal of Applied Polymer Science*, v. 112, p.89-98, 2008.

HUANG C-Y, CHEN C-M, LEE Y-D. Synthesis of high loading and encapsulation efficient paclitaxel-loaded poly(n-butyl cyanoacrylate) nanoparticles via miniemulsion. *International Journal of Pharmacy*, v.338, p.267-275, 2007.

HUANG H, CHEN Y, CHEN W, WU Y. Purging efficacy of $ZnPcH_1$-based photodynamic therapy on chronic myeloid leukemia bone marrow. International *Journal of Laboratory Hematololy*, v. 33, p.477-482, 2011.

HUANG X, BRAZEL C. S. On the importance and mechanisms of burst release in matrix-controlled drug delivery systems. *Journal of Controlled Release*, v. 73, p.121-136, 2001.

HUSSEIN M. T. Study β -phase Zn-Phthalocyanine nanostructure by high accuracy preparation with sublimation method. *International Journal of Science Advance Technology*, n.1, p.137-141, 2011.

INTERNATIONAL STANDARD: BIOLOGICAL EVALUATION OF MEDICAL DEVICES – Part 5: Tests for Cytotoxicity: in vitro methods. *ISO 10993-5*, (1992).

ISELE U, KESSLER R , VAN HOOGEVEST P, CAPRARO H. G. Pharmacokinetics and body distribution of liposomal zinc phthalocyanine in tumor-bearing mice: influence of aggregation state, particle size, and composition. *Journal of Pharmaceutical Science*, v. 84(2), p.166-173, 1995.

IWATSU F, KOBAYASHI T, UYEDA N. Solvent effects on crystal growth and transformation of zinc phthalocyanine. *Journal of Physical Chemitry*, n.84, p.3223-3230, 1980.

JAIN R, DANDEKAR P, LORETZ B, KOCH M, LEHR C-M. Dimethylaminoethyl methacrylate copolymer-siRNA nanoparticles for silencing a therapeutically relevant gene in macrophages. *Medical Chemical Communication*, v. 6, p.691-701, 2015.

JIA-JYUN L, JENN-SHING C, SHIH-JER H, JYUN-HAN K, YU-MING W, TING-LUNG C, LI-FANG W. Folic acid-Pluronic F127 magnetic nanoparticle clusters for combined targeting, diagnosis, and therapy applications. *Biomaterials*, v. 30, p.5114-5124, 2009.

KIM T-H, JEONG T-H, JIN S-G, PEI J, JUNG T-Y, MOON K-S, KIM I-Y, KANG S-S, JUNG S. Preparation of polylactide-co-glycolide nanoparticles incorporating celecoxib and their antitumor activity against brain tumor cells. *International Journal of Nanomedicine*, v.6, p.2621, 2011.

KLEIN E, WEBER N. J. In vitro test for the effectiveness of antioxidants as inhibitors of thiyl radical-induced reactions with unsaturated fatty acids. *Journal of Agriculture and Food Chemical*, v. 49 p.1224–1227, 2001.

KUMAR C. S. S. R, MOHAMAD F. Magnetic nanomaterials for hyperthermia-based therapy and controlled drug reléase. *Advance of Drugs Delivery Review*, v. 63(9), p.789-808, 2011.

KUMAR C. S. S. R, MOHAMAD F. Magnetic nanomaterials for hyperthermia-based therapy and controlled drug reléase. *Advance of Drugs Delivery Review*, v. 63(9), p.789-808, 2011.

KUMARI A, YADAV S. K, YADAV S. C. Development of biodegradable nanoparticles for delivery of quercetin. *Colloids and Surfaces B: Biointerfaces*, v.75, p.184-192, 2010.

KUMARI A, YADAVA S. K, PAKADE Y. B, SINGHC B, YADAV S. C. Photoelectric Properties of Soluble ZnPc-Epoxy Derivative Doped with C 60. *Colloids and Surfaces B: Biointerfaces*, v. 22(4), p.549-551, 2010.

LANDFESTER K, MAILANDER V. Nanocapsules with specific targeting and release properties using miniemulsion polymerization. *Expert Opinion Drugs Delivery*, v. 10, p.593-609, 2013.

LANDFESTER K. Miniemulsion polymerization and the structure of polymer and hybrid nanoparticles. *Angew Chemical*, v. 48, p.4488-4407, 2009.

LANDFESTER K.; MUSYANOVYCH V.; MAILANDER, A. From Polymeric Particles to Multifunctional Nanocapsules for Biomedical Applications Using the Miniemulsion Process. *Journal Polymer. Science. Part A: Polymer Chemical.* v. 48, 493-515, 2010.

LANDFESTER, K.; RAMIRES, L. P. Encapsulated magnetite particles for biomedical application. *Journal of Physics*, v.15, p.1345-1361, 2003.

LAPINA V. A, VOROBEY A. V, PAVICH T. A, OPITZ J. Targeting Diamond Nanoparticles into Folate-Receptor Expressing HeLa Cells. *Journal of Applied Spectroscopy*, v. 80, p.414-418, 2013.

LATTUADA M, HATTON T. A. Functionalization of monodisperse magnetic nanoparticles. *Langmuir*, v. 23, p.2158-2168, 2007.

LAURENT S, FORGE D, PORT M, ROCH A, ROBIC C, ELST V. L, MULLER R. N. Magnetic Iron Oxide Nanoparticles: Synthesis, Stabilization, Vectorization, Physicochemical Characterizations, and Biological Applications. *Chemical Review*, v. 108, p.2010-2064, 2010.

LEAMON C. P, LOW P. S. Delivery of macromolecules into living cells: a method that exploits folate receptor endocytosis. *Protocol Nat. Academic Science*, v. 88(13), p.5572–5576, 1991.

LEKSHMI U. M. D.; POOVI G.; KISHORE N.;REDDY P. N. In vitro characterization and in vivo toxicity study of repaglinide loaded poly (methyl methacrylate) nanoparticles. *International Journal of Pharmaceutics*, v.396 p.194–203, 2010.

LEOPOLD C. S, EIKELER D. Basic Coating Polymers for the Colon-Specific Drug Delivery in Inflammatory Bowel Disease. *Drug Development Industry Pharmaceutical*, v. 26(12), p. 1239-1246, 2000.

LEVY M, WILHELM C, SIAUGUE J-M, HORNER O, BACRI J-C, GAZEAU F. Magnetically induced hyperthermia: size-dependent heating power of γ-Fe(2)O(3) nanoparticles. *Journal of Physical Condensate. Matterial, v.* 20, p.204133, 2008.

LI C, WANG Z-H, YU D-G, WILLIAMS G. R. Tunable biphasic drug release from ethyl cellulose nanofibers fabricated using a modified coaxial electrospinning process. *Nanoscale Research Letters* v. 9(1), p.258-277, 2014.

LICCIARDI M, TANG Y, BILLINGHAM N. C, ARMES S. P. Synthesis of Novel Folic Acid-Functionalized Biocompatible Block Copolymers by Atom Transfer Radical Polymerization for Gene Delivery and Encapsulation of Hydrophobic Drugs. *Biomacromolecules*, v. 6, p.1085-1096, 2005.

LIN J-J, CHENB J-S, HUANG S-J, KO J-H, WANG Y-M, CHENC T-L, WANG L-F. Folic acid-Pluronic F127 magnetic nanoparticle clusters for combined targeting, diagnosis, and therapy applications. *Biomaterials*, v. 30, p.5114-5124, 2009.

LOCATELLI C, FILIPPIN-MONTEIRO F. B, CRECZYNSKI-PASA T. B. *European Journal of Medicinal Chemistry*, v. 60, p.233-239, 2013.

LONGO J. P. F, DE MELO L. N. D, MIJAN M. C, VALOIS C. R. A, JOANITTI G. A, SIMIONI A. R, TEDESCO A. C, AZEVEDO R. B. Photodynamic Therapy Mediated by Liposomal Chloroaluminum-Phthalocyanine Induces necrosis in oral cancer cells. *Journal of Biomaterial Tissue. Engineering*, v. 3, p.148-156, 2013.

LOSA C, MARCHAL-HESSELER L, ORALLO F, VILA JATO J. L, ALONSO M. J. Design of new formulations for topical ocular administration: polymeric nanocapsules containing metipranolol. *Pharmaceutical Research*, v. 10, p.80-87, 1993.

LUNOV O, SYROVETS T, LOOS C, BEIL J, DELACHER M, TRON K, NIENHAUS G. U, MUSYANOVYCH A, MAILANDER V, LANDFESTER K, SIMMET T. Differential uptake of functionalized

polystyrene nanoparticles by human macrophages and a monocytic cell line. *ACS Nano*, v. 5(3), p.1657-1669, 2011.

MADERUELO C, ZARZUELO A, LANAO J. M. Critical factors in the release of drugs from sustained release hydrophilic matrices. *Journal of Controlled Release*, v.154, p.2–19, 2011.

MAHDAVIAN A. R, ASHJARI M, MOBARAKEH H. S. Nanocomposite Particles with Core-Shell Morphology. I. Preparation and Characterization of Fe3O4–Poly(butyl acrylate-styrene) Particles via Miniemulsion Polymerization, v. 21, p.1242-1249, 2008.

MANNA S. K, KUO M. T. Overexpression of glutamylcysteine synthetase sup- presses tumor necrosis factor induced apopotosis and activation of nuclear transcription factor B and activator protein, *Oncogene*, v. 18, p.4371– 4382, 1999.

MARANHO D. S., LIMA R. G, PRIMO F. L, SILVA R. S, TEDESCO A. C.. Photoinduced nitric oxide and singlet oxygen release from ZnPC liposome vehicle associated with the nitrosyl ruthenium complex: synergistic effects in photodynamic therapy application. *Journal of Photochemistry and Photobiology*, v. 85, p.705-713, 2009.

MATHEW S. T, DEVI S.G, SANDHYA K. V. Formulation and evaluation of ketorolac tromethamine-loaded albumin microspheres for potential intramuscular administration. *AAPS Pharmaceutical Science Technology*, v. 8(1), p.71-79, 2007.

MEIORIN C, MURACA D, PIROTA K. R, ARAGUREN M. I, MOSIEWICKI M. A. Nanocomposites with superparamagnetic behavior based on a vegetable oil and magnetite nanoparticles. *European Journal Polymer*, v. 53, p.90-99, 2014.

MODY V. V, COX A, SHAH S, SINGH A, BEVINS W, PARIHAR H. Magnetic nanoparticle drug delivery systems for targeting tumor. *Applied Nanoscience*, v. 4, p.385-392, 2014.

MOHAPATRA S, S MALLICK K, KMAITI T, GHOSH S. K, PRAMANIK P. Synthesis of highly stable folic acid conjugated magnetite nanoparticles for targeting cancer cells. *Nanotechnology*, v.18, p.385102, 2007.

MORA-HUERTAS C. E, FESSI H, ELAISSARI A. Polymer-based nanocapsules for drug delivery. *International Journal Pharmaceutical*, v. 385, p.113-142, 2010

MUÑOS-BONILLA A, MARCELO G, CASADO C, TERAN F. J. Preparation of glycopolymer-coated magnetite nanoparticles for hyperthermia treatment. *Journal of Polymer Science* A, v. 50, p.5087-5096, 2012.

NAWALANY K, RUSINC A, KEPCZYNSKIA M, FILIPCZAKC P, KUMOREKA M, KOZIKA B, WEITMAND H, EHRENBERGD B, KRAWCZYKC Z, NOWAKOWSKA M. Novel nanostructural photosensitizers for photodynamic therapy: in vitro studies. *International Journal Pharmaceutical*, v. 430, p.129-140, 2012.

NORDIN M, WIESLANDER A, MARTINSON E, KJELLSTRAND P. Effects of exposure period of acetylsalicylic acid, paracetamol and isopropanol on L929 cytotoxicity. *Toxicologyi in Vitro*, v. 5, p.449-450, 1991.

NOWICKA A. M, KOWALCZYK A, JARZEBINSKA A, DONTEN M, KRYSINSKI P, STOJEK Z. Progress in targeting tumor cells by using drug-magnetic nanoparticles conjugate. *Biomacromolecules*, v. 14, p.828-833, 2013.

NUNES S. M. T, SEGUILIA F. S, TEDESCO A. C. Photophysical studies of zinc phthalocyanine and chloroaluminum phthalocyanine incorporated into liposomes in the presence of additives. *Brazilian Journal of Medical and Biology Research*, v.37(2), p.273-284, 2004.

OKUBO M, IZUMI J. Synthesis of micron-sized monodispersed, core-shell composite polymer particles by seeded dispersion polymerization. *Colloids and Surfaces A*, v. 153, p.297-304, 1999.

OLEINEICK N. L, MORRIS R. L, BELICHENKO I. The role of apoptosis in response to photodynamic therapy: what, where, why, and how. *Photochemistry and. Photobiololgy Science*, v. 1, p.1–21, 2002.

OSTERTAG F, WEISS J, MCCLEMENTS D. J. Low-energy formation of edible nanoemulsions: Factors influencing droplet size. *Journal of Colloid and Interface Science*, v. 388, p.95–102, 2012.

OW Y-Y, STUPANS T. Gallic Acid and Gallic Acid Derivatives: Effects on Drug Metabolizing Enzymes. *Current Drug Metabolism***,** v. 4(3), p.241-248, 2003.

PANARITI A, MISEROCCHI G, RIVOLTA I. The effect of nanoparticle uptake on cellular behavior: disrupting or enabling functions? *Nanotechnology Science Application*, v. 5, p.87-100, 2012.

PATIL R. M, SHETE P. B, THORAT N. D, OTARI S. V, BARICK K. C, PRASAD A, NINGTHOUJAM R. S, TIWALEA R. B, PAWAR S. H. Non-aqueous to aqueous phase transfer of oleic acid coated iron oxide nanoparticles for hyperthermia application. *RSC Advance*, v.4, p.4515, 2014.

PENGCHENG D, HUIYING Y, JIN Z, PENG L. Folic acid-conjugated temperature and pH dual-responsive yolk/shell microspheres as a drug delivery system. *Journal Materials Chemical B*, v. 1, p.5298, 2013.

PRADEEP, N, SREEKUMAR A. V. An in vitro investigation into the cytotoxicity of methyl methacrylate monomer. *The Journal of Contemporary Dental Practice*, v. 1(6), p.838-841, 2012.

PRIMO F. L, TEDESCO A. C. Combining photobiology and nanobiotechnology: a step towards improving medical protocols based on advanced biological models. *Nanomedicine*, v. 8(4), p.513-515, 2013.

QIU G, WANG Q, WANG C, LAU W. Polystyrene/Fe3O4 magnetic emulsion and nanocomposite prepared by ultrasonically initiated

miniemulsion polymerization. *Ultrasonics Sonochemistry*, v. 14, p.55-61, 2007.

RAI P, MALLIDI S, ZHENG X, RAHMANZADEH R, MIR Y, ELRINGTON S, KHURSHID A, HASAN T. Development and applications of photo-triggered theranostic agents. *Advances Drugs Delivery Review*, v. 62, p.1094-1124, 2010.

RAMIRES L. P, LANDFESTER K. Magnetic Polystyrene Nanoparticles with a High Magnetite Content Obtained by Miniemulsion Processes. *Macromolecular Chemical and Physical*, v. 204, p.22-31, 2003.

RAO J. P, GECKELER K. E., Polymer nanoparticles: Preparation techniques and size-control parameters. *Progress Polymer Science*, v. 36, p.887–913, 2011.

REN W. W, WU W, JIA M, DONG H, LI Y, OU Z. Reduction-Cleavable Polymeric Vesicles with Efficient Glutathione-Mediated Drug Release Behavior for Reversing Drug Resistance, *ACS Applied Materials and Interfaces*, v. 5, 10721-10731, 2013.

RICCI-JÚNIOR, E.; MARCHETTI, J. M. Zinc(II) phthalocyanine loaded PLGA nanoparticles for photodynamic therapy use. *International Journal of Pharmaceutics*, v. 310, p.187-195, 2006.

ROCHA M. S., LUCCI C. M, LONGO J. P, GALERA J. P, SIMIONI A. R, LACAVA Z. G, TEDESCO A. C, AZEVEDO R. B. Aluminum-chloride-phthalocyanine encapsulated in liposomes: activity against naturally occurring dog breast cancer cells. *Journal of Biomedical Nanotechnololy*, v.8(2), p.251-257, 2012.

ROMIO A. P, RODRIGUES H. H, PERES A, VIEGAS A. D. C, KOBITSKAYA E, ZIENER, U, LANDFESTER K, SAYER C, ARAÚJO P. H. H. Encapsulation of magnetic nickel nanoparticles via inverse miniemulsion polymerization**.** *Journal of Applied Polymer. Science*, v. 129, p.1426-1433, 2013.

ROTHEN-WEINHOLD A, SCHWACH-ABDELLAOUI K , BARR J, NG S. Y, SHEN H. R, GURNY R, HELLER J. Release of BSA from poly(ortho ester) extruded thin strands. *Journal of Controlled Release*, v. 71, p.31-37, 2001.

SABHARANJAK S, MAYOR S. Folate receptor endocytosis and trafficking. *Advanced Drug Delivery Reviews*, v. 8, p.1099-1109, 2004.

SAEKI, A. YUO, ISEMURA M, ABE I, SEKI T, NOGUCHI H. Apoptosis-inducing activity of lipid derivatives of gallic acid. *Biological and Pharmaceutical*, v. 23, p.1391-1394, 2000.

SAHOO B, SANJANA K, DEVI P, BANERJEE R, MAITI T. K, PRAMANIK P, DHARA D. Thermal and pH responsive polymer-tethered multifunctional magnetic nanoparticles for targeted delivery of anticancer drug. *ACS Applied Materials Interfaces*, v. 5, p.3884−3893, 2013.

SALTAN N, KUTLU HM, HÜR D, IZCAN A, RIDVAN S. Interaction of cancer cells with magnetic nanoparticles modified by methacrylamido-folic acid. *International Journal of Nanomedicine*, v. 6, p.477-484, 2011.

SAVOLAINEN J, LINDENA D, DIJKHUIZENA N, HEREK J. L. Characterizing the functional dynamics of zinc phthalocyanine from femtoseconds to nanoseconds. *Journal of Photochemistry and Photobiololy A*, v.1996, p.99-105, 2008.

SCHADE V. L, ROUKIS T. S. Role of polymethylmethacrylate antibiotic–loaded cement in addition to debridement for the treatment of soft tissue and osseous infections of the foot and ankle. *Journal of Foot and Ankle Surgery*, v. 49, p.55-62, 2010.

SCHAFFAZICK S. R, GUTERRES S. S, FREITAS L. L, POHLMANN A. L. Caracterização e estabilidade Físico-Química de sistemas Poliméricos nanoparticulados para administração de fármacos, *Química Nova*, v. 26, p.726-737, 2003.

SCHOCH Jr F. K, GREGGI JR J, TEMOFONATE T. A. Morphology of metal phthalocyanines thin films. *Journal of Vaccum Science and Technololy*, v.6, p.155-158, 1988.

SCOMPARIN A, SALMASO S, ELDAR-BOOCK A, BEN-SHUSHAN D, FERBER S, TIRAM G, SHMEEDA H, LANDA-ROUBEN N, LEOR J, CALICETI P, GABIZON A, SATCHI-FAINARO R. A comparative study of folate receptor-targeted doxorubicin delivery systems: Dosing regimens and therapeutic index. *Journal of controlled release*, v. 208, p. 106-120, 2015.

SERRANO A, PALACIOS C, ROY G, CESPON C, VILLAR M. L, NOCITO M, GONZALEZ-PORQUÉ, P. Derivatives of Gallic Acid Induce Apoptosis in Tumoral Cell Lines and Inhibit Lymphocyte Proliferation. *Archives of biochemistry and biophysics*, v. 350, p.49-54, 1998.

SHANG L, NIENHAUS K, NIENHAUS G. U. Engineered nanoparticles interacting with cells: size matters. *Journal Nanobiotechnology*, v. 12(1), p.5, 2014.

SHAO J, XUE J, DAI Y, LIU H, CHEN N, JIA L, HUANG J. Inhibition of human hepatocellular carcinoma HepG2 by phthalocyanine photosensitiser photocyanine: ROS production, apoptosis, cell cycle arrest. *European Journal Cancer*, v. 48, p.2086-296, 2012.

SHARMA G, VALENTA D. T, ALTMAN Y, SHERYL H, XIE H, MILTRAGOTRI S, SMITH J. W, JEFFREY. Polymer particle shape independently influences binding and internalization by macrophages. *Journal of Controlled Release*, v. 147(3), p.408-412, (2010).

SHI J, YU X, WANG L, LIU Y, GAO J, ZHANG J, MA R, LIU R, ZHANG Z. PEGylated fullerene/iron oxide nanocomposites for photodynamic therapy, targeted drug delivery and MR imaging. *Biomaterials*, v. 34(37), p.9666-9677, 2013.

SHORK J. F, LUO Y, SMULDERS W, RUSSUM J. P, BUTTE A, FONTENOT K. Miniemulsion Polymerization. *Advance Polymer Science*, v. 175, p.129-155, 2015.

SIMIONI A. R, PRIMO F. L, RODRIGUES M.M.A, LACAVA Z. G. M, MORAIS P. C, TEDESCO A. C. Binding and photophysical studies of biocompatible magnetic fluid in biological medium and development of magnetic nanoemulsion: A new candidate for cancer treatment. *IEEE Transactions on Magnetics*, v. 43(6), p.2459-2461, 2007.

SIQUEIRA-MOURA M. P, PRIMO F. L, ESPREAFICO E. M, TEDESCO A. C. Development, characterization, and photocytotoxicity assessment on human melanoma of chloroaluminum phthalocyanine nanocapsules. *Material and Science. Engineering C*, v.33, p.1744–1752, 2013.

SIVAKUMA M, RAO P. K. In vitro release of ibuprofen and gentamicin from PMMA functional microspheres. *Journal of Biomaterial Science Polymer edition*, v. 13(2), p. 111-126, 2002.

STAUDT T, MACHADO T. O, VOGEL N, WEISS C. K, ARAUJO P. H. H, SAYER C,
LANDFESTER K. Magnetic Polymer/Nickel Hybrid Nanoparticles Via Miniemulsion Polymerization. *Macromolecular Chemical and Physics*, v. 214, p.2213−2222, 2013.

STELLA B, ARPICCOA S, ROCCOA F, MARSAUDB V, RENOIRB J-M, CATTEL L, COUVREURB P. Encapsulation of gemcitabine lipophilic derivatives into polycyanoacrylate nanospheres and nanocapsules. *International Journal of Pharmaceutics*, v. 344, p.71–77, 2007.

SULISTIO A, LOWENTHAL J, BLENCOWE A, BONGIOVANNI M. N, ONG L, GRAS S. L, ZHANG X, QIAO G. G. Folic Acid Conjugated Amino Acid-Based Star Polymers for Active Targeting of Cancer Cells. *Biomacromolecules*, v. 12, p.3469–3477, 2011.

TANAKA H, HASHIMOTO K, YAMADA I, MASUMOTO K, OHSAWA T, MURAI M, HIRANO T. Interstitial Photodynamic

Therapy with Rotating and Reciprocating Optical Fibers. *Cancer*, v. 91, p.1791-1796, 2001.

TANG K. S, HASHMI S. M, SHAPIRO E. M. The effect of cryoprotection on the use of PLGA encapsulated iron oxide nanoparticles for magnetic cell labeling. *Nanotechnology*, v. 24, p.125-101, 2013.

TANIGUCHI T, SHIMIZU M, NAKAMURA H, HIRABAYASHI T, FUJINO H, MURAYAMA T. Hydrogen peroxide-induced arachidonic acid release in L929 cells; roles of Src, protein kinase C and cytosolic phospholipase A2alpha. *European Journal Pharmacololy*, v. 546, p.1-10, 2006.

TEIXEIRA M, ALONSO M. J, PINTO M. M. M, BARBOSA C. M. Development and characterization of PLGA nanospheres and nanocapsules containing xanthone and 3-methoxyxanthone. *European Journal Pharmaceutical Biopharmaceutical*, v. 59, p.491-500, 2005.

TEJA A. S, KOH P. Y. Synthesis, properties, and applications of magnetic iron oxide nanoparticles. *Progress in Crystal Growth and Characterization of Materials*, v. 255, p.45-55, 2009.

TIARKS F, LANDFESTER K, ANTONIETTI M, Silica nanoparticles as surfactants and fillers for latexes made by miniemulsion polymerization. *Langmuir*, v.17, p.575-5780, 2001.

TRIESSCHEIJN M.; BAAS P.; SCHELLENS H. M.; STEWART F.A. Photodynamic Therapy in Oncology. *The Oncologist*, v. 11, p. 1034 – 1044, 2006.

TRINDADE E. S, BOUÇAS R. I, ROCHA H. A. O, DOMINATO J, PAREDES-GAMERO E. J, FRANCO C. R. C, OLIVER C, JAMUR M. C, DIETRICH C. P, NADER H. B. Internalization and degradation of heparin is not required for stimulus of heparan sulfate proteoglycan synthesis. *Journal of cellular physiology*, v. 217(2), p. 360–366, 2008.

VAN DER ENDE A. E, SATHIYAKUMAR V, DIAZ R, HALLAHAN D. E, HARTH E. Linear release nanoparticle devices for advanced targeted cancer therapies with increased efficacy. *Polymer Chemistry*, v. 1, p.93-96, 2010.

WANG J. J., LIU K, SUNG K, TSAI C, FANG J. Y. Lipid nanoparticles with different oil/fatty ester ratios as carriers of buprenorphine and its prodrugs for injection. *European. Journal of Pharmaceutical Science*, v. 38(2), p.138, 2009.

WANG W, LI C, ZHANG J, DONGB A, KONG D. Tailor-made gemcitabine prodrug nanoparticles from well-defined drug–polymer amphiphiles prepared by controlled living radical polymerization for cancer chemotherapy. *Journal of Materials Chemical B*, v.2, p.1891-1901, 2014.

WEN L. Y, BAE S-M, CHUN H-J, PARK K-S, AHN W-S. Therapeutic effects of systemic photodynamic therapy in a leukemia animal model using A20 cells. *Lasers Medical Science*, v. 27, p.445-452, 2012.

WIBOWO S. A, SINGHA M, REEDERA K. M, CARTERA J. J, KOVACHA A. R, MENGA W, RATNAMB M, ZHANGA F, IIIA C. E. D. Structures of human folate receptors reveal biological trafficking states and diversity in folate and antifolate recognition. PNAS, v. 110(38), p.15180-15188, 2013.

WANG W, CHEN Q, JIANG CHA, YANG D, LIU X, XU S. One-step synthesis of biocompatible gold nanoparticles using gallic acid in the presence of poly-(N-vinyl-2-pyrrolidone). *Colloids and Surfavce* A, v. 301, p.73-79, 2007.

XIMENES V. F, LOPES M. G, NIO M. S. P, REGASINI L. C, SILVA D. H. S, FONSECA L. M. Inhibitory effect of gallic acid and its esters on 2,2'-azobis(2-amidinopropane)hydrochloride (AAPH)-induced hemolysis and depletion of intracellular glutathione in erythrocytes. *Journal of Agricultural and Food Chemistry*, v. 58, p.5355-5362, 2010.

XU C, SU S. New forms of superparamagnetic nanoparticles for biomedical applications. *Advance Drugs Delivery Review*, v. 65, p.732-743, 2013.

YANG H, LI Y, LI T, XU M, CHEN Y, WU C, DANG X, LIU Y. Multifunctional Core/Shell Nanoparticles Cross-linked Polyetherimide-folic Acid as Efficient Notch-1 siRNA Carrier for Targeted Killing of Breast Cancer. *Science Report*, v. 4, p.7072, 2014.

YOO H, MOON S-K, TAEWON H, SEOK K. Y, JOO-HWAN K, SUNG-WOOK C, JUNG HYUN K. Multifunctional Magnetic Nanoparticles Modified with Polyethylenimine and Folic Acid for Biomedical Theranostics. *Langmuir*, v. 29, p.5962-5967, 2013.

YU D. G, WANG X, LI X. Y, CHIAN W, LI Y, LIAO Y. Z. Electrospun biphasic drug release polyvinylpyrrolidone/ethyl cellulose core/sheath nanofibers. *Acta Biomaterialia*, v. 9, p.5665–5672, 2013.

YU T, MALUGIN A, GHANDEHARI H. Impact of silica nanoparticle design on cellular toxicity and hemolytic activity. *ACS Nano*, v. 5(7), p.5717-5728, 2011.

ZANGE R, KISSEL T, Comparative *in vitro* biocompatibility testing of polycyanoacrylates and poly (D, L-lactide-co-glycolide) using different mouse fibroblast (L929) biocompatibility test models. *European Journal Pharmaceutical and Biopharmaceutical*, v. 44, p.149-157, 1997.

ZEE J. V. Heating the patient: a promising approach? *Annal Oncology*, v. 13, p.1173–1184, 2002.

ZHANG B, LI W, FANG C-Y, CHANG C-C, CHEN C-S, CHEN Y-Y, CHANG H-C. Receptor-mediated cellular uptake of folate-conjugated fluorescent nanodiamonds: A combined ensemble and single-particle study. *Small*, v. 5, p. 2716-2721, 2009.
ZHANG B, LI W, FANG C-Y, CHANG C-C, CHEN C-S, CHEN Y-Y, CHANG H-C. Receptor-mediated cellular uptake of folate-conjugated

fluorescent nanodiamonds: A combined ensemble and single-particle study. *Small*, v. 5, p. 2716-2721, 2009.

ZHANG J. L, SRIVASTAVA R. S, MISRA R. D. K. Core-Shell Magnetite Nanoparticles Surface Encapsulated with Smart Stimuli-Responsive Polymer: Synthesis, Characterization, and LCST of Viable Drug-Targeting Delivery System. *Langmuir*, v. 23(11), p.6342–6351, 2007.

ZHANG Y, YANG M, PORTNEY N. G, CUI D, BUDAK G, OZBAY E, OZKAN M, OZKAN C. S. Zeta potential: a surface electrical characteristic to probe the interaction of nanoparticles with normal and cancer human breast epithelial cells. *Biomedical Microdevices*, v. 10(2), p.321-328, 2008.

ZHAO B, GU M. Gallic acid reduces cell viability, proliferation, invasion and angiogenesis in human cervical cancer cells. *Oncology letter*, v. 6(6), p.1749-1755, 2013.

ZHAO D. L, ZHANG H. L, ZENG X. W, XIA Q. S, TANG J. T. Inductive heat property of Fe3O4/polymer composite nanoparticles in an AC magnetic field for localized hyperthermia. *Biomedical Materials*, v. 1, p.198-201, 2013.

ZHAO X, ZHAO H, YUAN H, LAN M. Multifunctional Superparamagnetic Fe_3O_4@SiO_2 Core/Shell Nanoparticles: Design and Application for Cell Imaging. *Journal Biomedical Nanotechnology*, v. 10, p.262-270, 2014.

ZHEN Z, TANG W, GUO C, CHEN H, LIN X, LIU G, FEI B, CHEN X, XU B, XIE J. Ferritin nanocages to encapsulate and deliver photosensitizers for efficient photodynamic therapy against cancer. *ACS nano*, v.4(8), p.6988-6996, 2013.

ZHENG N, YIN L, SONG Z, MA L, TANG H, GABRIELSON N. P, LU H, CHENG J. Maximizing gene delivery efficiencies of cationic helical polypeptides via balanced membrane penetration and cellular targeting. *Biomaterials*, v. 35, p.1302-1314, 2014.

ZHENG W, GAO F, GU H. Magnetic polymer nanospheres with high and uniform magnetite content. *Journal of Magnetic and Magnetism Material*, v. 288, p.403-410, 2005.

ZHOU Q, ZHANG Z, CHEN T, GUO X, XHOU S. Preparation and characterization of thermosensitive pluronic F127-b-poly(ε-caprolactone) mixed micelles. *Colloids and Surfaces B: Biointerface*, v. 86(1), p.45-67, 2011.